QATAR UNIVERSITY

COLLEGE OF ENGINEERING

STRENGTHENING OF REINFORCED CONCRETE BEAMS WITH

TEXTILE- REINFORCED MORTARS

BY

MUHAMMAD SHEKAIB AFZAL

A Thesis Submitted to the Faculty of

College of Engineering

in Partial Fulfillment

of the Requirements

for the Degree of

Master of Science

January, 2016

COMMITTEE PAGE

The members of the Committee approve the thesis of Muhammad Shekaib Afzal defended on 27/12/2015.

_____

Dr. Usama Ebead
Thesis Supervisor

_____

Dr. Antonio Nanni
Committee Member

_____

Dr. Mohammed Al-Ansari
Committee Member

_____

Dr. Wael Al-Nahhal
Committee Member

Approved:

_____

Dr. Rashid Alammari, Dean, College of Engineering

ABSTRACT

This study involves an experimental work for using textile reinforced mortar (TRM) to increase the flexural strength of reinforced concrete (RC) beams. Two different types of textiles namely carbon and Polyparaphenylene benzobisoxazole (PBO) were used as strengthening materials. The studied parameters included the type of mortar, type of strengthening material, number of TRM layers, and reinforcement ratio. Eighteen 18 beams were tested under four-point loading until failure. The beams were reinforced with 2D10, 2D12 and 2D16 as main steel reinforcement. Three beams were tested as control specimens namely R1, R2 and R3 respectively. Nine beams were externally reinforced with one layer $(EA)_c^1 = 12.56$ kN/mm, two layers $(EA)_c^2 = 25.12$ kN/mm and three layers $(EA)_c^3 = 37.68$ kN/mm of the carbon TRM system. The other six beams were strengthened using one $(EA)_{PBO}^1 = 6.4$ kN/mm and two layers $(EA)_{PBO}^2 = 12.8$ kN/mm of the PBO TRM system.

The experimental work concluded that a reasonable gain in the flexural strength was achieved for both the strengthening systems, with an average increase of 38% when carbon TRM system was used and an average of 26.7% for the PBO TRM system compared to their respective control specimen. The highest increase in the load carrying capacity was 77.51% for a specimen having the main reinforcement of D12 and was strengthened with carbon TRM system using three layers of carbon textile $(EA)_c^3 = 37.68$ kN/mm. The lowest increase in the ultimate load capacity was 6.60%

for a specimen having the main reinforcement of D16 and was strengthened with one layer of the PBO $(EA)^1_{PBO} = 6.4$ kN/mm strengthening system.

Further, PBO system showed comparatively stronger interfacial bond behavior within the TRM system and further between the TRM layer and concrete substrate, which resulted in higher ductility index and higher energy absorption. Moreover, during the experimentation, it was seen that the technique of applying the TRM system also considers the contractor's ease where the construction workers (although not very skilled) can easily implement the technique after being given simple demonstrations.

TABLE OF CONTENTS

LIST OF FIGURES

LIST OF TABLES

NOMENCLATURE

Abbreviations

RC   Reinforced Concrete

FRP   Fiber Reinforced Polymer

CFRP   Carbon Fiber Reinforced Polymer

T_g Glass transition temperature

TRM   Textile Reinforced Mortar

PBO   Polyparaphenylene Benzobisoxazole

FRM   Fiber Reinforced Mortar

AR   Aluminum Resistance

FRCM   Fabric Reinforced Cementitious Mortar

W:C   water-to-cement

MF   Mechanically Fastened

Symbols

σ_f Flexural strength (Modulus of rupture)

ρ_s Longitudinal steel reinforcement ratio

ρ_f Longitudinal TRM reinforcement ratio

ΔI Ductility Index

Ψ Energy Absorption

A_s Area of steel bar

A_s' Area of compression steel bar

M_n	Nominal Moment
E_s	Steel Modulus of Elasticity
E_c	Elastic Modulus of Carbon Textile
E_{PBO}	Elastic Modulus of PBO Textile
f_y	Yield strength of steel
$f_c{}'$	Nominal compressive strength
$\in_{cu}$	Compressive ultimate strain
A_f	Area of textile / fabric
f_f	Tensile strength of textile
L_b	Length of beam
W_b	Width of beam
d	Effective depth of steel reinforcement
h	Thickness of the beam
d'	Effective depth of compression steel
d_f	Effective depth of textile
t_f	Thickness of textile
b_f	Width of single textile / fabric
N	Number of textile / fabric along the width

ACKNOWLEDGEMENTS

First of all, I would like to thank Allah Almighty for providing me the courage and the blessing to complete this project.

I am sincerely grateful to all who supported me in completing this project effectively and on time. I put forward my supreme appreciation to my project supervisor, Dr. Usama Ebead, for his counseling and advice throughout the project. Dr. Ebead has always been a source of inspiration for me. The way of his thinking and taking good decisions at critical situations are really a good support for me. I thank him again for his assistance and for all his technical support and for never letting me down at any stage.

I would also like to put my sincere thanks to Dr. Kshitij, Post-doctoral Researcher, for helping me in all the experimental work as well as for his comments and recommendations for the betterment of my Master Thesis. He always treats me like a brother and he always support me in all the challenges which I face during the experimental work. Also I would like to thank Eng. Abdul Aziz, Senior Lab Technician, for helping me out in carrying all the experimental work. I gratefully acknowledge his constant help during all the experimental work.

Finally, I would like to thank my parents and my relatives who have supported me to study abroad and helped me out morally and financially in this endeavor.

CHAPTER 1
INTRODUCTION

In this chapter, a background information is given to the strengthening of concrete beams by using different techniques. Brief introduction to the factors that influence the damage in the reinforced concrete structures are discussed. New strengthening techniques and their significance have also been highlighted. Finally, the aims and objectives of this project have been stated with an explained project methodology.

1.1 Background

Concrete is the main construction material in the Gulf region, which is characterized by its high temperatures, severe humidity and high chloride content in soil and concrete materials. Such severe environment is the main cause of corrosion and deterioration of the reinforcing steel bars in concrete structures which significantly reduces the life span of structures. Coastal structures suffer from extensive carbonation and chloride attack, which causes reinforcement corrosion, concrete spalling and cracks after ten years of their age [1]. In a recent study [2], the surface chloride build-up rate was reported as 0.3% of concrete weight per year in the tidal zone of the Arabian Gulf, as compared to 0.04-0.15% in other marine environments. Moreover, most of the surface coatings do not prevent the penetration of chloride in to the concrete due to the harsh environment interaction of the Gulf region.

The damage of concrete structures can be mitigated by applying effective strengthening techniques. Several techniques have been investigated and applied by

previous research as discussed in later sections of this thesis. The cost of rehabilitation and strengthening of concrete structures is usually estimated in millions of dollars [3]. Therefore, looking for a reliable technique to counter the corrosion consequences in the Gulf environment seems to be a challenge for engineers and researchers.

1.2 Strengthening techniques for RC beams

Different strengthening techniques are available in the market depending on the purpose needed for strengthening. The composite plates may be used to strengthen a structural member with different reinforcement materials, in different proportions and by using different matrix materials [4]. An economical solution depends on the market availability of the materials and the ease of application of the strengthening technique.

1.2.1 Ferrocement as a strengthening material

In the traditional method of strengthening the damaged structures, the corroded bars are replaced with new steel rebars and the deteriorated concrete layers are substituted with the fresh concrete layers. A strengthening technique that is appealing for strengthening is the use of ferrocement as external reinforcement, in which steel meshes are embedded between layers of cementitious mortars.

A recent study [5] showed that ferrocement is a good strengthening technique for the loaded reinforced concrete beams and is mainly targeted for the developing countries

where it is not possible to carry out the strengthening process while releasing all the live loads.

The uniform dispersion of reinforcement in the mesh offers improvement in strength, ductility, and crack width control. However, despite the advantages of this technique, it does not prevent the re-initiation of corrosion after strengthening due to the presence of the steel mesh.

1.2.2 Fiber reinforced polymers with epoxy as external reinforcement

Extensive applications of fiber-reinforced polymer (FRP) materials as a relatively new strengthening material have been accomplished and provided an attractive alternative to the ferrocement technique and other traditional strengthening techniques. The great success of using FRP products in the strengthening of concrete structures was driven by their anti-corrosive properties, lightweight, and high tensile strength.

FRP has been used to strengthen the reinforced concrete structures subjected to corrosion [6]. The fatigue capacity of beams with corroded steel reinforcement has been increased when prepared with carbon fiber reinforced polymer (CFRP) sheets beyond that of the control un-strengthened beams having the un-corroded steel reinforcement.

A comparable fatigue performance was achieved for the beams that were strengthened with carbon fabric reinforced polymer (CFRP) at a medium level of corrosion and then were further corroded to high level corrosion before the start of the

test to those that were strengthened and were tested directly to a high corrosion level [7].

1.2.3 Drawbacks of fiber reinforced polymers

In Gulf region where the climate is mostly hot, the problem with the failing of bond strength at high temperature is a significant issue. The CFRP does not show a proper bond strength with the concrete surface at high temperatures [8]. In fact, the curing process for the epoxy resins, which are normally used to glue the FRP composite to concrete substrate, starts at a low glass transition temperature (T_g) which will affect the mechanical properties of the adhesive. The bond performance can be influenced by this reduction, compromising the effectiveness of reinforcing techniques [9].

1.2.4 New strengthening technique – Textile reinforced mortar

This study proposes a new technique that utilizes textile-reinforced mortar (TRM) to strengthen concrete beams. TRM system consist of one or more layers of textiles made of carbon or Polyparaphenylenebenzobisoxazole (PBO) grids among others that are sandwiched between layers of cementitious mortars (Figure 1). If the mortar is polymer modified, the maximum content of organic compounds (dry polymers) in the matrix is limited to 5 percent by weight of cement. . Also, the TRM in North America is known as fiber reinforced cementitious mortar (FRCM) when used as a repair material [10]. With this technique, corrosion can be mitigated after strengthening due to the non-corrosive nature of the textile grids. Meanwhile, the cement-based mortar used in TRM acts as a barrier against chloride ions penetration thus protecting the

main reinforcing bars from corrosion attack. Its lightweight, high tensile strength and ease of application makes the system attractive. This technique also surmounts the epoxy-bonded FRP systems that lack fire resistance as the embedded grid is protected between the mortar layers; thus reducing its vulnerability hazard as the organic matrix is no longer present.
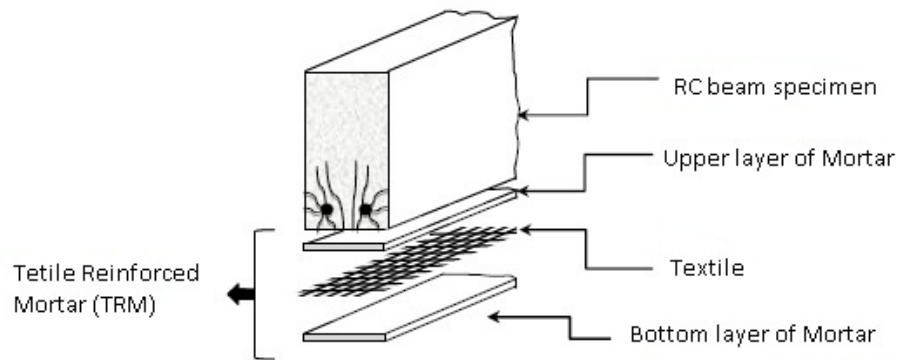
Figure 1: Schematic representation of TRM system

1.3 Motivation and significance

Qatar is significantly investing in construction industry of civil infrastructure for the 21st century, and it is of outmost importance for the country to have available maintenance, repair, and strengthening strategies that allow for safe, continuous, uninterrupted, and efficient functionality. The majority of these construction work projects in Qatar utilize reinforced concrete (RC) and the country is surrounded by the Arabian Gulf; a fact which means that these RC structures are more readily subjected to "*seawater exposure*" in the form of humidity or even direct splashing for sea-level and offshore structures. Also, Qatar is characterized by its high temperature,

severe humidity and high chloride content in concrete materials. Such severe environment is the main cause for reducing the life span of the structure to 10 - 15 years. In some cases, the owner may decide to demolish the whole building simply because it reaches a "*beyond repair*" stage, which means that either it cannot be safely repaired or it becomes much expensive to repair than to demolish and rebuild.

This study proposes an "*optimum strengthening technique*" for RC structures to mitigate the prevailing conditions of Qatar. This relatively new technique utilizes textile-reinforced mortar (TRM) to strengthen concrete beams. The potential of TRM for the repair and strengthening of concrete structures is not just the result of its physio-mechanical performance but also the ease and simplicity of installation that does not require any sophisticated equipment or retraining of the construction work. From past experience, the TRM technique might be the best alternative compared to traditional epoxy-based composites.

1.4 Organization of thesis

A review of the literature in the areas related to the strengthening of the reinforced concrete structures using Textile Reinforced Mortars (TRM) are summarized in Chapter 2. Moreover the limitations of past studies and the methodology applied is also highlighted.

Chapter 3 introduces the material characterization of all the material. Further, the preparation of beam specimens and steps followed for the strengthening technique application has also been discussed.

Chapter 4 covers the detailed test results of each specimen. The test results include the graphs of load vs displacement, steel strain and concrete strain respectively. Moreover the crack patterns and the mode of failure of each specimen has also been reported in this chapter. The latter section covers a summary of the test result and also the effect of different parameters in order to understand the behavior of each system and to make comparisons between the two TRM systems.

Chapter 5 deals with the computation of theoretical load value calculations. It includes step-by-step formulations adopted for calculating the flexural resistance of typical doubly-reinforced concrete beam with and without TRM strengthening.

Chapter 6 briefly summarizes the work reported in this thesis, highlighting the main findings and finally proposes the recommendations for further studies.

CHAPTER 2
LITERATURE REVIEW

The detailed literature study is conducted in this chapter about the topics related to strengthening of the reinforced concrete structures using textile reinforced mortars (TRM). The limitations of the past research studies and the methodology will also be highlighted.

2.1 Fiber reinforced polymer (FRP) composite versus textile reinforced mortar (TRM)

Deterioration or the strict design requirements lead to the rehabilitation and strengthening of existing concrete structures. One of the most common strengthening technique for reinforced structures is fiber reinforced polymers (FRP) [11], [12]. The FRP has attained the increasing popularity in the modern era due to the attractive properties, such as; corrosion resistance, high strength to weight ratio, ease and speed of application and minimal change in geometry [10-11].

However, the FRP strengthening techniques bring about certain drawbacks, which are accredited to organic resins normally used to fix and saturate the fibers [15]. These disadvantages may include: (a) poor behavior at temperatures above the glass transition temperature; (b) de-bonding of FRP from concrete substrate; (c) relatively high cost of epoxy resins; (d) non-applicability on damp surfaces; (e) lack of vapor permeability, which lead to damage of concrete structure; (f) incompatibility of resins

and substrate materials; (g) difficulty to conduct post-earthquake damage evaluation under (undamaged) FRP jackets [13].

TRMs systems are based on inorganic (cementitious) matrixes. Unlike polymer binders, cementitious matrixes cannot fully impregnate individual fibers. Therefore the typical fiber sheets which are used in FRP are installed by manual layup are replaced in TRM with a structural reinforcing mesh (fabric). The fibers used in the TRM mesh are bonded together without any polymer resin but there is a coating on the mesh as a whole. If a polymer is used to either cover or bond the strands, such polymer does not fully penetrate and impregnate the fibers as it would in FRP That is why, the TRM mesh is a dry fiber because the fibers are free from the polymer resin [10].

Fiber matrix relations could be attained when continuous fiber sheets are changed by the textiles, resulting in the generation of new material, called as textile reinforced mortars (TRM) and this might be considered as an alternative technique to FRP in the field of strengthening [13].
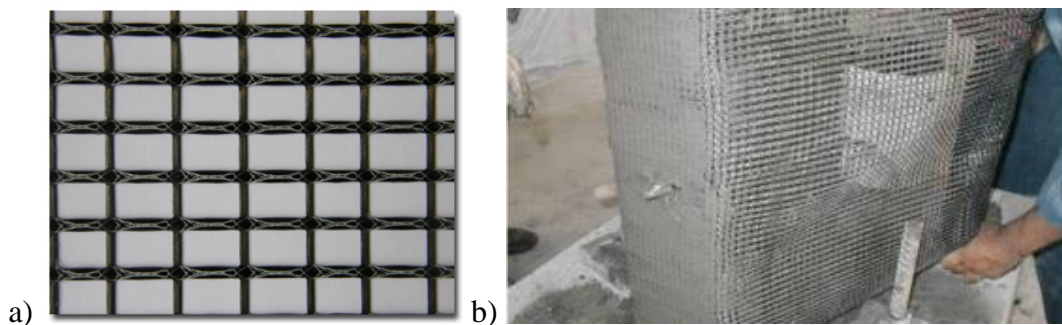
Figure 2: **a)** Two directional carbon fiber based textile [16] **b)** Application at the base of reinforced concrete column [17]

2.2 Textile reinforced mortar (TRM)

Textile (Figure 2) in TRM comprises of fabric meshes made of long woven, knitted or even unwoven fiber rovings in at least two typically orthogonal directions (primary and secondary direction. The spacing and the amount of rovings in each direction can be controlled and by this it will affect the mechanical characteristics of textile as well as the penetration of the mortar matrix through the mesh openings [13].

Polymer modified cementitious matrix having the maximum content of organic compounds in matrix limited to 5 percent by weight of cement, should meet the following requirements: a) no shrinkage, b) high workability (trowel can be used easily for the application), c) high viscosity, d) low rate of workability loss (application of each mortar layer should be possible while the previous one is still in fresh condition), and e) enough shear strength [13] in order to avoid premature de-bonding.

TRM systems have several advantageous which are documented in [10] as

a) Compatibility with chemical, physical and mechanical properties of concrete or masonry substrate.

b) Ease of installation as traditional plastering or trowel trades can be used

c) Porous matrix structure that allows air and moisture transport both into and out of the substrate

d) Good performance at elevated temperatures in addition to partial fire resistance

e) Ease of reversibility (which means the ability to undo the repair without damaging the original structure).

Characteristics of the composite of the textile reinforced concrete are greatly influenced by the properties, amount and arrangements of the fiber material. Therefore, certain demands have to be fulfilled by the fiber material and its textile. Besides the high fiber tenacity and breaking elongation, the modulus of elasticity should be much higher than concrete. Without losing the properties, fiber material has to withstand the alkaline medium permanently in order to ensure the life- long reinforcing effect [15].

2.3 Previous research studies:

Previous research studies have proven a great success of TRM in enhancing the performance of RC structures [18], [19], [20], [21]. Most of these studies were motivated by the desire to remedy the lack of fire resistance of epoxy based bonding agents and to use recycled materials that have a low impact on the environment [18]. Some of the important and most relevant research studies related to strengthening of RC beams using TRM are summarized in Tables 1, 2 and 3 respectively.

As far as reinforced concrete strengthening is concerned, TRM systems have been developed to strengthen existing concrete structures. The feasibility of using carbon TRM to strengthen RC beams in flexure is reported in [22]. One control beam (un-

strengthened) was tested and the second beam was strengthened with four-layer mesh TRM. The TRM-strengthened beam displayed a failure mechanism that was ruled by an inter-laminar shear and showed a good pseudo-ductility.

Elsanadedy et al. [23] checked the flexural strengthening of reinforced concrete beams experimentally as well as numerically. The summary of the tested specimen details and their results has also been summarized in Table 1. Their study comprises the type of mortar, number of TRM layers and the type of strengthening material. Six simply supported small scale beams (150 x 200 x 2000 mm) were tested under four point loading. Two beams were used as control specimens while three beams were strengthened by TRM in which basalt was used as a textile and in the last beam a single layer of CFRP laminates was used for strengthening. The beams were reinforced with 2D10 longitudinal rebars on top as well as at the bottom with a cover of 25 mm. Cementitious and polymer-modified cementitious mortar were utilized in the study. U-shaped technique having 10 numbers of layers was used in TRM strengthened beams while a single layer of CFRP sheet was applied only at the soffit in FRP- strengthened beams. A displacement rate of 1 mm/min was used to test all the beam specimens that were loaded monotonically until the failure. The experimental result proved that polymer modified cementitious mortar gives better bond between the concrete surface and TRM layers as compared to cementitious mortars. The flexural capacity of reinforced concrete beams were increased from 39% to 91% using the basalt textile reinforced mortar. The results also showed that TRM

based strengthening system is more effective in terms of deflection ductility and is slightly less effective in enhancing the flexural strength compared with CFRP.

D. Ambrisi and Focacci have discussed the experimental results of RC beams that were strengthened in flexure with various types of TRM materials [24]. Carbon and PBO meshes and the two types of cementitious matrices were tested. The failure of TRM-strengthened beams was initiated by loss of strengthening action as a result of fiber debonding, three different debonding modes were identified. In most cases, the fiber debonding involved the fiber/matrix interface instead of the concrete substrate. Polyparaphenylene benzobisoxazole (PBO) TRM performed better than carbon TRM. The fiber strain at beam failure was estimated at 0.8 to 0.9 percent in carbon TRM and 1.3 to 1.5 percent for PBO TRM. The performance of TRM materials is strongly dependent on the matrix design and constituents as they affect the fibers/matrix bond.

Kotynia et al. [25] presented the experimental and numerical study of the reinforced concrete beams (RC) that were strengthened in flexure with different externally bonded carbon fiber-reinforced polymers (CFRP) as well as the wet lay-up sheets. The summary of the adopted strengthening techniques and test results is shown in Table 1. A total of ten rectangular specimens (150 x 300 x 4450 mm) with a clear span of 4200 mm were tested in order to calculate the effect of using the additional U – shaped CFRP systems on the intermediate crack debonding of bottom laminate. U-shaped wet lay-up sheets and spaced side- bonded CFRP L-shaped laminates were proposed as the additional strengthening system. Based on the experimental results,

the observed mode of failure for all the tested specimens was the intermediate crack debonding of bottom FRP flexural strengthening reinforcement. Also a debonding plane was seen in the concrete cover. While using the wide laminates and transverse FRP continuous U wrap system, the ultimate load carrying capacity was increased due to additional CFRP reinforcement.

Papanicolaou et al. [26] made experimental and analytical investigations on the use of carbon and glass TRM to strengthen 2 x 2 m two-way slabs that were subjected to central concentrated forces. The load-carrying capacity of the TRM-strengthened slabs using one and two carbon, and three glass fabric layers increased by more than 25, 50, and 20 percent, respectively, over that of the control specimen.

Si Larbi, Agbossou, and Hamelin [27] reported an experimental and numerical study on repair and strengthening of reinforced concrete beams using textile reinforced concrete (TRC), hybrid solutions (TRC + carbon and glass rods) and carbon fiber-reinforced polymers (CFRP) solutions. The complete summary has been shown in Table 3. The investigated parameters include the bearing capacity and different failure modes. The TRC used in this study consisted of a selected mortar of fine particles and textile (AR glass) reinforcement. Two variables were selected. The first TRC was consisted of three layers of alkali-resistant fabric that was embedded inside the mortar and second one combined the two layers of alkali resistant fabric with carbon rods (TRC +JV) or the combination of carbon and glass (TRC + JVC). Five reinforced concrete (RC) beam specimens (150 x 250 x 2300 mm) have been tested.

The beams were internally reinforced with 12 mm rebars at the bottom side and two 8 mm rebars at the top. Out of the total five, one was the control specimen and rests were strengthened as TRC, CFRP, TRC+JC and TRC+JVC. In order to check the performance of reinforcement in case of repair, three beams were loaded prior of strengthening (CFRP, TRC+JC and TRC+JVC) until longitudinal steel yields and are named as damaged beams. The control specimens and TRC were undamaged beams. The static monotonic load were applied under the load control (1 kN / min) until the specimens fails. Load cell of 200 kN capacity was used to measure the load value.

The experimental results of the work done by Si Larbi, Agbossou, and Hamelin [27] showed that the TRC alone cannot be considered for increasing the bearing capacity as it significantly improves the ultimate capacity. Although TRC showed a multi-cracking behavior, but it did not provide any relevant gain in terms of ductility. For the concrete cracks, the average crack spacing was inversely proportional to axial stiffness of the reinforcement and the stress transfer between the longitudinal steel and external reinforcement will also be increased while increasing the axial stiffness.

Gencoglu and Mobasher [28], [29] strengthened plain concrete flexural members with alkali-resistant (AR) glass TRM. The results obtained showed an increase in the load carrying capacity as well the increase in the pseudo-ductility by using different layers of AR glass mesh. A design procedure based on composite laminate theory was proposed [30] to address the contribution of TRM, where an algorithm produces a

moment-curvature relationship for the section, which in turn can be used to calculate the load-deflection response of a structural member [31].

Verbruggen, Tysmans, and Wastiels [32] focused on the cracking behavior for the textile reinforced cement (TRC) or carbon fiber reinforced polymer (CFRP) strengthened reinforced concrete beams. A total of 17 beam specimens having five different types were studied in which three beam types (control, TRC reinforcement or CFRP reinforcement) were used to study the effect of external reinforcement on the behavior of internally reinforced concrete beams. All the beams were simply supported small scale (100 x 100 x 650 mm) and were tested under the four point bending with third point loading. The main longitudinal rebar in all the beams were 2D8. In the TRC –matrix, Inorganic Phosphate cement (IPC) was used along with the glass fibers.

The experimental results of Verbruggen, Tysmans, and Wastiels [32] showed that the stability of inner steel reinforcement was increased when external reinforcement was added to the concrete beam without affecting the mode of failure, total number of cracks and ultimate load capacity. However, the immediate opening of already existing cracks reduces the initial high uncracked stiffness of the beam.

S. Babaeidarabad et al. [33] investigated the feasibility of fabric- reinforced cementitious mortar (FRCM) materials to be used as an alternative external strengthening technique using dry- fabric. The experimental setup consisted of testing eigtheen reinforced concrete beams (260 x 152 x 1829 mm) strenthened in flexure

using one and four layers of PBO-fabric. The beams were fabricated using low and high strength concrete. The three-point bending test was conducted with instrumentation including the laod cell, linerar variable differential transducers (LVDTs) and strain gauges. Six strain guages were installed to measure the strain at different locations which are; two on the longitudinal steel bars; two on FRCM (tension face) and two on concrete surface (compression side). Displacement control mode of loading rate 3.05mm/min was used to test all the beam specimens in quasistatic loading and unloading cycles for a total of six cycles.

The experimental result reported in S. Babaeidarabad et al. [33] showed that by using one ply of FRCM , the avereage ultimate load recorded was 67.7 kN and 63 kN for low strength concrete and high strength concrete specimen respectively. However, the beams that were strengthened with four ply of FRCM, reached the highest peak load value with an average of 99 kN for low strength concrete speciemns and an average of 96.8 kN for high strength concrete specimens and both of them are almost 1.5 times than that of 1 ply specimens. Also the test results identified two modes of failure which were named as the fabric slip within the FRCM layer and second one was FRCM delamination from concrete substrate. Moreover the analysis and design were conducted to calculate the flexural capaicty of beams and while comparing the results with the experimental database, it showed comparatively satisfactory results with a lillte variation from the experimental results.

D. Arboleda et al. [34] focused on the characterization of tensile behavior of FRCM composites. Two setups were investigated in this study namely clevis grip and a clamping grip. A trilinear curve of stress-strain behavior of FRCM was observed with having the main difference in the stresses that were generated by the grips used in two different methods. Shear stresses were only transferred in the first case while in the second one compression and shear stresses were transferred. Five different FRCM systems were used in this study named as Polyparaphenylene benzobisoxazole (PBO), two types of carbon fiber (C fiber and cC fiber), and two types of glass fabric (G fiber and cG fiber). Each fabric was laid with its associated mortar which were given by the manufacturer. Moreover the recommendations for the tensile characterization of FRCM materials has also been provided in this study.

Triantafillou [13] focused on the effectiveness of TRM as externally applied flexural strengthening reinforcement for reinforced concrete (RC) beams. The detail of test specimens and their experimental results has also been illustrated in Table1. Three under-reinforced beams (150 x 250 x 2000 mm) were tested under four point bending having the main reinforcement of 2D12. Self-compacting concrete having the 28 days compressive strength of 34.5 MPa was used for the casting of beam specimens. Out of three, one of the specimen was tested as a control specimen (un-strengthened). The second one was strengthened using four layers of textile fabric bonded with cement based mortar and the third specimen was strengthened by four layers but bonded with epoxy resin based matrix. The beams were tested monotonically as the load was applied using a vertically positioned actuator and a heavy spread beam. Two

differential transducers were mounted on both sides of the beams in order to get the displacements at the mid span. The experimental results showed that the bilinear response was displayed for the control specimen and the deflection at maximum load (83 kN) was nearly 40 mm. The beam strengthened by epoxy impregnated textile showed an increased strength and increased stiffness by approximately 50%. The beam failed suddenly (at 125 kN) because of the tension fracture of externally bonded reinforcement at mid-span. The other beam strengthened by cement based mortar, displayed almost the similar characteristics, but its response was a little more ductile means the steel tends to yield at lower load value; the ultimate load (111 kN) was even lower. The mode of failure was the debonding at the end of the TRM layer due to the inter-laminar shearing. In short, the TRM based strengthening was approximately 30% less effective in terms of flexural strength, but 30 % more effective in terms of ductility (displacement).

2.3.1 Concrete surface abrasion techniques

The concrete surface was prepared so that the overlays or coatings should make a strong bond with the underlying concrete [35]. Separate techniques and different types of equipment can be used in order to roughen the surface. Scarifiers, scabblers, abrasive blasters and water blasters are some of the machines that can be used for roughening the surface.

2.3.1.1 Abrasive blasters

Abrasive blasters include the sand blasting as well as shot blasters technique [35].
The details for both the methods are given below.

Sandblast:

Most of the contractors are familiar with the sand blasting machines (Figure 3) as abrasive blasters. The machine uses compressed air to eject a high speed stream of sand from the nozzle.

Figure 3: Sand blasting machine [36]

Dust may cause health issues when sandblasting is used. Workers have to wear an air-fed helmets as breathing heavy concentration of dust over an extended period is harmful. There is some sandblasting systems which inject water along with the sand and this also provides a wash down of cleaned surface instead of holding down the dust [35].

Shot blasters:

A metallic abrasive steel shot has been used in shot blasting machine (Figure 4) to roughen the concrete surface. The shot is pushed by a rotating wheel, influences on the concrete surface and bounces back into a recovery unit. One of the major advantages of shot blasters is the good control of the dust. As, there is no need of water, the surface is immediately ready for the application of coating which requires a dry surface. It is typically used for cleaning to depth up to 1/8 inch [35].

Figure 4: Shot blasting equipment [37]

2.3.1.2 Water blasters

Newly developed high pressure water blasters (Water Jetting Machine) are now being used to prepare concrete surfaces for repairing purposes (Figure 5). With these water blasters around 2 to 3 inches of removal depth are most commonly done in bridges and parking decks [35].

Figure 5: Water jetting machine [38]

High pressure water jets used for concrete removal typically develop pressures ranging from 16,000 to 25,000 psi. Water consumption is at the rate of about 20 to 26 gallons per minute. Depth of the removal is controlled by adjusting water pressures and speed of the machine. The main advantage of using water jetting machine is that no dust is created and machine removes deteriorated concrete selectively and leaves good concrete intact [35].

Table 1: Summary 1 of existing experimental work on flexural strengthening using TRM technique

Experimental Detail	Elsanadedy et al. [23]	Kotynia et al. [25]	Triantafillou [13]
Test Specimen Details	6 RC Beams (150 x 200 x 2000 mm) with 2 beams as control specimen.	10 RC beams (150 x 300 x 4200 mm)	3 RC beams (150 x 250 x 2000 mm) with one as control specimen
Type of FRCM	i. Basalt textile (3-beams) ii. CFRP laminates (1- beam)	i. CFRP Laminates ii. Wet layup sheet	i. Carbon fiber with cement based mortar ii. Epoxy resin-based matrix material
Reinforcement Type	2D10 on top and bottom sides	2 D12 on bottom and 2 D10 on top sides	2 D12 on bottom and top sides
Mortar matrix Type	i. Cementitious ii. Polymer modified cementitious	Associated cement mortar	i. Cement based mortar ii. Epoxy resin
Strengthening Technique	i. U shaped ii. Flat shape	i. Flat strips ii. Continuous U shaped Laminates ii. Spaced L shaped Laminates (spacing 200 mm)	Flat type
No. of Layers of Textile	i. 10 layers ii. 1 layer	i. 3layers ii. 1 layer ii. 2 layers	4 layers
Increase in Flexural Strength (%)	i. 40 % ii. 22 %	i. U shaped ;34 % ii. L shaped; higher load values	i. 25 % ii. 50 %
Observed Failure	i. TRM debonding ii. Textile rupture	CFRP debonding	i. TRM debonding ii. Tensile fracture

Table 2: Summary 2 of existing experimental work on flexural strengthening using TRM technique

Experimental Detail	T. Sen and H. N. Jagannatha Reddy [39]	Al-Salloum[14]
Test Specimen Details	7 beams with 3 main groups (140 x 200 x 1400 mm) with one group as control specimen	10 beams (150 x 200 x 1500 mm) with one as control specimen
Type of FRCM	i. Full length wrapping 90° (Jute, Carbon and Glass) FRP ii. Strip wrapping 90° (Jute, Carbon and Glass) FRP (62 mm strips at 124 mm C/C)	Basalt based textile with different orientation
Reinforcement Type	2 D8 and 3 D 8	4 D10 at bottom and 2 D10 at top side
Mortar matrix Type	Associated Mortar	Cementitious Polymer-modified cementitious
Strengthening Technique	U –wrap three sided	2 sides in shear span
No. of Layers of Textile	One layer for all three groups	2 layers 4 layers
Increase in Flexural Strength (%)	i. 62.5, 150 and 125 ii. 25, 50 and 37.5	36 -88% in shear capacity
Observed Failure	i. Debonding of FRP ii. Flexural crack	Shear failure

Table 3: Summary 3 of existing experimental work on flexural strengthening using TRM technique

Experimental Detail	Si Larbi, Agbossou, and Hamelin [27]
Test Specimen Details	5 RC beams (150 x 250 x 2300 mm) with one control specimen
Type of FRCM	i. TRC ii. CFRP ii. TRC(glass fabric) & JC (carbon rod) v. TRC (glass fabric) & JCV(glass and carbon rod)
Reinforcement Type	2D12 and 2D8
Mortar matrix Type	Associated Mortar of fine particles (diameter less than 0.8mm)
Strengthening Technique	Flat type (Soffit of beam)
No. of Layers of Textile	i. 3 glass AR fabric ii. Carbon Fiber ii. (2 glass fabric)+(8 carbon rods) v. (2 glass fabric)+(12 Glass rod and 4 carbon rods)
Increase in Flexural Strength (%)	i. 28.1 % ii. 86.5 % ii. 57.3 % v. 63.5 %
Observed Failure	i. Strengthening plate failure ii. Peeling off ii. Peeling off v. Strengthening plate failure

2.4 Limitations of past research studies

Strengthening of RC structures with TRM is a promising technique that can be as effective as epoxy-based FRP systems. The use of TRM provides better interaction between the cement-based mortars used and the concrete substrate. Additionally, it is more compatible with the typical construction workers' skills being a trowel-trade. However, many parameters that might influence the performance of TRM-strengthening need to be thoroughly investigated. Their effects on the performance of the structure have not been fully documented. Examples include the existing steel reinforcement ratio, different TRM system having different volume fraction, stiffness (EA) of TRM system and the strengthening scheme, etc.

Research studies on TRM as a strengthening material are relatively recent compared to those on FRP strengthening system. Such studies need to provide more understanding of the performance of TRM-strengthened structures. The current research aims at contributing to such research to add the knowledge on TRM as a strengthening technique. It is believed that the findings of this research will provide practicing engineers and contractors with new perspectives in the rehabilitation field.

2.5 Objectives of the present work

The main objectives of this research are:

1. Investigating experimentally the feasibility of using the TRM systems to upgrade the service flexural performance and the ultimate capacity of reinforced concrete beams

2. Investigating the parameters (steel reinforcement ratio, stiffness of TRM system and amount of TRM) that most influence the flexural performance of reinforced concrete beams strengthened with TRM.

3. Attempting to optimize the configuration of the TRM strengthening technique in terms of the type of TRM used and the number of layers of fabrics while altering the original steel reinforcement ratio of the beam specimens.

4. To verify the ACI-549 [10] by making the theoretical model.

2.6 Methodology

The proposed program aims at investigating the flexural performance of reinforced concrete beams strengthened with TRM systems. The tests were carried out on a medium-scale reinforced concrete beams. The detailed design of the beam specimen was accomplished in early stages of the testing program. The beams strengthened with TRM systems were tested under monotonic loading. Un-strengthened beams served as control specimens.

The aim here is investigating the static flexural performance of RC beams strengthened with the TRM systems and to quantify the effect of various parameters

on their performance. The mechanical behavior of the TRM material system used to strengthen the beams was also assessed. Un-strengthened and strengthened beams were tested under four-point monotonic loading. Tests were performed under displacement control mode with a loading rate of 1mm / min until failure occurs. The following three parameters were investigated in this research.

1. Steel reinforcement ratio

The beam specimens were designed according to the ACI-318 provisions. Three reinforcement ratios determined as percentages of the balanced ratio of the studied cross section were considered. The ratios simulated two cases of in-service beams; namely, (a) flexure-deficient beams with flexural capacities less than the minimum capacity specified by the code. These beams were designed with a steel ratio well below the balanced value and (b) typical under-reinforced beams that need to be upgraded to accommodate the anticipated increase in-service load. The selection of the number of bars associated with each reinforcement ratio was part of the initial design of the parameters at the beginning of the work. The outcome of testing these beams aims to quantify the efficiency of TRM in strengthening RC beams with various reinforcement ratios. Results focused on quantifying the efficiency of TRM in upgrading the serviceability and the capacity of the strengthened beams.

2. TRM system

Beam specimens were strengthened with two TRM types, namely the carbon- and PBO- TRM systems. The strengthening technique was applied to the soffit of the

beam (flat-shape). Test results compared the efficiency of each system in enhancing the ductility and load capacity of the strengthened beams. Prior to strengthening, the concrete substrate was prepared and recommendation for best practices for concrete surface preparation has also been given.

3. Volume fraction of TRM

Different volume fractions of TRM were achieved by altering the number of layers (one layer of carbon $(EA)_c^1 =$ 12.56 kN/mm , two layers of carbon $(EA)_c^2 =$ 25.12 kN/mm , three layers of carbon $(EA)_c^3 =$ 37.68 kN/mm , one layer of PBO $(EA)_{PBO}^1 =$ 6.4 kN/mm and two layers of PBO $(EA)_{PBO}^2 =$ 12.8 kN/mm) of textile that are embedded in the mortar. Volume fractions have been assessed according to enhancement level in the ultimate capacity of beams strengthened with one layer of textile. The ductility and energy absorption values were also determined by altering the number of layers of fabric / textile and were compared between the two TRM systems.

CHAPTER 3
EXPERIMENTAL PROGRAM

This chapter provides details on material characterization tests performed on all the materials. Furthermore, the preparation of beam specimens and the procedure adopted for the strengthening technique application has also been highlighted.

3.1 Material characterization

In this section the material properties used in the experimental program of TRM strengthened beams are discussed.

3.1.1 Concrete and steel reinforcement

Ready mix concrete with a compressive strength of 67 MPa was used to cast the beam specimens. All the beams were casted using the same transit mixer (Figure 6) at one time. For each cubic meter, the mixture proportions were 1,100 kg of gravel, 800 kg of sand, 370 kg of ordinary Portland cement and 167 L of water. The total density was 2466 kg/m^3. The water-to-cement (W:C) ratio was kept at 0.45.

Figure 6: Ready mix Concrete (Transit Mixer)

Eight standard concrete cylinders having dimensions of 150mm in diameter and 300mm in height to evaluate the compressive strength of concrete. Also, six prisms (100 x 100 x 500 mm) were tested to measure the flexural strength (modulus of rupture) of concrete. Flexural strength can be determined by $\sigma_f = \frac{3PL}{4bd^2}$. The samples were tested (Figure 7) after five months from the day of casting as the beams were also tested after four to six months respectively after applying the appropriate strengthening techniques. The average flexural and compressive strength is presented in Tables 4 and 5 respectively.

a)   b)
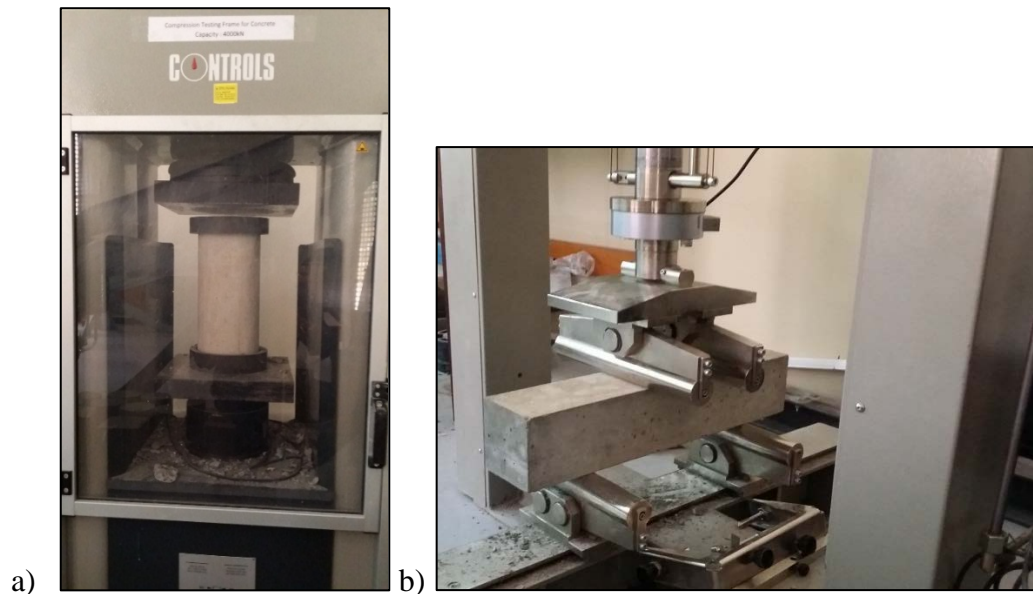
Figure 7: Apparatus to measure a) Compressive strength and b) Flexural strength

Table 4: Measured flexural strength of concrete specimens

Specimen Type	Peak Flexural Load (kN)	Flexural Strength (MPa)	Mean Flexural strength (MPa)	Standard deviation (MPa)
Concrete Prism (100 x 100 x 500) mm	23.345	8.75	9.63	0.62
	26.898	10.08		
	23.591	8.85		
	26.015	9.76		
	27.727	10.39		
	26.602	9.96		

Table 5: Measured compressive strength of concrete specimens

Specimen type	Compressive strength (MPa)	Mean compressive strength (MPa)	Standard deviation (MPa)
Concrete Cylinders (D = 150 mm) (H = 300 mm)	66.39	67.46	1.64
	65.61		
	69.00		
	70.18		
	67.06		
	66.52		
	65.71		
	69.20		

Steel bars (of diameter of 8, 10, 12 and 16 mm) were used for the steel reinforcement in the construction of beams (Figure 8). The bars of diameter 8 mm were used for all transverse steel reinforcement (stirrups) and also used in the compression reinforcement for all the beams, while the 10, 12 and 16 mm bars were used for the

main flexural reinforcement. The properties of steel reinforcement are illustrated in Table 6 [40].

Figure 8: Steel rebars

Table 6: Properties of steel reinforcement

Bar No.	Nominal Area (mm^2)	Yield Strain	Yield Stress (MPa)	Ultimate Stress (MPa)	Modulus of Elasticity (GPa)
8 mm	50.2	0.00268	512	551	191
10 mm	78.5	0.00267	515	555	193
12 mm	113.1	0.00268	519	553	194
16 mm	201.1	0.00266	525	560	197

3.1.2 Textile reinforced mortar (TRM)

The TRM systems consist of two main elements, a cementitious matrix and a fiber network or mesh (fabric). Two commercially available TRM systems have been

utilized in this study. The first system is the Ruredil X Mesh Gold and the second one is the Carbon fiber Armo Mesh L600 with Sika Mono top-612 Mortar.

The Ruredil X Mesh Gold system comprises of a Polyparaphenylene benzobisoxazole (PBO) mesh and a stabilized inorganic matrix (Ruredil X Mortar M750).

3.1.2.1 Textile properties

Textile contain fabric meshes made of long woven, knitted or even unwoven fiber rovings in typically two orthogonal direction, consisting of primary direction (PD) and secondary direction (SD).The orientation of the main fabrics in the textile reinforcement is an important feature that has to be taken into account. In case of carbon fiber ARMO Mesh L600, the applied forces are resisted by the fibers which run in Primary direction (PD) whereas in the case PBO textile , the applied forced are resisted by fibers both in primary as well as in secondary direction. The carbon and PBO fabrics used in the experiment can be seen in Figure 9.

a)   b)
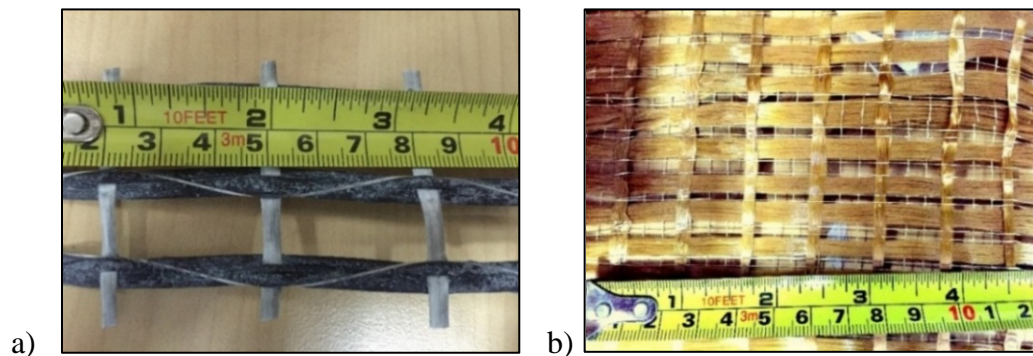
Figure 9: Textile fabric used: (a) Carbon, (b) PBO

The properties of TRM fabrics system are shown in Table 7 and Table 8 respectively.

Table 7: Properties of fabrics used in the TRM system [41], [42] and [10]

TRM Properties	Carbon	PBO
Density, g/cm³	1.79	1.56
Tensile strength, GPa	4.30	5.80
Modulus of Elasticity, GPa	80	128
Ultimate deformation	0.0175	0.0215
Break down temperature, °C	2500	650
Ultimate tensile strength f_{fu} (MPa)	1031	1664
Ultimate tensile strain ε_{fu} (mm/mm)	0.016	0.018

Table 8: Mesh properties of fabrics used in the TRM system [41], [42].

Fiber Mesh Properties	Carbon	PBO
Weight of PBO fibers in the mesh, g/m²	187	88
Fiber area by unit width A_f (mm^2/mm)	0.157	0.05
Equivalent fiber thickness in the direction of warp (mm)	0.156	0.0455
Equivalent fabric thickness in the direction of the weft (mm)	-	0.0115
Ultimate tensile stress of warp per unit of width, kN/m	450	264
Ultimate tensile stress of the weft per unit of width, kN/m	-	66.5

3.1.2.2 Mortar characterization (ASTM C109)

Test specimens of cubes of size 50 mm were prepared with test cubes as per ASTM C109 [43] (Figure 10-a). The specimens were prepared by hand tamping the mortar in two layers during casting, after mechanical mixing the mortar matrix. Mix design and mixing procedure adopted was based on the manufacturers' recommendation. Immediately upon completion of molding, the mold was placed in a moist room for 24 hours. The specimens were removed from the mold after 24 hours and were cured

in water for 7 days and 28 days compressive strength. Two mortar types are studied here: Sika MonoTop-612 and Ruredil X Mortar 750. The test set-up on the compression testing machine is shown in Figure 10-b. The test results are presented in Table 9.

Table 9: Measured compressive strength of mortars used in TRM composites

Mortar type	Test day	Compressive strength (MPa)	Mean compressive strength (MPa)	Standard deviation (MPa)
Sika MonoTop-612	7-day	11.328	13.315	1.846
		11.340		
		15.132		
		14.684		
		14.092		
	28-day	20.416	19.674	1.112
		19.360		
		18.384		
		19.044		
		21.168		
Ruredil X Mortar 750	7-day	23.332	23.810	1.237
		22.996		
		24.944		
		25.292		
		22.488		
	28-day	26.544	29.062	2.094
		31.532		
		30.820		
		28.732		
		27.684		
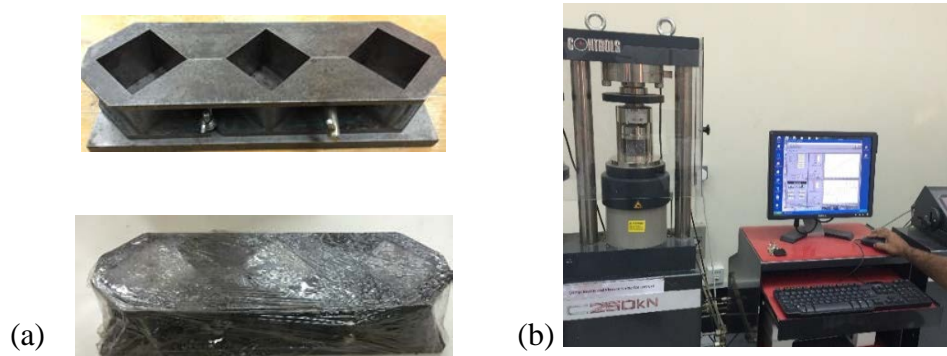
Figure 10: Compressive strength test of mortar, ASTM C109: (a) Test mold, (b) Test set-up

3.2 Detailing of beam specimens

A total of eighteen beam specimens were used in this research. Three beams were used as control specimens having the main rebar of 2D10, 2D12 and 2D16 respectively. The beams were designed in such a way that they will be having a pure flexural failure while testing. The effective depth of the beam is fixed (d=210 mm) for all the three types of beam specimens by differing in the concrete cover (at the bottom sides) of 37, 36 and 34 mm for 2 D10, 2 D12 and 2 D16 specimens respectively. The detailed sections of beam specimens having the main longitudinal rebar of 2 D10, 2 D12 and 2D16 are shown in Figure 11(a, b and c) respectively.
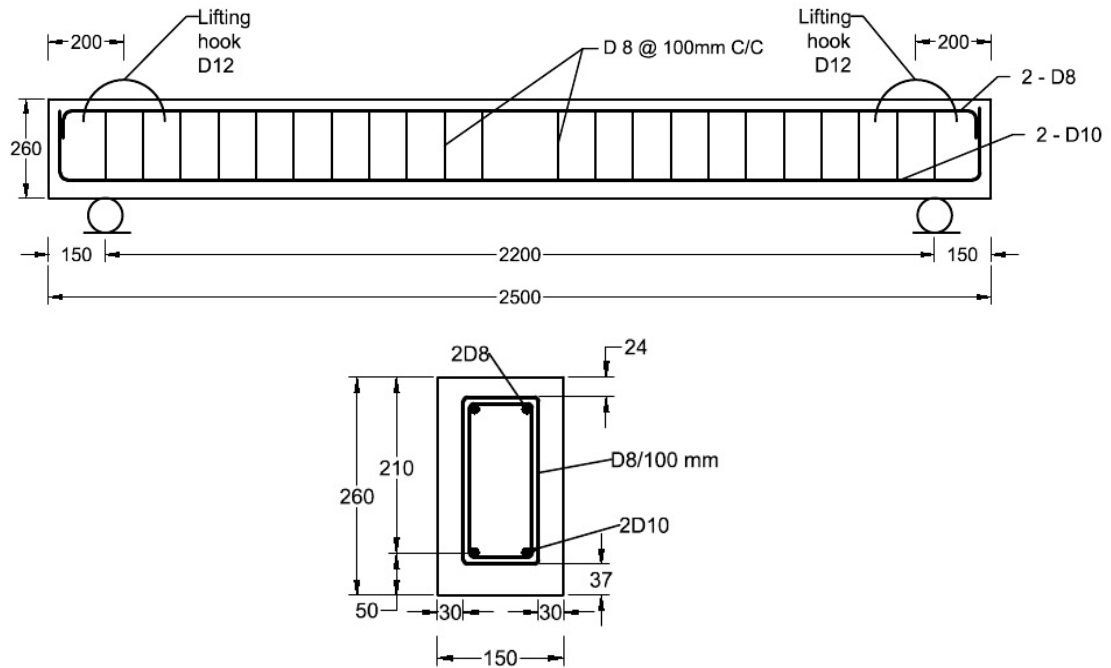
a) Longitudinal and mid span cross-section of 2 D10 specimen (Dimensions are in mm)
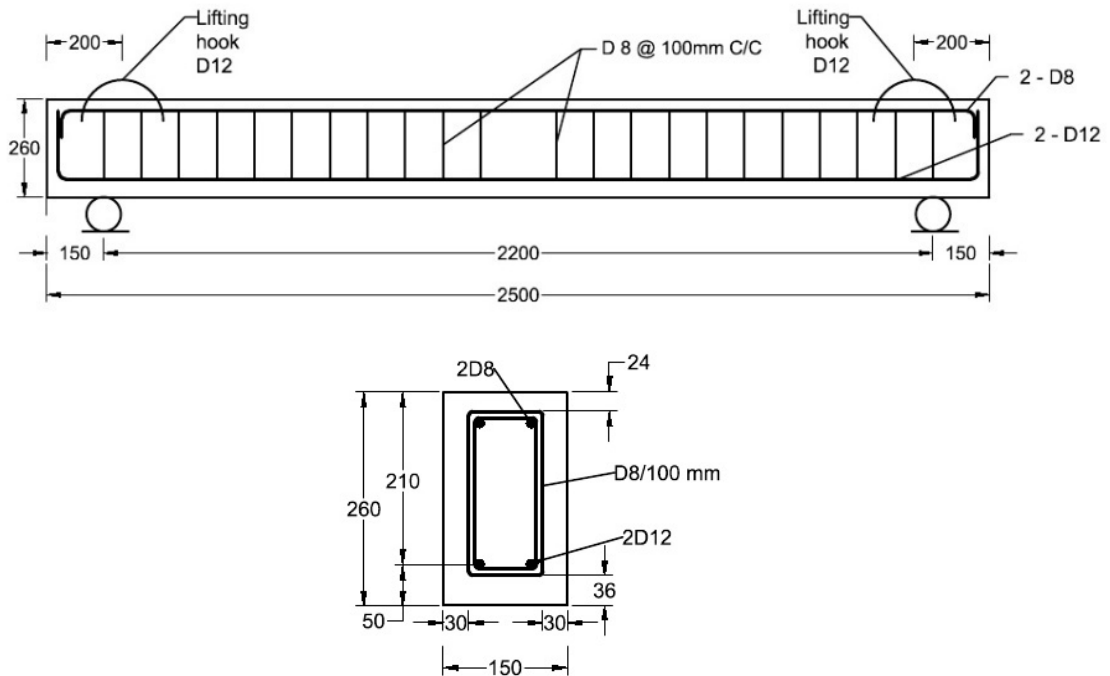
b) Longitudinal and mid span cross-section of 2 D12 specimen (Dimensions are in mm)
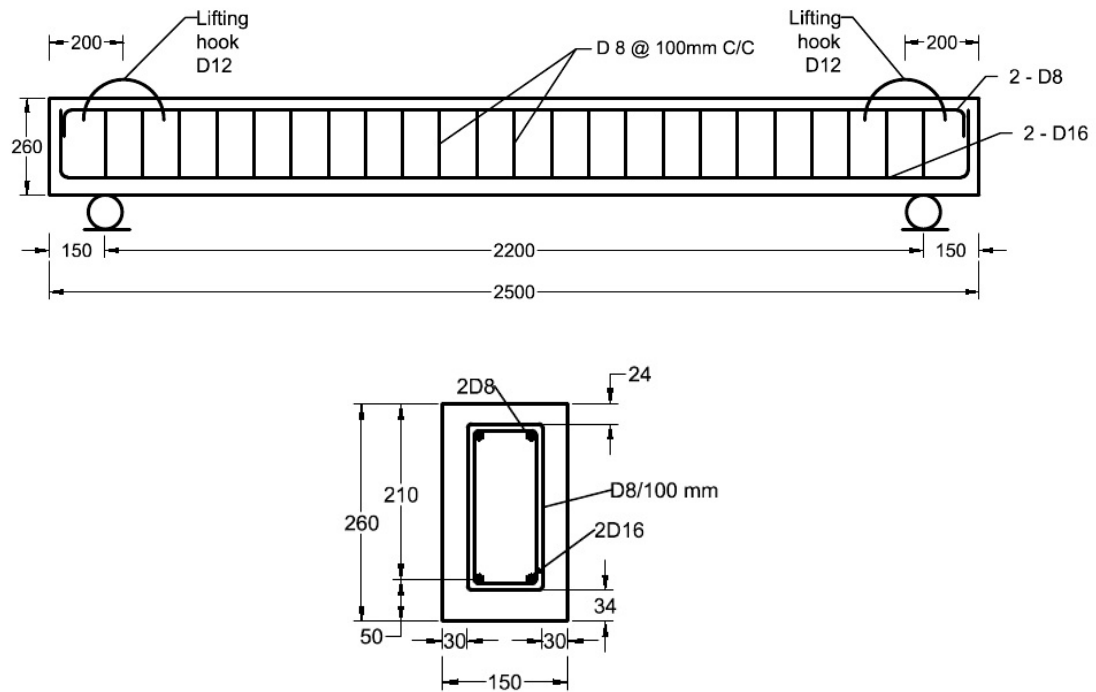
c) Longitudinal and mid span cross-section of 2 D16specimen (Dimensions are in mm)

Figure 11: Longitudinal and mid span cross-section **a)** 2 D10 **b)** 2 D12 **c)** 2 D16

3.2.1 Detailing of strengthened beam specimens

The strengthening technique is applied so that the textiles are sandwiched between the two layers of cementitious mortar. The total thickness of the TRM mortar layer ranged from 10 to 18 mm (10 mm thickness for single layer, 15 mm for double layer and 18 mm for three layers of textile respectively). The details are given in Section 3.6. The longitudinal and a mid-span cross section of a typical TRM strengthened beam specimen is shown in Figure 12. All the dimensions are in mm.
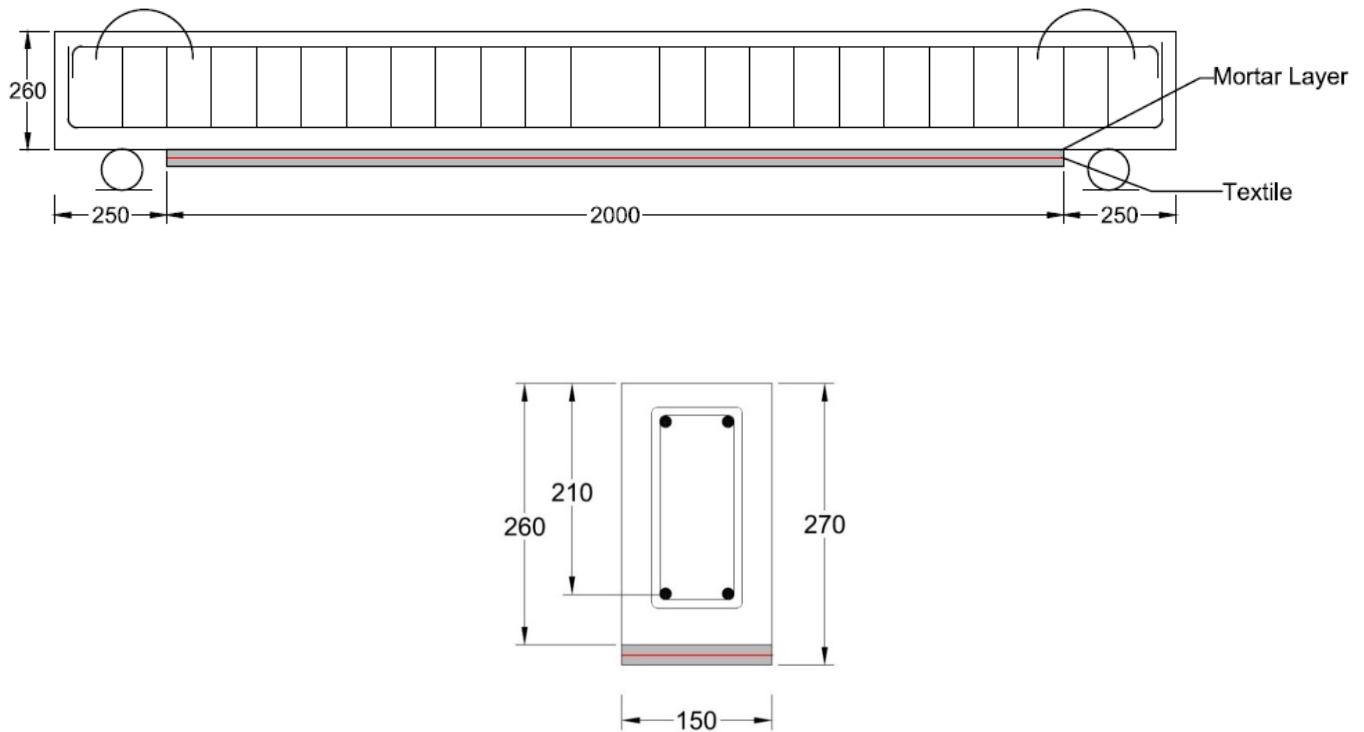
Figure 12: Longitudinal and mid span cross-section of strengthened specimen

3.3 Test matrix

Table 10 shows the test matrix for all the beam specimens.

3.4 Preparation of beam specimens

This section describes the preparation of beam specimens by focusing on each part separately. Further, applying of strengthening technique had also been discussed in this section.

Grinding of the rebar surface

Before casting the beams, the strain gauges were installed on the rebars. In order to install strain gauges on steel rebar, the surface of rebar should be smooth / flat enough so that the strain gauge will have the maximum contact area to the rebar.

Table 10: Test matrix for RC beam specimens

No.	Beam[a]	TRM type	Reinforcement	No. of Layers	ρ_s (%)	$(EA)_f$ (kN/mm)	Strengthening scheme
1	R1	-	2D10	-	0.50	-	-
2	R2	-	2D12	-	0.72	-	-
3	R3	-	2D16	-	1.27	-	-
4	C-R1-V1-F	Carbon	2D10	1	0.50	12.56	Full-length
5	C-R1-V2-F	Carbon	2D10	2	0.50	25.12	Full-length
6	C-R1-V3-F	Carbon	2D10	3	0.50	37.68	Full-length
7	C-R2-V1-F	Carbon	2D12	1	0.72	12.56	Full-length
8	C-R2-V2-F	Carbon	2D12	2	0.72	25.12	Full-length
9	C-R2-V3-F	Carbon	2D12	3	0.72	37.68	Full-length
10	C-R3-V1-F	Carbon	2D16	1	1.27	12.56	Full-length
11	C-R3-V2-F	Carbon	2D16	2	1.27	25.12	Full-length
12	C-R3-V3-F	Carbon	2D16	3	1.27	37.68	Full-length
13	P-R1-V1-F	PBO	2D10	1	0.50	6.4	Full-length
14	P-R2-V1-F	PBO	2D12	1	0.72	6.4	Full-length
15	P-R3-V1-F	PBO	2D16	1	1.27	6.4	Full-length
16	P-R1-V2-F	PBO	2D10	2	0.50	12.8	Full-length
17	P-R2-V2-F	PBO	2D12	2	0.72	12.8	Full-length
18	P-R3-V2-F	PBO	2D16	2	1.27	12.8	Full-length

Note: ρ_s = longitudinal steel reinforcement ratio, $\rho_s = A_s / bd$

[a]C is for Carbon textile, P is for PBO textile, R1 is for D10, R2 is for D12, R3 is for D16, V1 is for 1 layer of textile, V2 is for 2 layers of textile and V3 is for 3 layers of textile.

Now the grinding of the rebar can be done either by sand paper, hand grinder or by using any other technique. HILTI grinder was used for grinding the rebar surfaces (Figure 13).
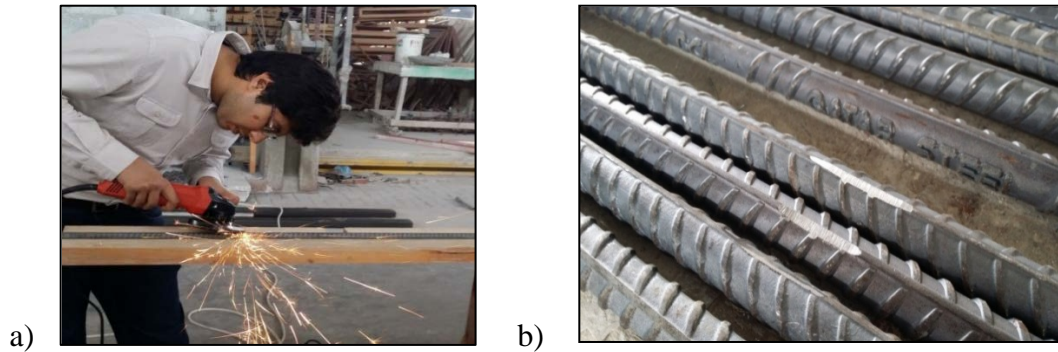
Figure 13: a) Grinding the steel rebars, b) Grinded steel rebars

Fixing / placing of steel rebars

After grinding all the required rebar, they were assembled according to the required design in order to form steel cages (Figure 14).

Figure 14: Steel cages

Installation of strain gauges

Strain gauges were installed in the middle of each bottom bar to measure the strains at mid-span of beams during the test. Two strain gauges were attached to bottom rebars. The insulation tape was wrapped around the strain gauge (Figure 15) in order to protect the strain gauge while casting of concrete.

Figure 15: Fixing of strain gauges

Casting of beam specimens

Finally the steel cages were placed into the wooden formwork (Figure 16) by taking into consideration that the wires of strain gauges were not damaged while placing them in wooden formwork and while during casting of concrete.

Figure 16: Steel reinforcement cages inside the wooden form work

Before casting the beam specimens, wooden formwork was cleaned using compressed air to make sure that there was no dust and the contact surface between the concrete and the formwork was clean. Further, during casting, a vibrator (Figure 17) was used to make proper compaction of concrete and to avoid any air bubbles.
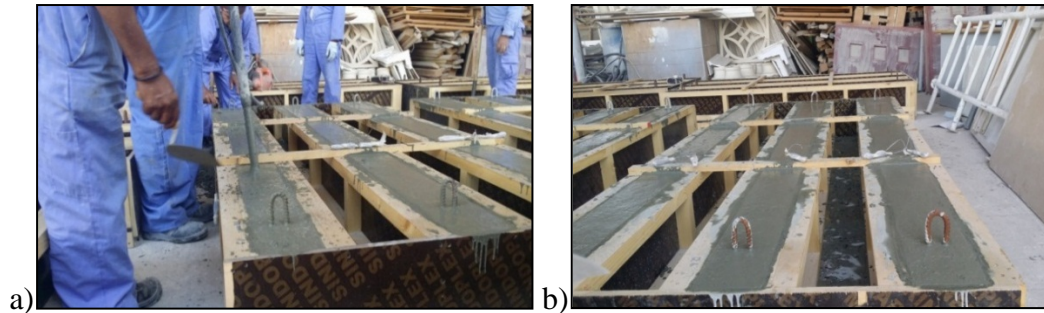
Figure 17: Casting of beams **a)** use of vibrators; **b)** Finishing of concrete

Curing of the specimens

In the process of curing, the concrete is sheltered from loss of moisture and kept in a reasonable temperature range. Gain in strength and decrease in the permeability is the main result of this process. Cracks can be mitigated during the curing process which strictly impacts durability. Open access for harmful materials is allowed by the cracks to avoid the low permeability concrete near the surface.

All the specimens were cured for 28 days after casting stage in order to achieve the required compressive strength of concrete. The beams were covered with hessian cloth and were placed under a shaded area (Figure 18). Water was sprinkled over the specimens twice a day for 28 days. After the curing period, all specimens were kept in shaded area before the test day.

Figure 18: Curing of beam specimens

Concrete substrate abrasion technique adopted in this research

Sand blasting technique was used in this research for the roughening of all the beam specimens. In order to apply the strengthening technique to the soffit of the beam, the bottom surface was roughened to have a good contact between the concrete substrate and the strengthening TRM layer. Figure 19 shows the sand blasted beam specimen.

a) b)
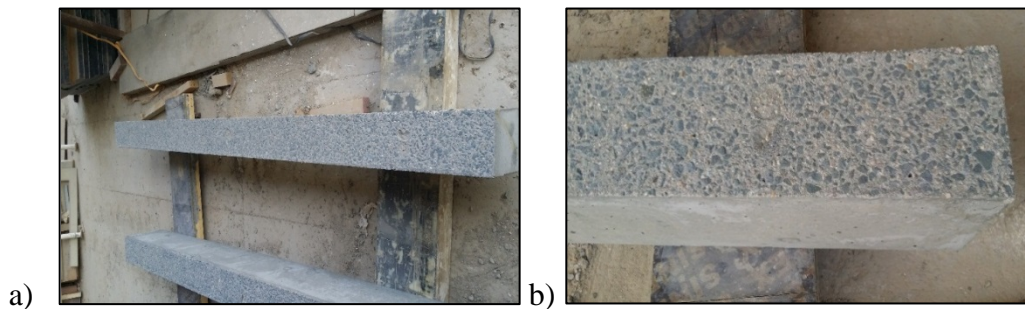
Figure 19: Roughened concrete surfaces a) and b)

3.6 Steps for strengthening of concrete beams

Pre-saturation of beams

Before application of strengthening technique, the contact surface of the beam specimen should be saturated surface dry. For this purpose, the beams were covered with hessian cloth (Figure 20) and water was sprinkled over the beam for at least 40 minutes prior to application of the mortar layer.

Figure 20: Saturating the beam specimens prior of strengthening

Mixing of mortar

Electric mixer (Figure 21) was used to mix the mortar with water according to the specifications given for each mortar type respectively.

Figure 21: Mixing of mortar

Laying of mortar and textile layers

The textile was placed so that it should be sandwiched between the layers of mortar. The first layer of mortar was laid with a thickness of approximately 5mm and the textile was placed over this mortar layer so that it was impregnated (Figure 22) inside the mortar. The second layer of 5 mm thickness was applied over the textile with proper finishing.

For multi-layer TRM specimens, mortar having a thickness of 3 to 4 mm was provided between textile layers (Figure 23, 24).

The final layer of mortar (having the thickness of 2 to 3 mm) was applied with proper finishing (Figure25). Afterwards, the strengthened layer was allowed to cure for 28 days in order to achieve the maximum strength of mortar. Similar technique was used for both the carbon and PBO TRM systems.

47
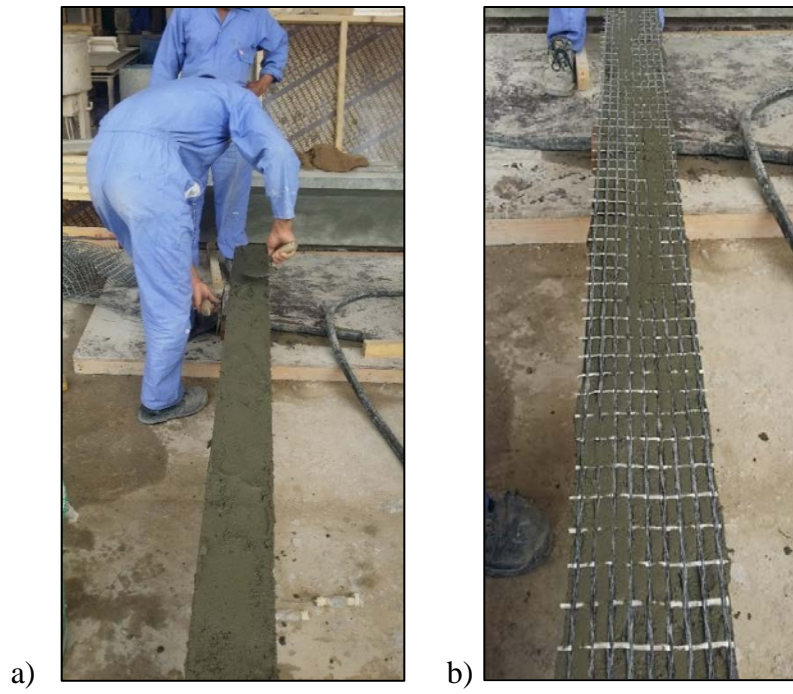
Figure 22: a) Mortar laying over concrete surface and b) First layer of textile over mortar

Figure 23: a) Laying the second layer of mortar and b) Textile over the second mortar layer

a)   b)
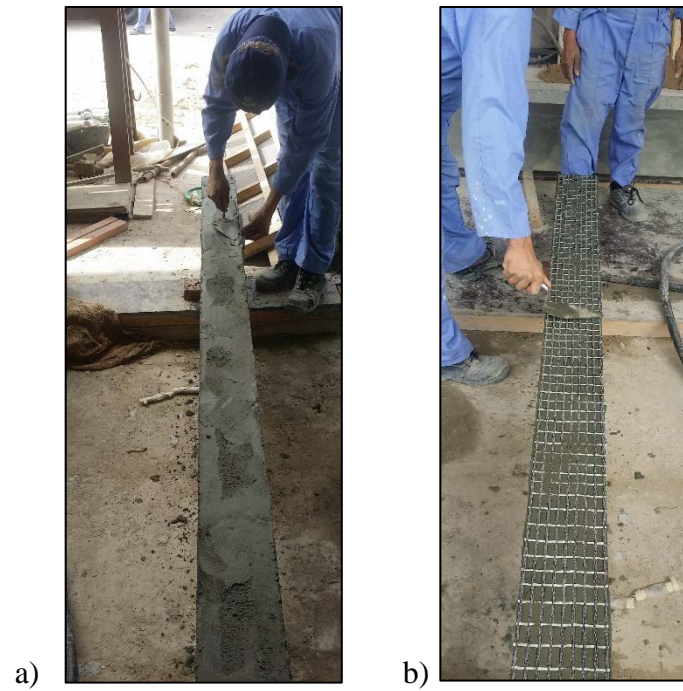
Figure 24: a) Laying the third layer of mortar and b) Textile over the third mortar layer

Figure 25: Final layer of mortar laying and finishing

3.7 Test set-up and instrumentation

The detail of the loading pattern adopted for all the specimens is illustrated in Figure 26. The test was performed under displacement control mode with loading rate of 1 mm / min. Displacement measurements at the mid-span of the specimen were measured using displacement transducers. Two strain gauges (TML FLA-5-11) reading for the rebars were made at the mid-span location. Concrete strain gauge (TML PL-60-11) was attached at the top of the concrete beam mid-span location. The measurements were recorded using a data acquisition system TC-32K data logger with CSW-5B switch-box (Figure 28) at a frequency of 1Hz. The test beam mounted in Instron 1500HDX Static Hydraulic Universal Testing machine along with the displacement transducers and data acquisition system is shown in Figure 29.
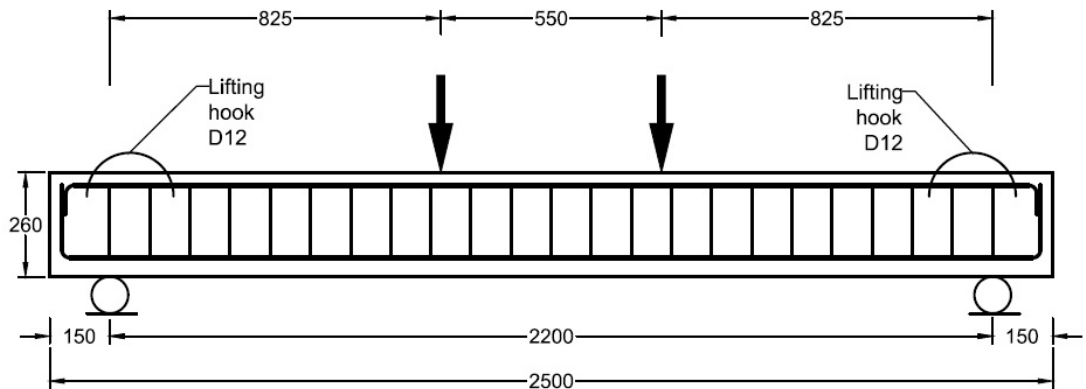
Figure 26: Detail of loading pattern

Figure 27: Instron 1500HDX Static Hydraulic Universal Testing Machine (Front View)
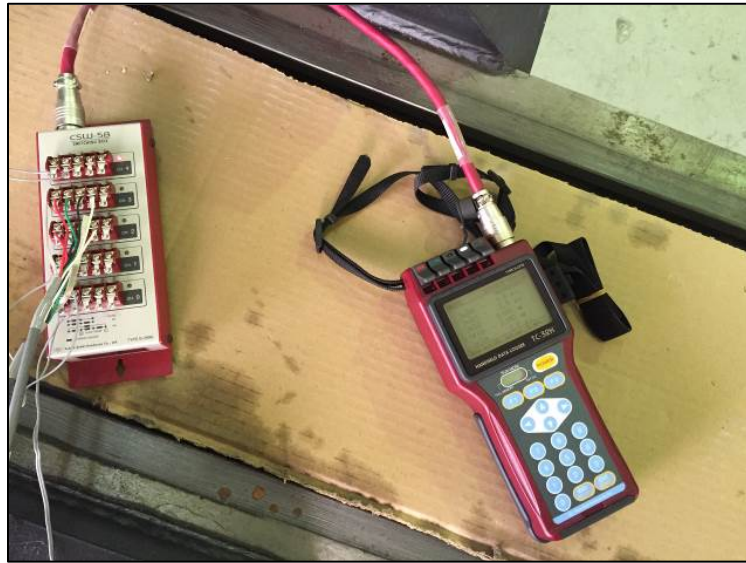
Figure 28: Data acquisition system TC-32K data logger with CSW-5B switch-box
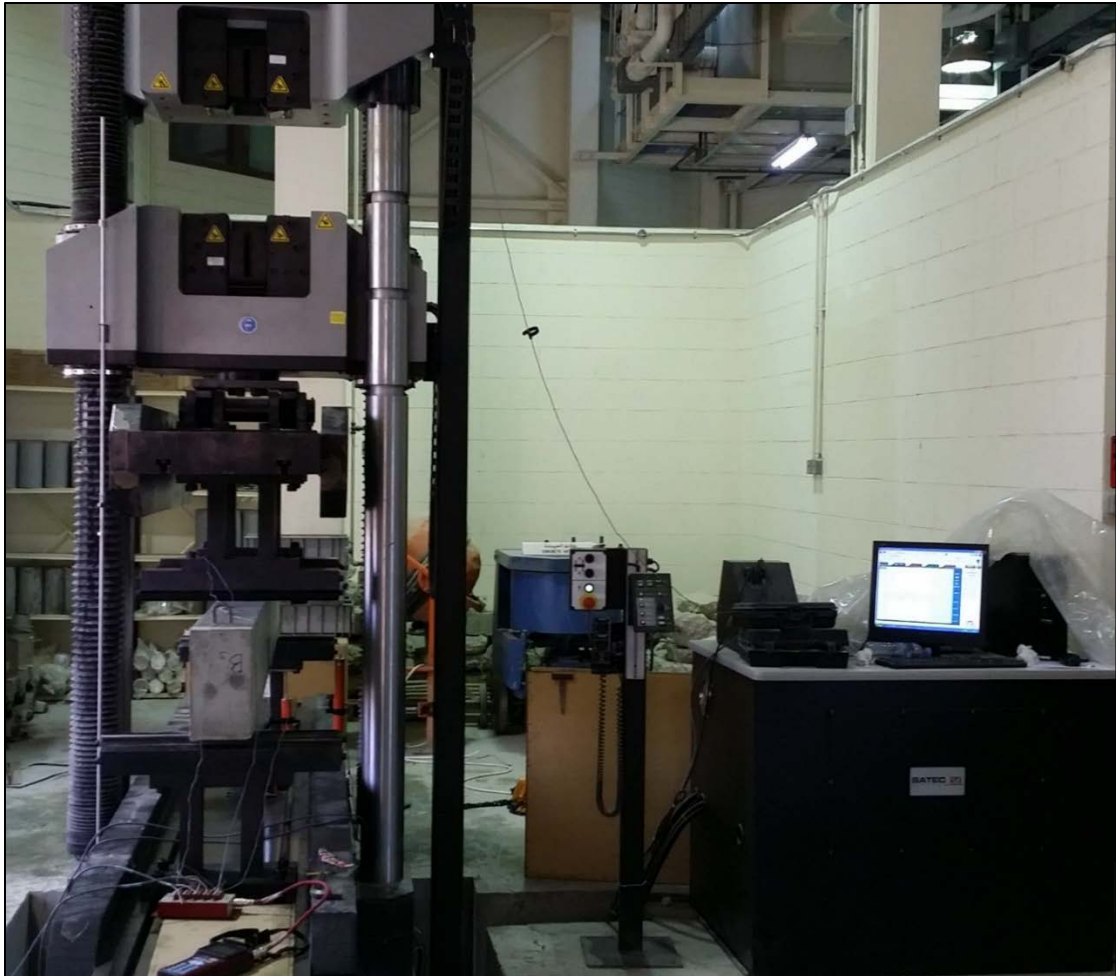
Figure 29: Beam mounted in Instron 1500HDX Static Hydraulic Universal Testing Machine along with the displacement trasnducers and data acquisition system

CHAPTER 4
RESULTS AND DISCUSSIONS

The detailed test results of each specimen are discussed in this chapter. The test results include the graphs of load vs displacement, steel strain and concrete strain respectively. Load values were recorded using the load cell attached to the Instron testing machine. Average of the two steel strain readings recorded for the two bottom rebars have been plotted. The crack pattern and mode of failure of each specimen has also been reported.

Tables 11 and 12 show the summary of all the test results. Column 3 and 4 in Table 11 list the ultimate load carrying capacity (P_u) for each specimen and gain in P_u (in terms of strengthened beams). The yield load values are listed in Column 2 of Table 11. Ductility Index (ΔI) and energy absorption (Ψ) values for all the specimens are shown in Table 12 and their details are given in section 4.17.2 and 4.17.3 respectively. Moreover, the sample calculation to calculate the ductility Index and Energy absorption has also been shown in Appendix C.

The name of the beam specimens were categorized based on the reinforcement ratio and the number of layers of textile; C is for Carbon textile, P is for PBO textile, R1 is for D10, R2 is for D12, R3 is for D16, V1 is for 1 layer of textile, V2 is for 2 layers of textile and V3 is for 3 layers of textile.

Different modes of failure (F+C, F+T+C, F+S+C, F+L+C) were observed while testing the strengthened specimens. F+C is for flexural failure with yielding of steel

rebar having concrete crushing as final mode of failure; F+T+C is for flexural failure associated with textile slippage at the mid span followed by the concrete crushing; F+S+C is flexural failure associated with the TRM separation from concrete substrate and crushing of the concrete and F+L+C is flexural failure associated with cracking within TRM layer as well as slippage of textile followed by the crushing of concrete. Column 5 in Table 11 depicts the mode of failure.

The effects of different studied parameters on these quantities are discussed in later sections. The detailed discussion of the test results, mode of failure and the crack pattern of each specimen is provided in the sections below.

4.1 Control specimens (R1, R2 & R3)

The three control specimens R1, R2 and R3 showed the standard response characteristics of pure flexural failure for under–reinforced beams (Figure 30). They failed in flexure with the yielding of steel rebar through the formation of wide flexural cracks at the mid span with the concrete crushing as the final mode of failure (Figure 31). The tests were stopped at approximately 30-50% reduction in the maximum recorded load. The ultimate loads recorded were 47.90 kN, 69.13 kN and 110.84 kN at a displacement of 36.5 mm, 43.46 mm and 39.51 mm for R1, R2 and R3 specimens respectively.

Table 11: Summary of test results

1	2	3	4	5
Specimen	Yield Load P_y (kN)	Ultimate Load P_u (kN)	Gain in P_u (%)	Mode of failure[a]
R1	41.21	47.895	N.A	F+C
R2	61.54	69.14	N.A	F+C
R3	90.78	110.32	N.A	F+C
C-R1-V1-F	50.12	66.084	37.97	F+T+C
C-R1-V2-F	51.64	72.94	52.29	F+T+C
C-R1-V3-F	59.62	80.40	67.85	F+S+C
C-R2-V1-F	66.18	85.15	23.13	F+T+C
C-R2-V2-F	77.32	89.12	28.90	F+T+C
C-R2-V3-F	70.53	122.71	77.51	F+S+C
C-R3-V1-F	108.15	126.17	14.40	F+T+C
C-R3-V2-F	107.27	142.29	28.97	F+T+C
C-R3-V3-F	112.19	160.36	45.41	F+S+C
P-R1-V1-F	41.25	59.72	24.69	F+L+C
P-R1-V2-F	52.76	79.74	66.49	F+L+C
P-R2-V1-F	62.36	84.68	22.47	F+L+C
P-R2-V2-F	67.91	88.15	27.51	F+L+C
P-R3-V1-F	105.7	117.6	6.60	F+L+C
P-R3-V2-F	101.6	123.86	12.31	F+L+C

[a]F+C is for flexural failure with yielding of steel rebar having concrete crushing as final mode of failure; F+T+C is for flexural failure associated with textile slippage at the mid span followed by concrete crushing; F+S+C is flexural failure associated with the TRM separation from concrete substrate and crushing of the concrete and F+L+C is flexural failure associated with cracking within TRM layer as well as the slippage of textile followed by the crushing of concrete

Table 12: Summary of test results (Continued)

Specimen	δ_Y (mm)	δ_u (mm)	Ductility Index (ΔI)	Energy Absorption Ψ (kN-mm)
1	6	7	8	9
R1	15.03	36.49	2.43	1491.7
R2	7.14	43.46	6.09	2724.9
R3	8.8	39.51	4.49	3692.1
C-R1-V1-F	8.38	20.33	2.43	998.7
C-R1-V2-F	7.74	17.29	2.23	1132
C-R1-V3-F	8.15	24.17	2.97	1485
C-R2-V1-F	8.02	19.33	2.41	1210.7
C-R2-V2-F	11.91	17.97	1.51	1358.8
C-R2-V3-F	7.99	26.33	3.30	1623.8
C-R3-V1-F	10.50	20.93	1.99	1959.3
C-R3-V2-F	10.29	18.81	1.83	2025.4
C-R3-V3-F	10.06	24.53	2.44	2719.5
P-R1-V1-F	6.7	35.14	5.24	1665.1
P-R1-V2-F	5.61	36.52	6.51	2323.2
P-R2-V1-F	8.05	40.45	5.02	2804.2
P-R2-V2-F	8.38	34.56	4.12	2980.1
P-R3-V1-F	10.13	21.54	2.13	2266.5
P-R3-V2-F	10.39	30.15	2.90	2943.2

Figure 30: Load –deflection curve for control specimens R1, R2 and R3
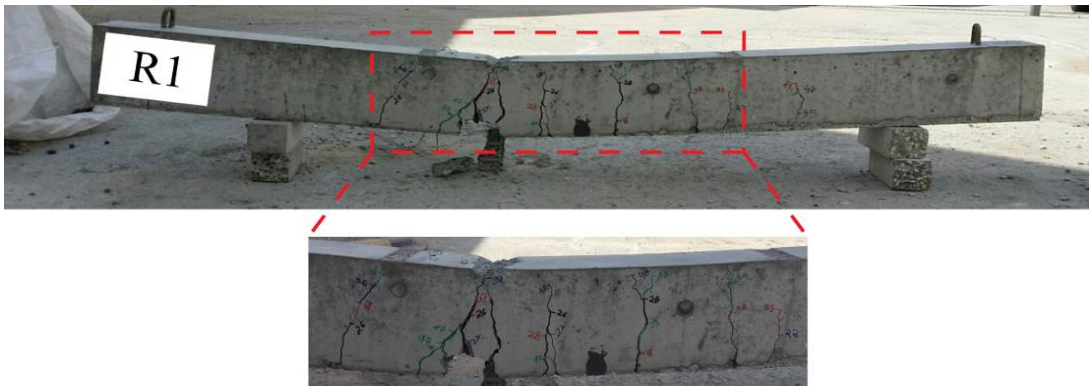
(a) Control specimen R1(Values shown are in kN)
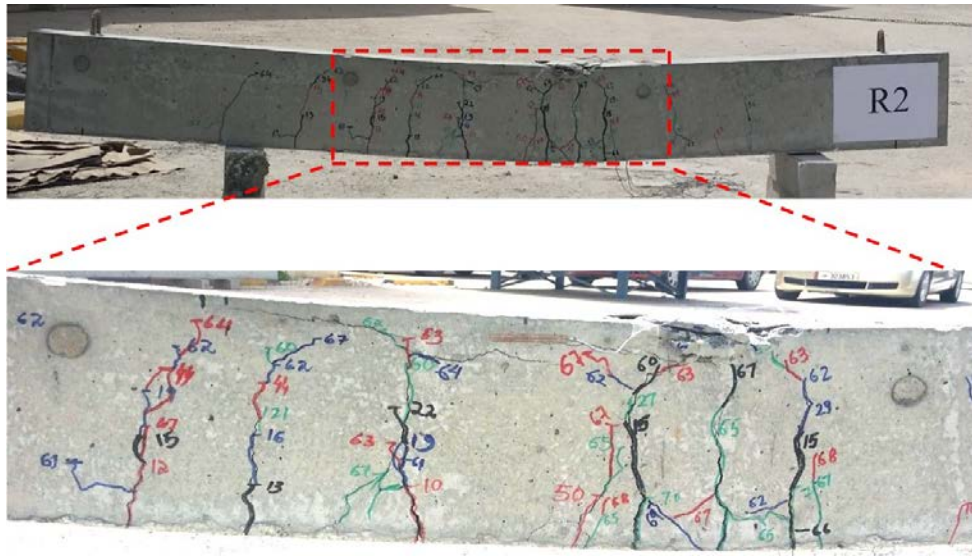
(b) Control specimen R2 (Values shown are in kN)
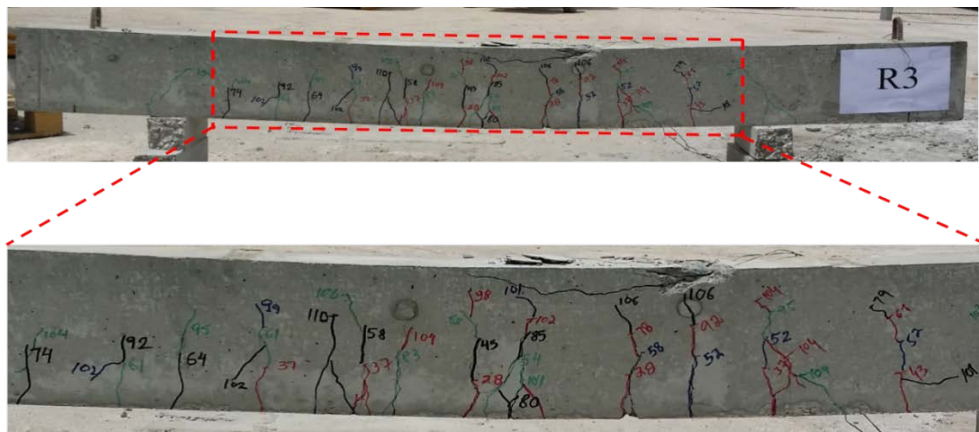
(c) Control specimen R3 (Values shown are in kN)

Figure 31: Modes of failure and crack patterns for control beam specimens R1, R2 and R3

4.2 Specimen C-R1-V1-F

C-R1-V1-F beam specimen used 2D10 as the main longitudinal reinforcement and was strengthened with carbon TRM system using one layer of carbon textile $(EA)_c^1 = 12.56 \ kN/mm$. The load-displacement relationship, along with its associated control specimen is shown in Figure 32-a while load versus steel and concrete strains are

shown in Figure 32- b and 32-c respectively. The first crack appeared in the middle of the specimen at 21kN and then the cracks spread evenly at both sides (Figure 33). The steel reinforcement started to yield at around 0.24% strain as shown in Figure 32-b. The corresponding yield flexural load for this beam was 50.12kN. The ultimate load recorded for the beam was 66.08kN and the load dropped afterwards. The mode of failure observed in this specimen was flexural failure associated with textile rupture at the mid span as well as concrete crushing (F+T+C). The gain in ultimate load was 37.97 % with respect to the control specimen. Slippage and breaking of steel strain gauge occurred after initiation of rebar yielding.

Figure 32: Test results for specimen C-R1-V1-F a) load vs displacement; b) load vs steel strain and c) load vs concrete strain

Figure 33: Mode of failure and crack patterns for test beam C-R1-V1-F (Values are in kN)

4.3 Specimen C-R1-V2-F

C-R1-V2-F beam specimen used 2D10 as the main longitudinal reinforcement and was strengthened with carbon TRM system using two layers of carbon textile $(EA)_c^2 = 25.12 \, kN/mm$. The load-displacement relationship, along with its associated control specimen is shown in Figure 34-a while load versus steel and concrete strains are shown in Figure 34- b and 34-c respectively. The beam reached yield at 51.64 kN and the displacement recorded at the yield load was 7.74 mm. The ultimate load recorded was 72.94 kN and then the load dropped suddenly afterwards. The gain in the ultimate load was 52.29% with respect to the control specimen. The observed mode of failure was the flexural failure associated with textile rupture at the mid span as well as concrete crushing (F+T+C) as shown in Figure 35.

Figure 34: Test results for specimen C-R1-V2-F a) load vs displacement; b) load vs steel strain and c) load vs concrete strain

Figure 35: Mode of failure and crack patterns for test beam C-R1-V2-F (Values are in kN)

4.4 Specimen C-R1-V3-F

C-R1-V3-F beam specimen used 2D10 as the main longitudinal reinforcement and was strengthened with carbon TRM system using two layers of carbon textile $(EA)_c^3 = 37.68 \, kN/mm$. The load-displacement relationship, along with its associated control specimen is shown in Figure 36-a while load versus steel and concrete strains are shown in Figure 36- b and 36-c respectively. The yield and ultimate load recorded were 59.62kN and 80.39kN respectively. Load dropped twice prior to reaching the ultimate load. The first load-drop occurred due to formation of cracks within the TRM layer and the second drop of the load was due to the initiation of slip between the TRM layer and the concrete substrate. The observed mode of failure was the flexural failure associated with the TRM slippage from concrete substrate (F+S+C) up to the support on the right side of the beam specimen (Figure 37) and was followed by concrete crushing. The gain in the ultimate capacity was 67.85% to that of the control specimen. Slippage and breaking of steel strain gauge occurred after initiation of rebar yielding. The concrete was crushed prior to reaching the maximum concrete strain value.

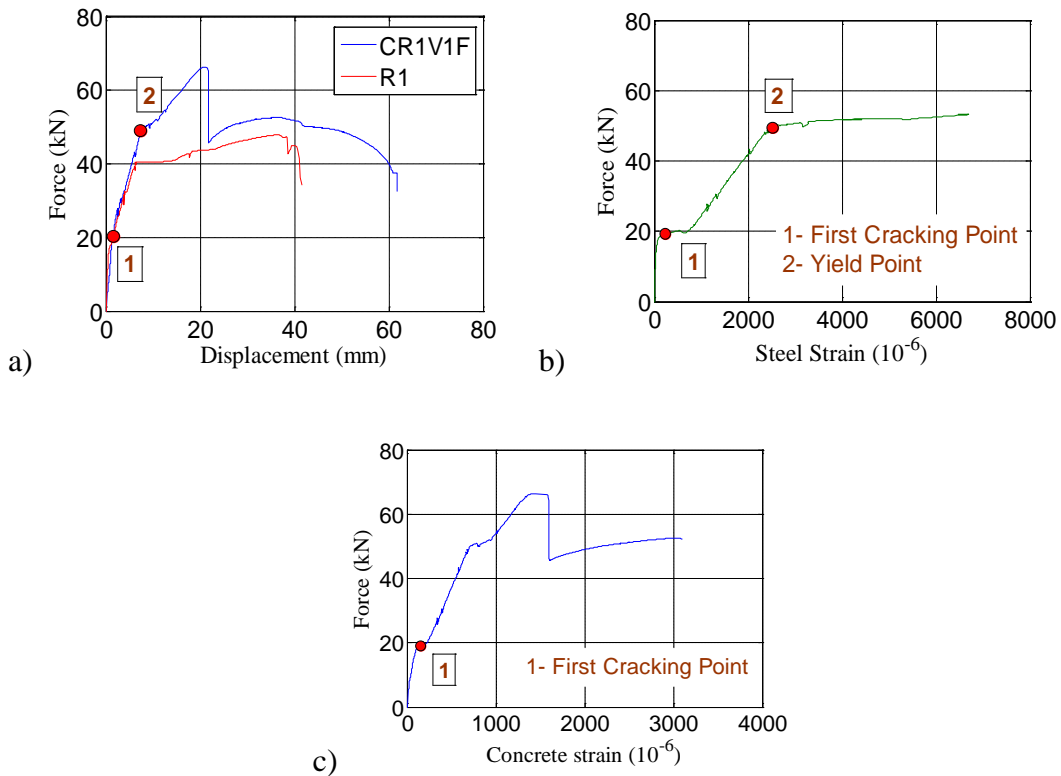a)   b)

c)

Figure 36: Test results for specimen C-R1-V3-F a) load vs displacement; b) load vs steel strain and c) load vs concrete strain
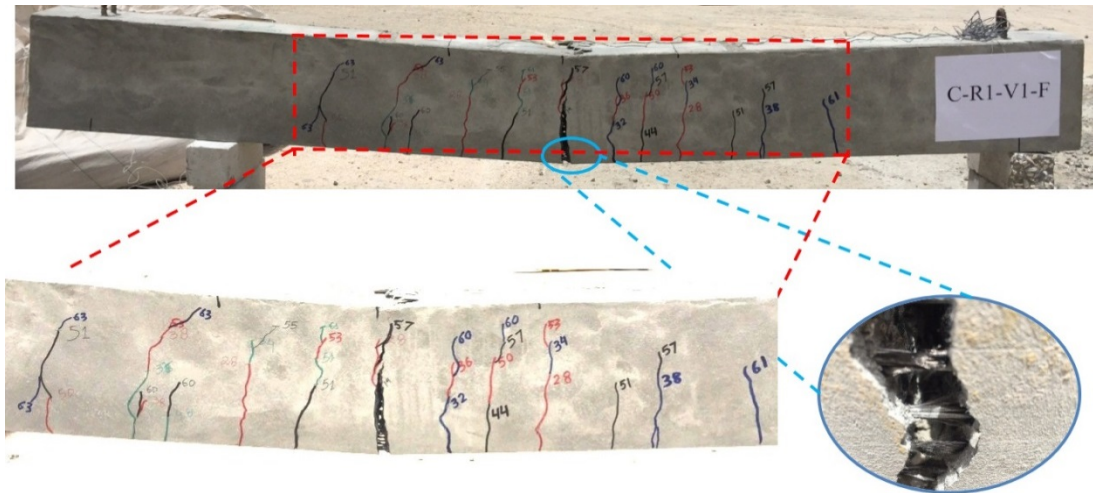

Figure 37: Mode of failure and crack patterns for test beam C-R1-V3-F (Values are in kN)

4.5 Specimen C-R2-V1-F

C-R2-V1-F specimen having the main longitudinal reinforcement of D12 was strengthened with single layer of carbon TRM system $(EA)_c^1 = 12.56 \; kN/mm$. Load

versus mid span deflection curve is shown in Figure 38-a along with the control specimen R2. Steel and concrete strain relationship with the applied load are shown in Figure 38-b and 38-c respectively. The first crack occurred at 24kN and then the cracks spread equally at both sides (Figure 39). The beam reached yield at 66.18kN. However, at maximum load of 85.15kN, the beam failed due to the flexural failure associated with textile rupture at the mid span as well as concrete crushing (F+T+C). The gain in the ultimate load was 23.13% with respect to its control specimen. At failure, the flexural capacity dropped down suddenly followed by concrete crushing.
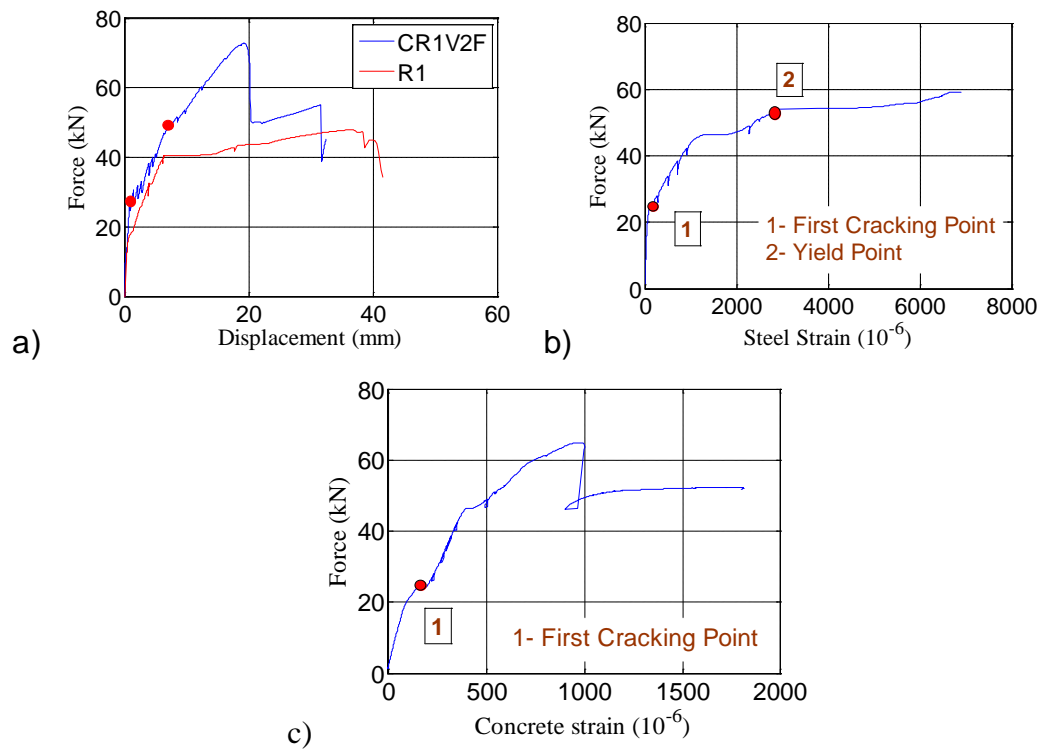

Figure 38: Test results for specimen C-R2-V1-F a) load vs displacement; b) load vs steel strain and c) load vs concrete strain

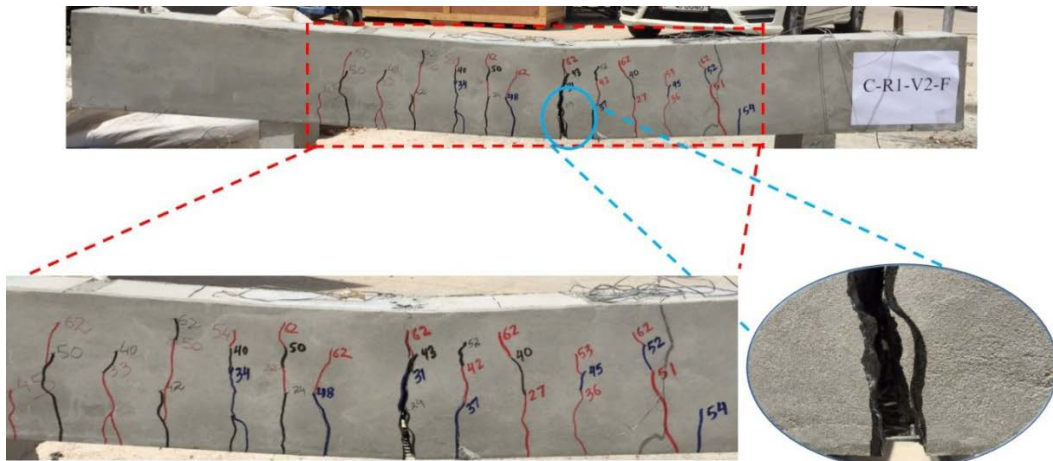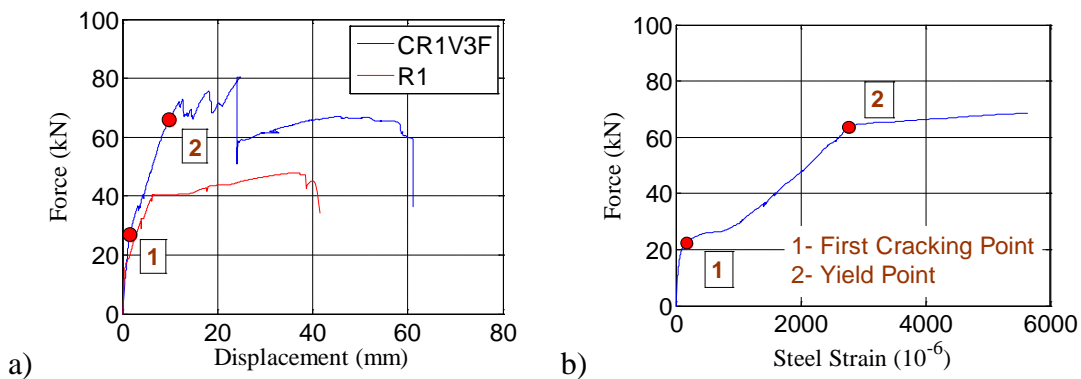Figure 39: Mode of failure and crack patterns for test beam C-R2-V1-F

4.6 Specimen C-R2-V2-F

C-R2-V2-F beam specimen used 2D12 as the main longitudinal reinforcement and was strengthened with carbon TRM system using two layers of carbon textile $(EA)_c^2 = 25.12 \ kN/mm$. The load-displacement relationship, along with its associated control specimen is shown in Figure 40-a while load versus steel and concrete strains are shown in Figure 40- b and 40-c respectively. The first crack appeared at 31kN near the mid span (Figure 41) and then the cracks spread at both sides of the beam. The mode of failure observed was the flexural failure associated with textile rupture at the mid span followed by the concrete crushing (F+T+C). The yield and ultimate load recorded were 77.3 kN and 89.12 kN respectively. The gain in the ultimate load was 28.90 % of that of the control specimen R2.
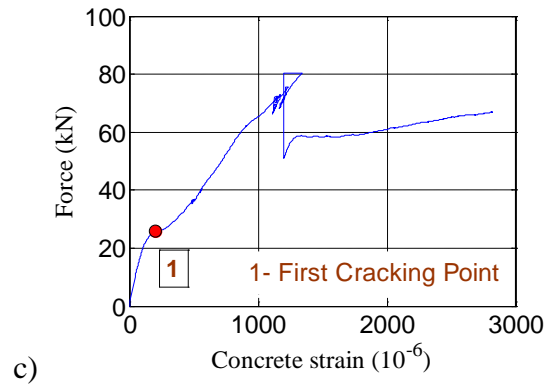
Figure 40: Test results for specimen C-R2-V2-F a) load vs displacement; b) load vs steel strain and c) load vs concrete strain

Figure 41: Mode of failure and crack patterns for test beam C-R2-V2-F (Values are in kN)

4.7 Specimen C-R2-V3-F

C-R2-V3-F specimen having the main longitudinal reinforcement of D12 was strengthened with three layers of carbon TRM system $(EA)_c^3 = 37.68 \, kN/mm$. Load versus mid span deflection curve is shown in Figure 42-a along with the control specimen R2. Steel and concrete strain relationship with the applied load are shown in Figure 42-b and 42-c respectively. Before reaching the ultimate value, load dropped due to the formation of cracks within the TRM layer and the initiation of slippage between the TRM layer and the concrete substrate. After failure, the load dropped suddenly due to the complete slippage between the TRM and concrete substrate. So, the observed mode of failure was the flexural failure associated with the TRM slippage from concrete substrate and crushing of the concrete (F+S+C). Wide flexural cracks occurred from TRM substrate towards the point of application of load on the left side of the beam specimen (Figure 43). The test was stopped for safety as the deflection of the beam was more than 60mm. The ultimate load value was increased to 122.71kN and the yield value was also increased to 70.53kN. The increase in the ultimate load was 77.51% with respect to the control specimen R2. Also, the steel strain gauge slips at higher load, so the yield load value had not been captured by the strain gauge.
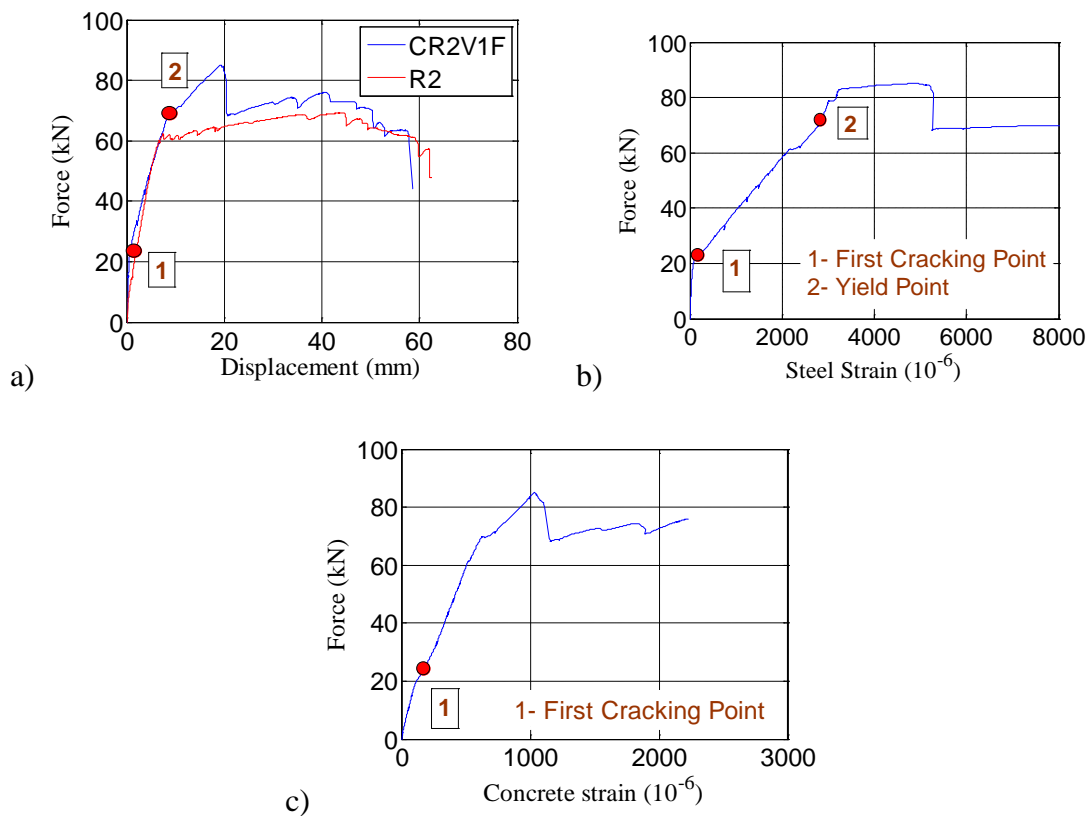
Figure 42: Test results for specimen C-R2-V3-F a) load vs displacement; b) load vs steel strain and c) load vs concrete strain
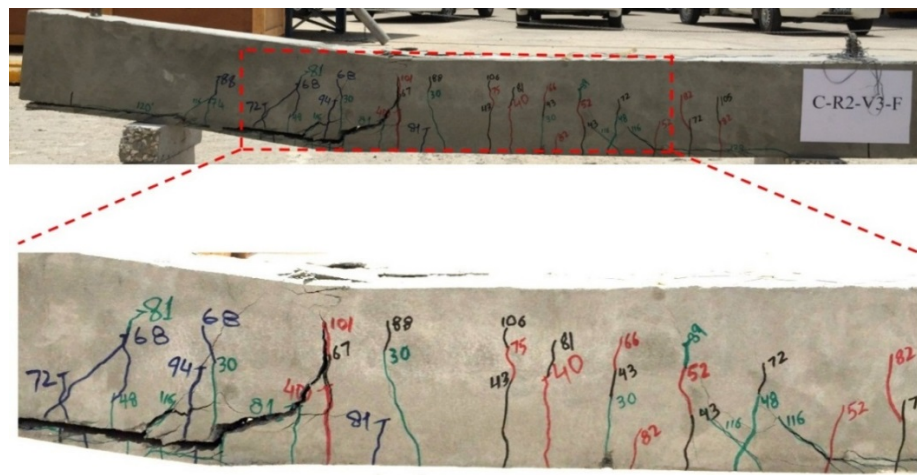
Figure 43: Mode of failure and crack patterns for test beam C-R2-V3-F (Values are in kN)

4.8 Specimen C-R3-V1-F

C-R3-V1-F beam specimen used 2 D16 as the main longitudinal reinforcement and was strengthened with carbon TRM system using one layer of carbon textile $(EA)_c^1 = 12.56 \, kN/mm$. The load-displacement relationship, along with its associated control specimen is shown in Figure 44-a while load versus steel and concrete strains are shown in Figure 44- b and 44-c respectively. The first crack appeared at 33kN in the middle of the specimen. At ultimate load, the load drops suddenly due to the rupture of textile at the mid span. The observed mode of failure was the flexural failure associated with textile rupture at the mid span (F+T+C) followed by the crushing of concrete (Figure45). The respective yield and ultimate load values were 108.15kN and 126.17kN. The gain in the ultimate load was 14.40% of the control specimen R3.

a)   b)

69

Figure 44: Test results for specimen C-R3-V1-F a) load vs displacement; b) load vs steel strain and c) load vs concrete strain
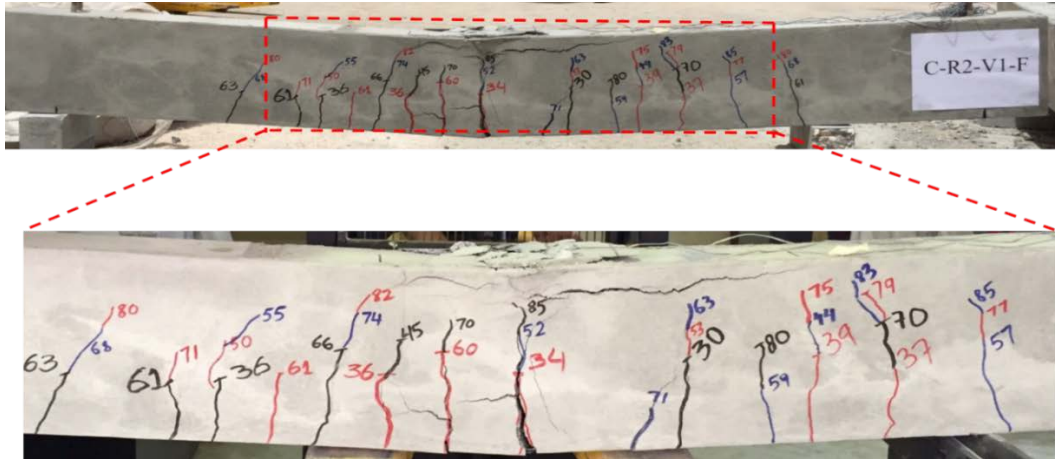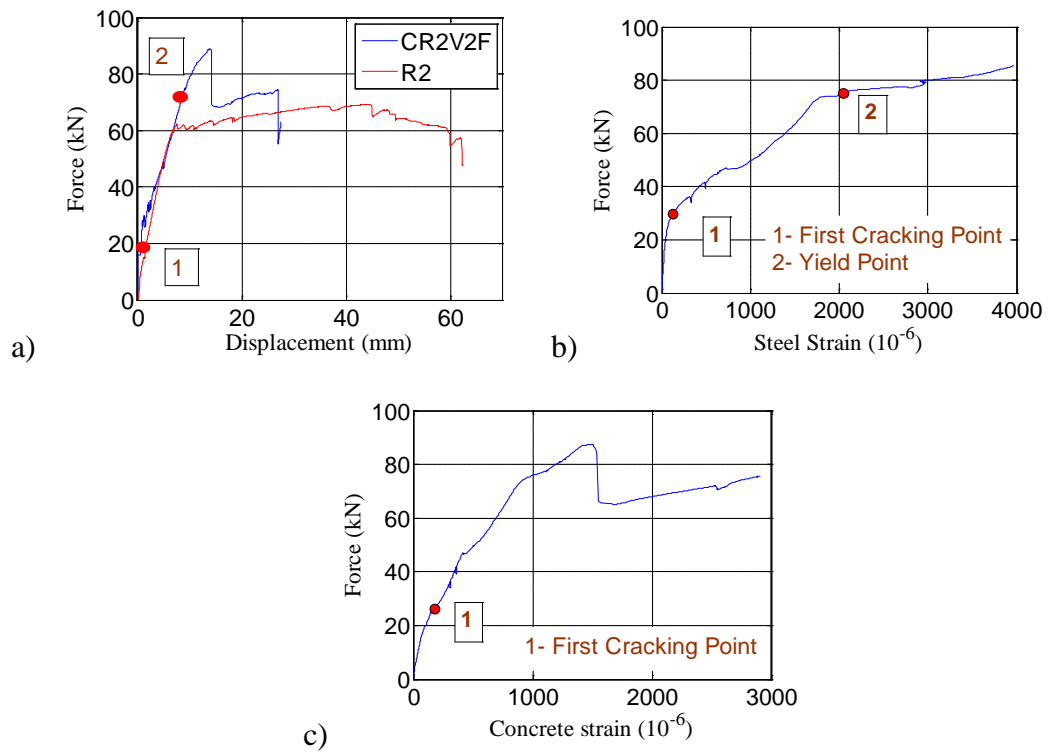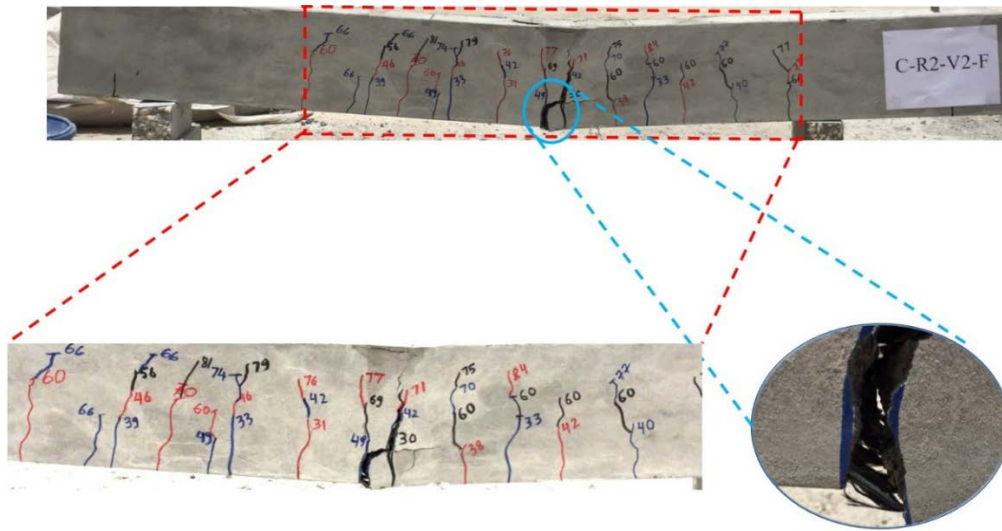

Figure 45: Mode of failure and crack patterns for test beam C-R3-V1-F (Values are in kN)

4.9 Specimen C-R3-V2-F

C-R3-V2-F specimen having the main longitudinal reinforcement of D16 was strengthened with two layers of carbon TRM system $(EA)_c^2 = 25.12 \ kN/mm$. Load versus mid span deflection curve is shown in Figure 46-a along with the control

specimen R3. Steel and concrete strain relationship with the applied load are shown in Figure 46-b and 46-c respectively. The first crack appeared at 32kN in the middle of the beam specimen. The respective yield and ultimate load values were 107.27kN and 142.29kN respectively. The gain in the ultimate load was 28.97% with respect to the control specimen R3. At ultimate load, the load dropped suddenly due to textile slippage and the mode of the failure observed was the flexural failure associated with textile rupture at the mid span as well as concrete crushing (F+T+C) at the top of the beam specimen (Figure 47).
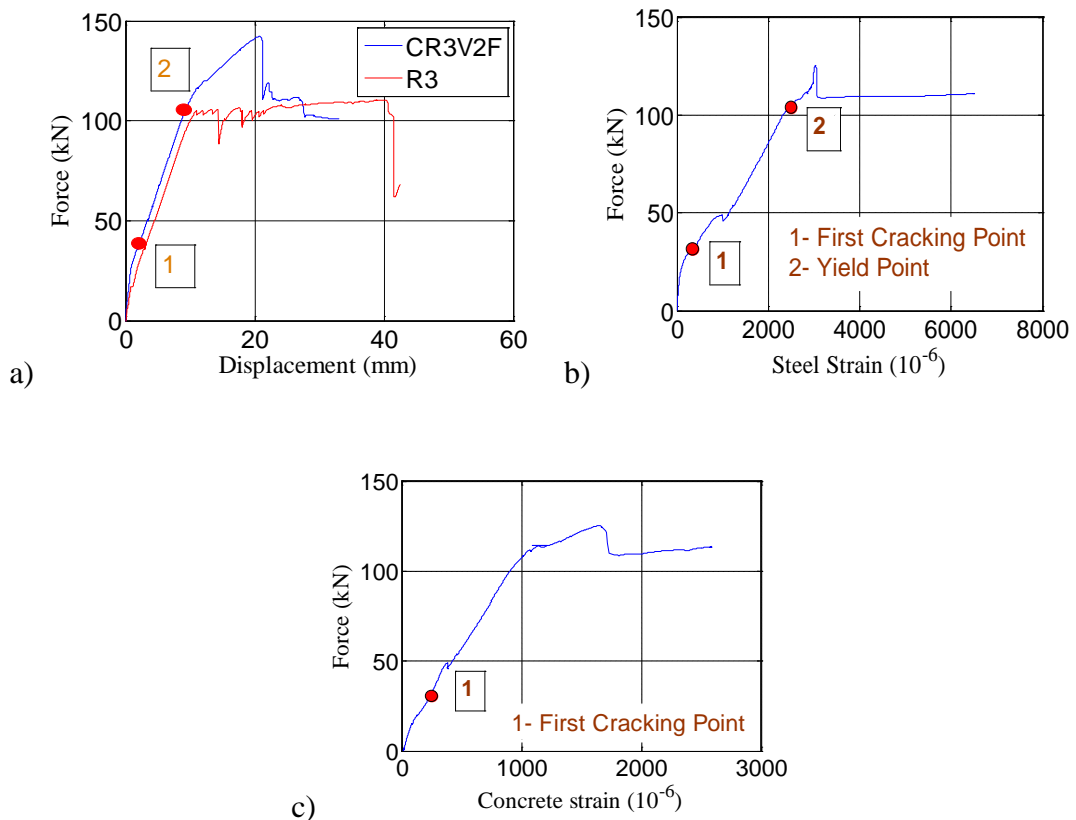
Figure 46: Test results for specimen C-R3-V2-F a) load vs displacement; b) load vs steel strain and c) load vs concrete strain

View from top

View from bottom

Figure 47: Mode of failure and crack patterns for test beam C-R3-V2-F (Values are in kN)

4.10 Specimen C-R3-V3-F

C-R3-V3-F beam specimen used 2 D16 as the main longitudinal reinforcement and was strengthened with carbon TRM system using three layers of carbon textile $(EA)_c^3 = 37.68 \, kN/mm$. The load-displacement relationship, along with its associated control specimen is shown in Figure 48-a while load versus steel and concrete strains are shown in Figure 48- b and 48-c respectively. With three layers of carbon textile, a remarkable increase in the ultimate and yield load was observed. The yield and ultimate load values were 112.19 kN and 160.36 kN respectively. The gain in the ultimate load was 45.41% of control specimen R3. Even after the ultimate load value, there was no sudden drop in the load value. Slippage occurred between TRM layer (Figure 48) and concrete substrate on the left side of beam specimen at higher deformation levels, which was the final mode of failure followed by the concrete crushing (F+S+C). The test was stopped for safety as the deflection had gone beyond 60 mm.
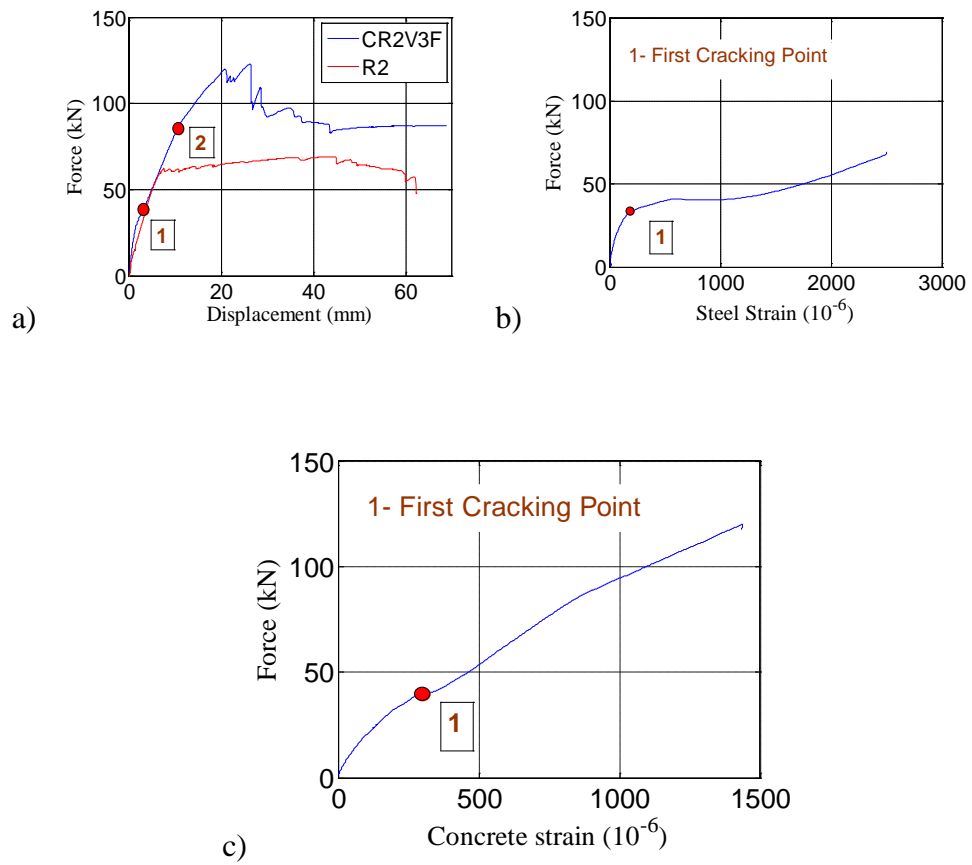
Figure 48: Test results for specimen C-R3-V3-F a) load vs displacement; b) load vs steel strain and c) load vs concrete strain
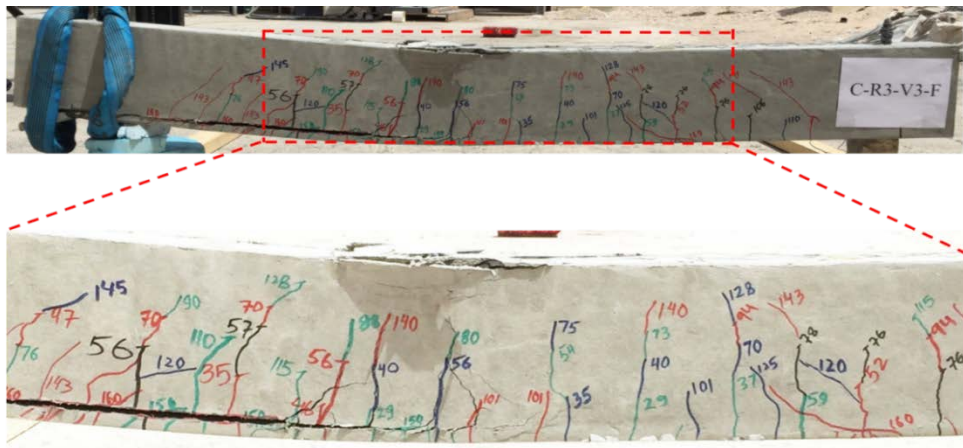
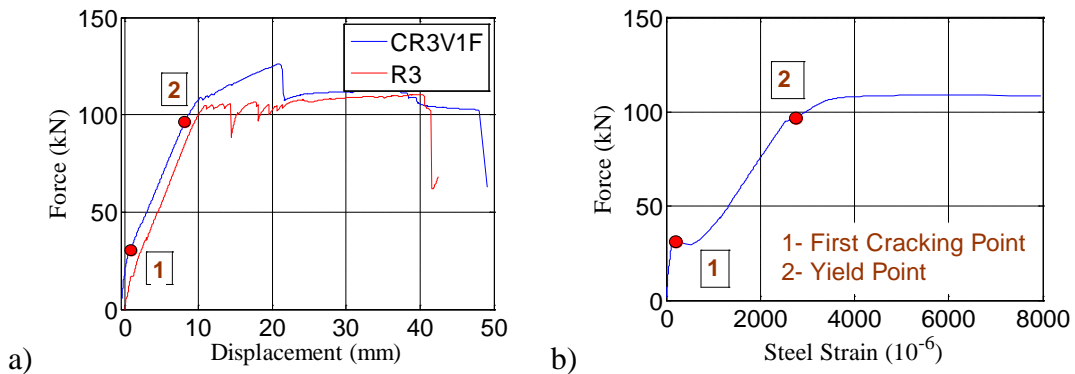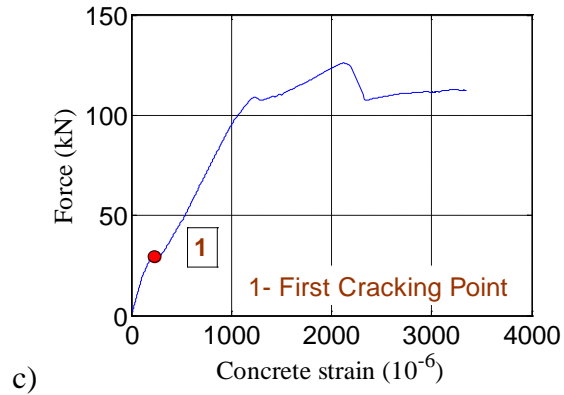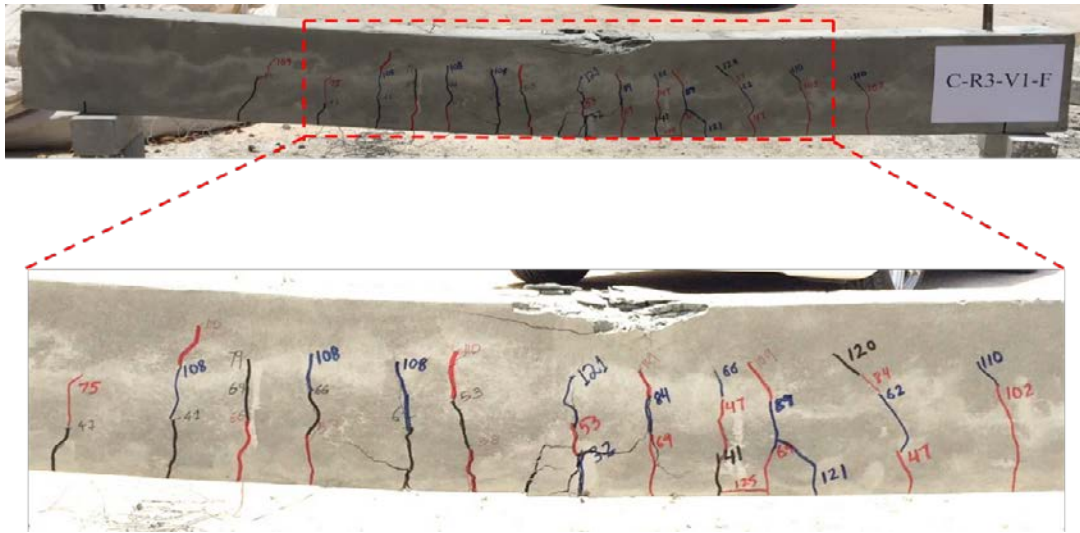Figure 49: Mode of failure and crack patterns for test beam C-R3-V3-F (Values are in kN)

4.11 Specimen P-R1-V1-F

P-R1-V1-F specimen having the main longitudinal reinforcement of D10 was strengthened with one layer of PBO TRM system $(EA)^1_{PBO} = 6.4 \, kN/mm$. Load versus mid span deflection curve is shown in Figure 50-a along with the control specimen R1. Concrete strain relationship with the applied load is shown in Figure 50-b.Steel strain gauges were not working in this specimen due to the slippage of strain gauges from steel rebars while applying the vibrator during casting of concrete. The ultimate load recorded was 59.72 kN at a displacement of 35.14 mm and then the load dropped suddenly. The gain in the ultimate load capacity was 24.7% of control specimen R1. After this sudden drop, the load tends to increase as well, but could not reach to the maximum value and then decreased gradually until the textile ruptured which was the final mode of the failure (Figure 51). At a load of 52 kN, the cracks started to appear within the mortar layer, but it did not go towards the bond failure.
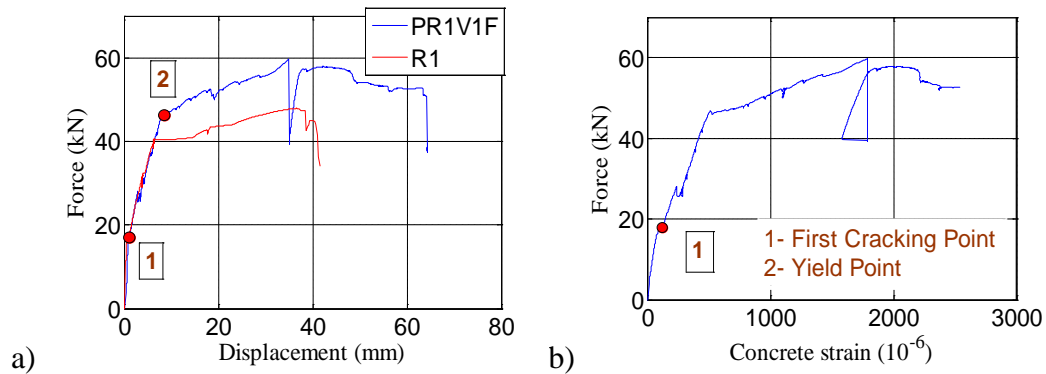
Figure 50: Test results for specimen P-R1-V1-F a) load vs displacement and b) load vs concrete strain

View from bottom

Figure 51: Mode of failure and crack patterns for test beam P-R1-V1-F (Values are in kN)

4.12 Specimen P-R1-V2-F

P-R1-V2-F beam specimen used 2 D10 as the main longitudinal reinforcement and was strengthened with PBO TRM system using two layers of PBO textile $(EA)^2_{PBO} = 12.8\ kN/mm$. The load-displacement relationship, along with its associated control specimen is shown in Figure 52-a while load versus steel and concrete strains are shown in Figure 52- b and 52-c respectively. The first crack appeared at 28kN just in the middle of the specimen. The beam reached the yield at 52.76kN while the slippage of steel strain occurred at higher loads. The ultimate load recorded was 79.74kN and the gain in the ultimate load capacity was 66.5% with respect to the control specimen R1. At 64kN cracks tend to appear within the mortar layer and at 79kN, the bond slippage occurred between the concrete substrate and mortar layer (Figure 53). A wider crack appeared near to the center of the beam leading towards the failure of mortar layer. The observed mode of failure was the flexural failure

associated with cracking within TRM layer followed by the crushing of concrete (F+L+C).

Figure 52: Test results for specimen P-R1-V2-F a) load vs displacement; b) load vs steel strain and c) load vs concrete strain

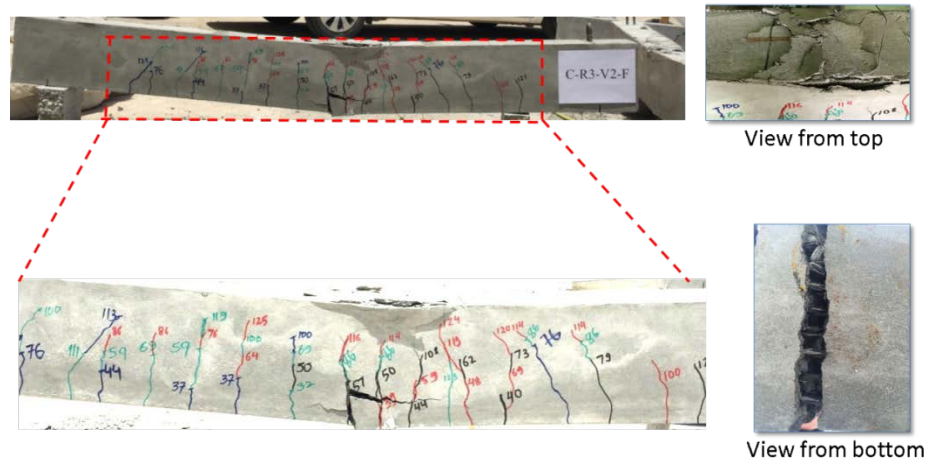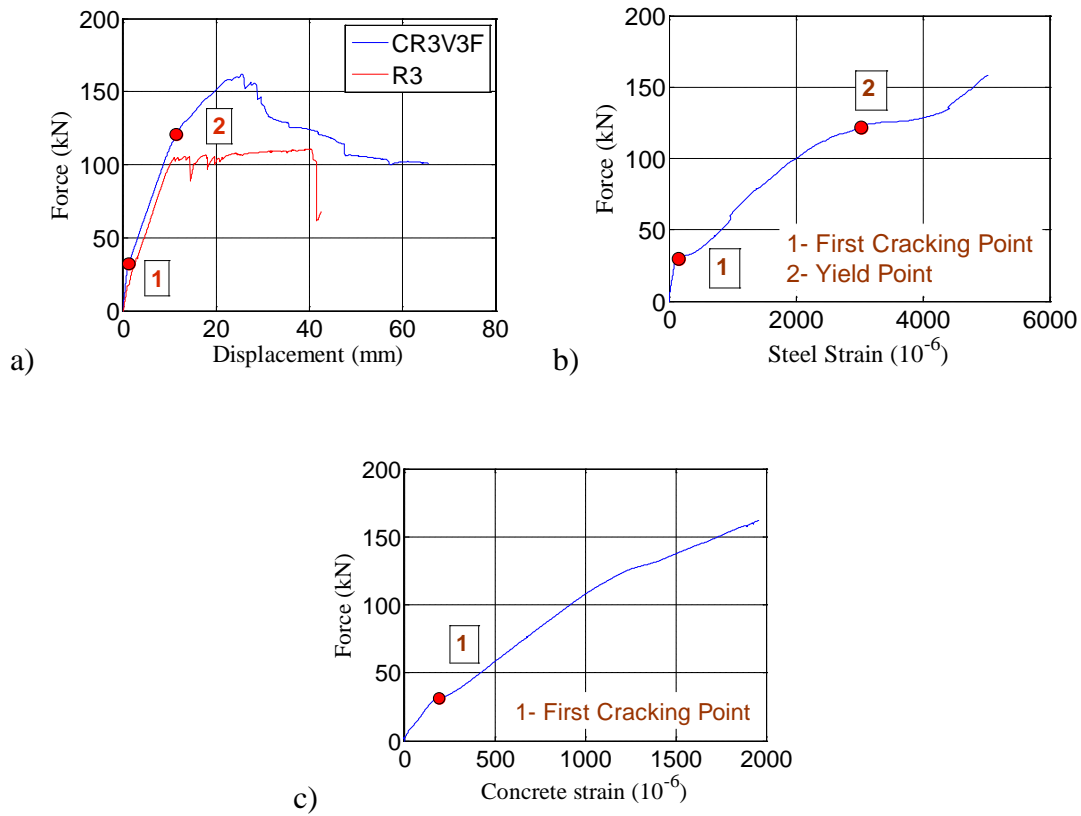Figure 53: Mode of failure and crack patterns for test beam PR1V2F (Values are in kN)

4.13 Specimen P-R2-V1-F

P-R2-V1-F specimen having the main longitudinal reinforcement of D12 was strengthened with one layer of PBO TRM system $(EA)^1_{PBO} = 6.4\ kN/mm$. Load versus mid span deflection curve is shown in Figure 54-a along with the control specimen R2. Steel and concrete strain relationship with the applied load are shown in Figure 54-b and 54-c respectively. The load in this specimen also dropped down suddenly at the displacement of 40.45 mm after reaching its ultimate load value of 84.68 kN. The gain in the ultimate load was 22.47% of the control specimen R2. The yield load recorded was 62.357 kN at a displacement of 8.05 mm. After the first drop the load increased suddenly as well and at 77 kN, the cracks were appearing within the mortar layer (Figure 55). The final mode of failure was due to flexural failure associated with cracking within TRM layer followed by the crushing of concrete (F+L+C).

a)   b)

c)
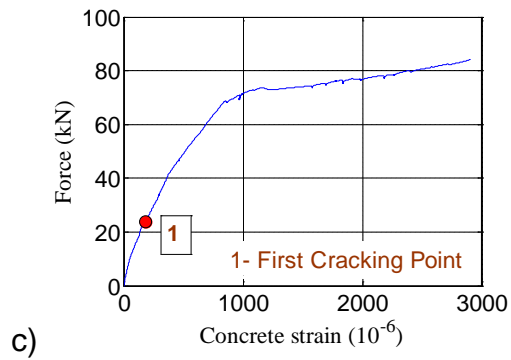
Figure 54: Test results for specimen P-R2-V1-F a) load vs displacement; b) load vs steel strain and c) load vs concrete strain

View from bottom
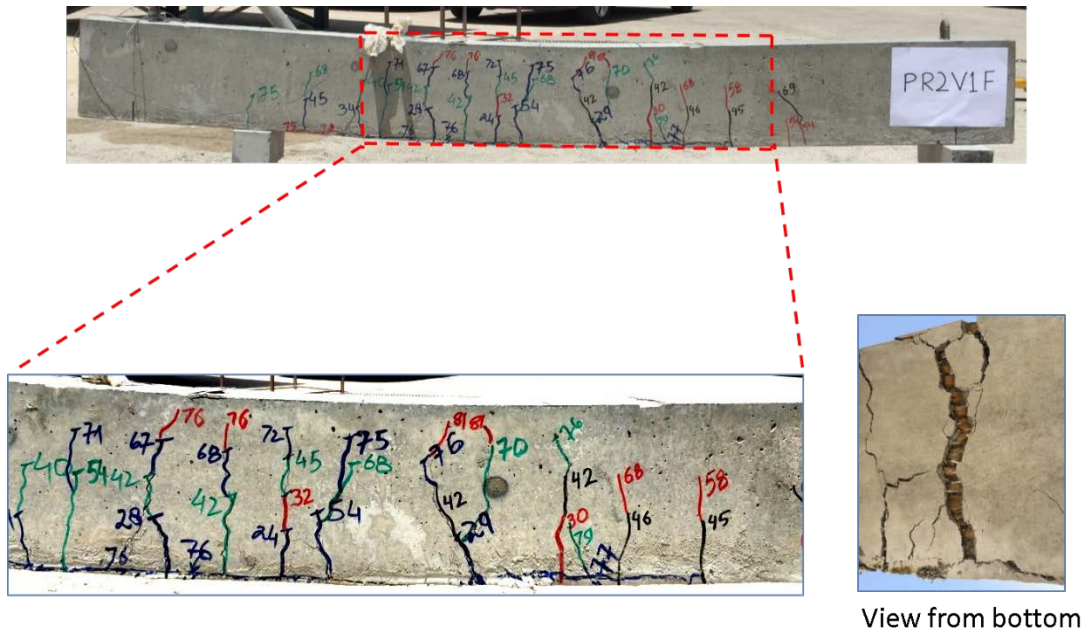
Figure 55: Mode of failure and crack patterns for test beam P-R2-V1-F (Values are in kN)

4.14 Specimen P-R2-V2-F

P-R2-V2-F beam specimen used 2 D12 as the main longitudinal reinforcement and was strengthened with PBO TRM system using two layers of PBO textile $(EA)^2_{PBO} = 12.8 \, kN/mm$. The load-displacement relationship, along with its associated control

78

specimen is shown in Figure 56-a while load versus steel and concrete strains are shown in Figure 56- b and 56-c respectively. The first crack appeared at 22 kN (Figure 57). The ultimate and yield load recorded were 88.15 kN and 67.91 kN respectively. The gain in the ultimate load capacity was 27.51% of the control specimen R2. Prior to reach the ultimate load value, the load dropped once due to the failure of first textile layer and as a result of the major cracks within the mortar layer followed by the concrete crushing (F+L+C). The test was stopped due to the safety as the deflection was more than 60 mm.
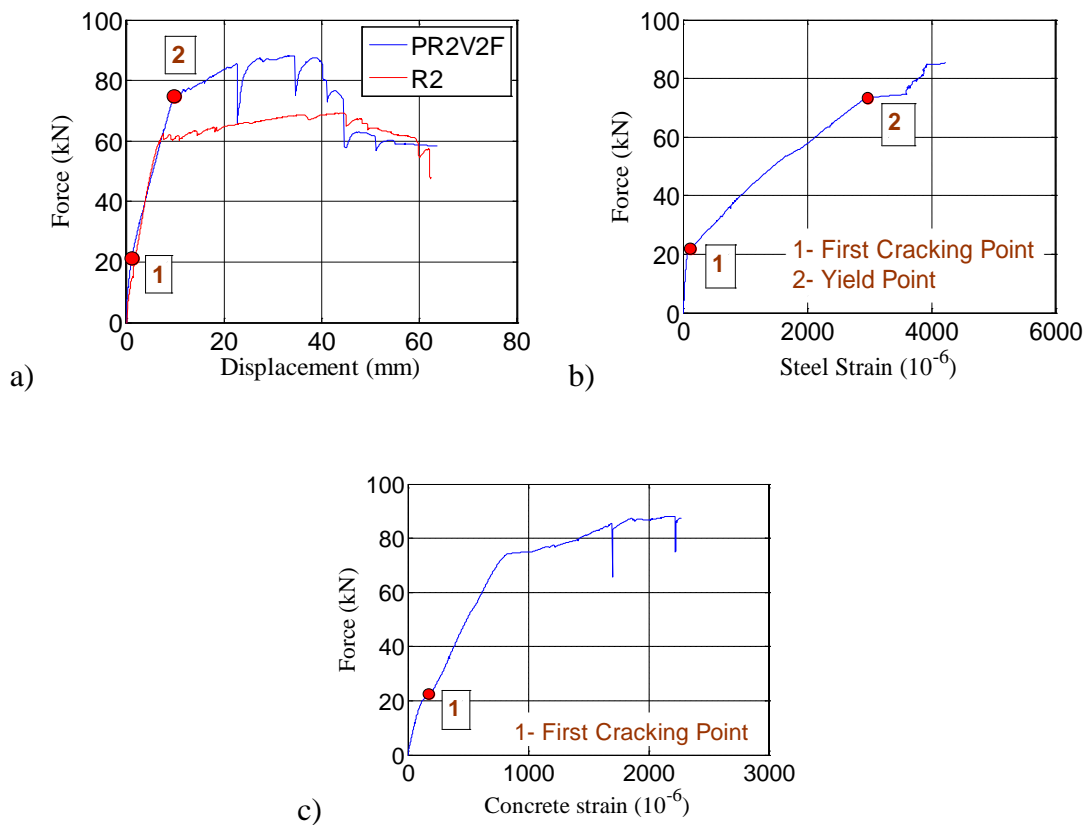
Figure 56: Test results for specimen P-R2-V2-F a) load vs displacement; b) load vs steel strain and c) load vs concrete strain
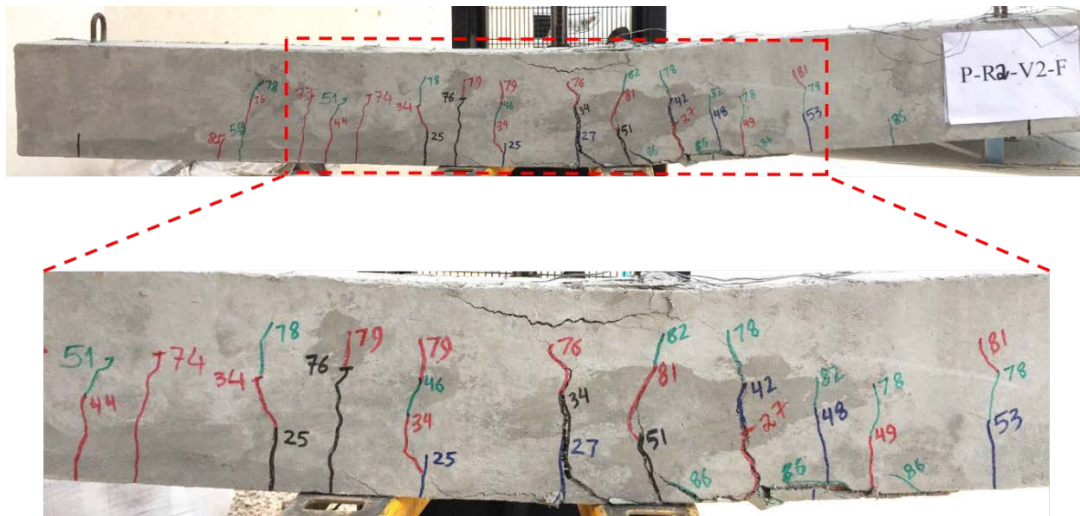
Figure 57: Mode of failure and crack patterns for test beam P-R2-V2-F

4.15 Specimen P-R3-V1-F

P-R3-V1-F specimen having the main longitudinal reinforcement of D16 was strengthened with one layer of PBO TRM system $(EA)^1_{PBO} = 6.4\ kN/mm$.. Load versus mid span deflection curve is shown in Figure 58-a along with the control specimen R3. Steel and concrete strain relationship with the applied load are shown in Figure 58-b and 58-c respectively. The mortar layer started to crack at 81 kN but it did not go up to the bond failure between the concrete substrate and TRM layer. The final mode of failure (F+L+C) was the flexural failure associated with cracking within TRM layer followed by the crushing of concrete as there was no clear sign of rupturing of textile (Figure 59). The load dropped twice prior of reaching the final load value. The corresponding yield flexural load for beam was 105.7kN. The ultimate load (117.6kN) recorded was before the first drop of the load. The increase in the load capacity was only 6.60% of the control specimen R3.
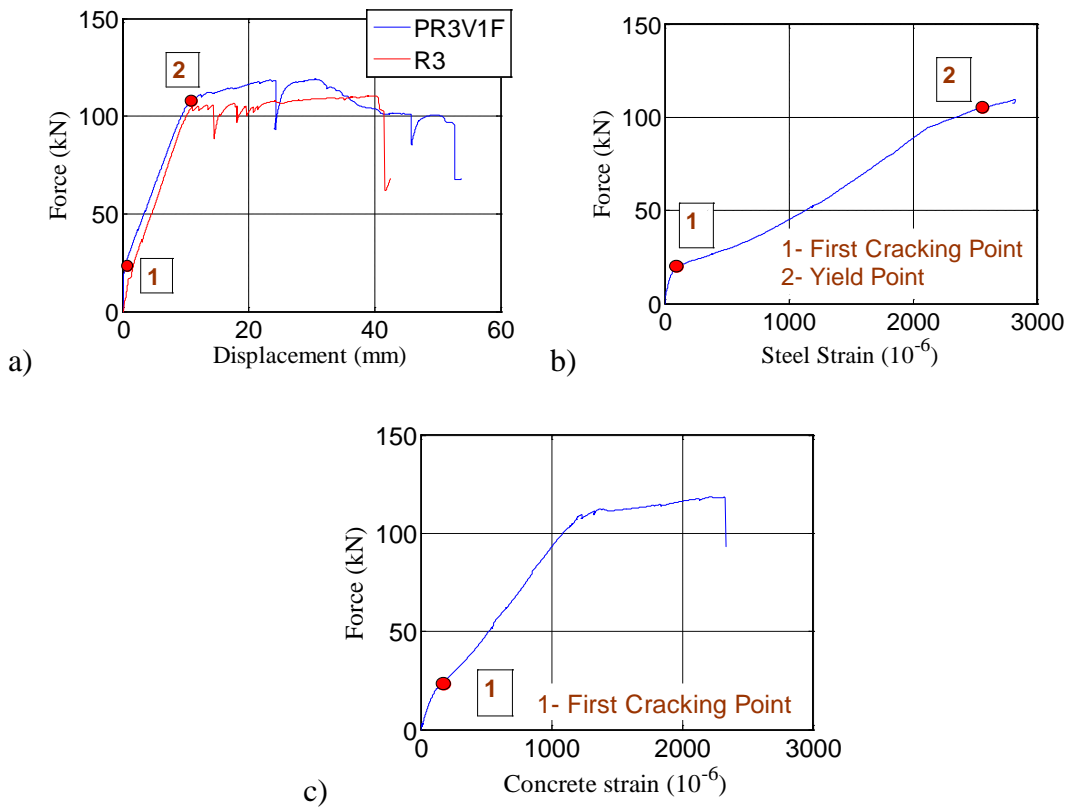
Figure 58: Test results for specimen P-R3-V1-F a) load vs displacement; b) load vs steel strain and c)

load vs concrete strain
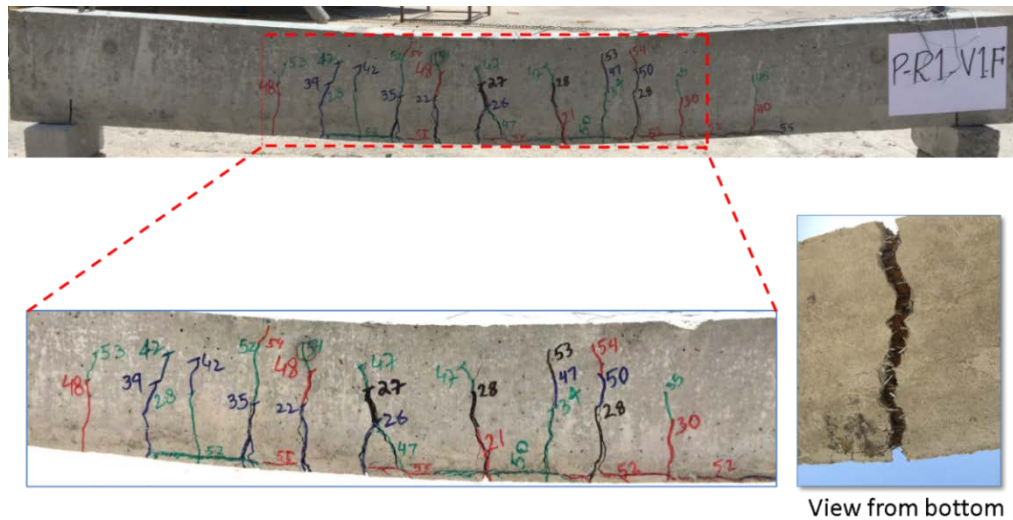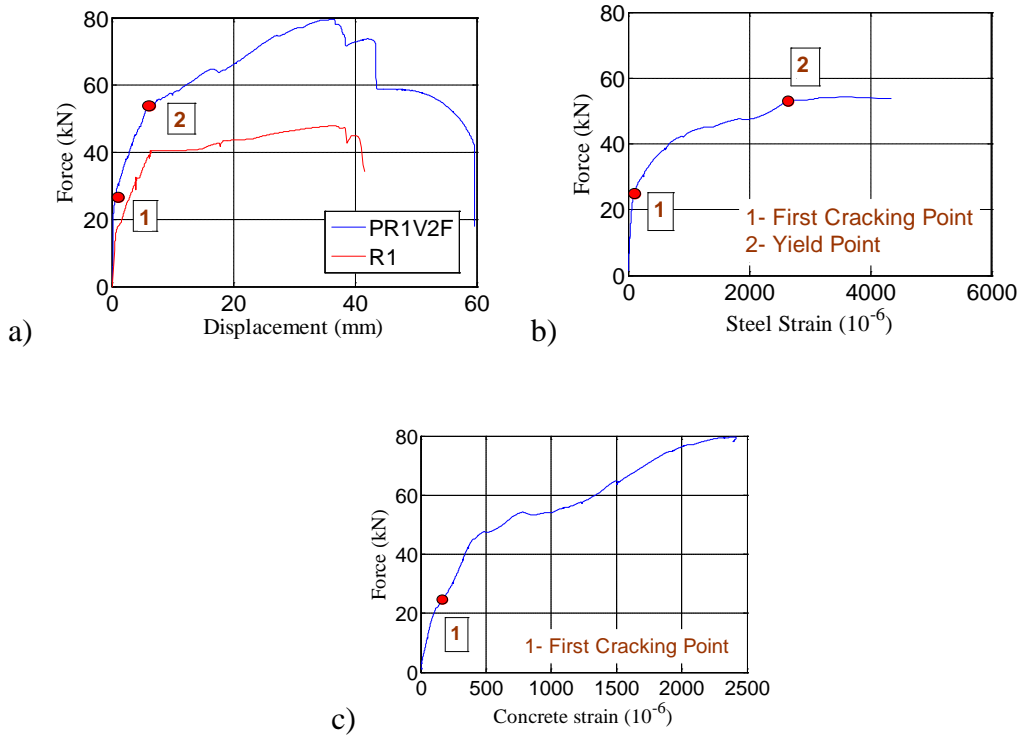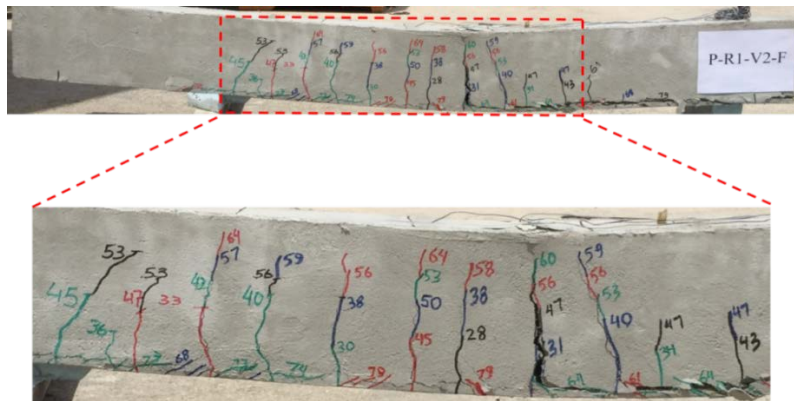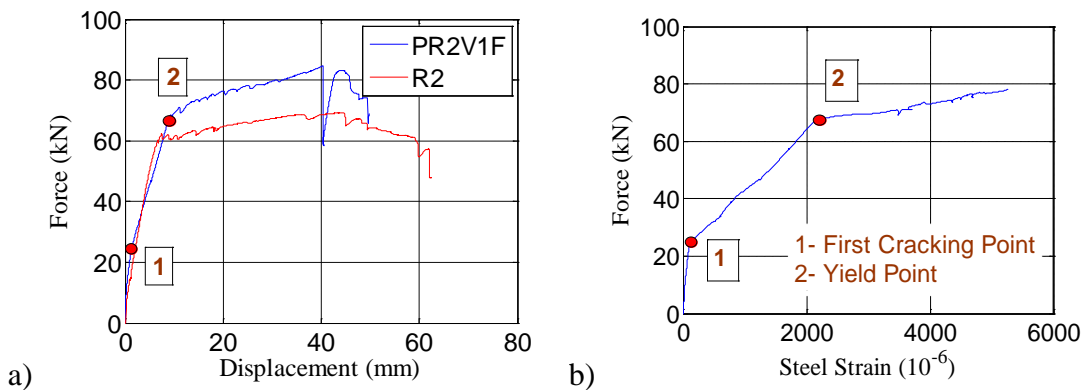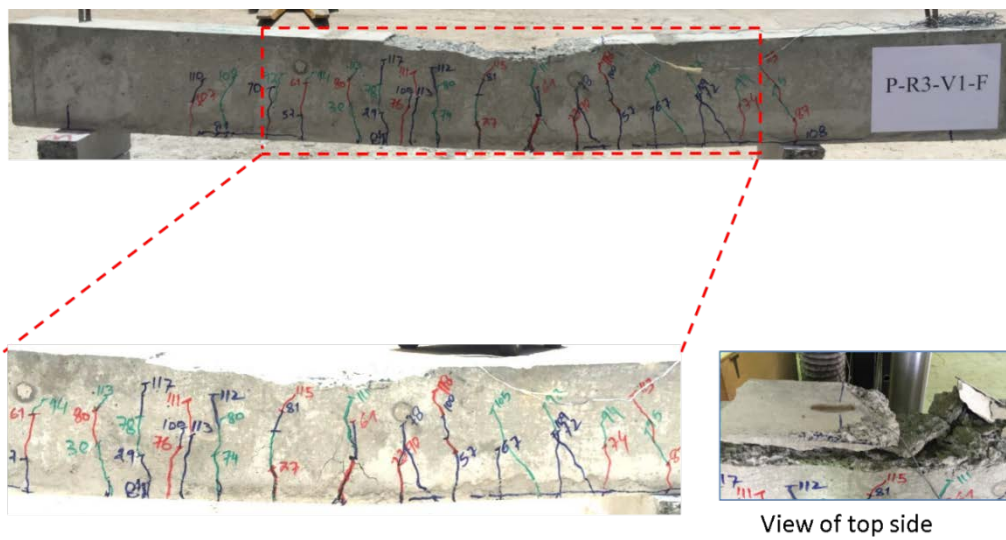

Figure 59: Mode of failure and crack patterns for test beam P-R3-V1-F

4.16 Specimen P-R3-V2-F

P-R3-V2-F beam specimen used D16 as the main longitudinal reinforcement and was strengthened with PBO TRM system using two layers of PBO textile $(EA)_{PBO}^2 = 12.8 \, kN/mm$. The load-displacement relationship, along with its associated control specimen is shown in Figure 60-a while load versus concrete strain is shown in Figure 60- b. The steel strain gauges were not working in this beam specimen. The reason might be it slips or breaks while the preparation of beam specimens or while applying the vibrator during casting of concrete. The first crack appeared at 33 kN in the middle of beam specimen (Figure 61). The cracks in the mortar layer started at 121 kN. There was no sudden drop in the load value and the final mode of failure was the flexural failure associated with cracking within TRM layer followed by the crushing of concrete (F+L+C). The yield and the ultimate load recorded were 101.6 kN and 123.86 kN respectively. The gain in the ultimate load capacity was 12.31% with respect to the control specimen R3.
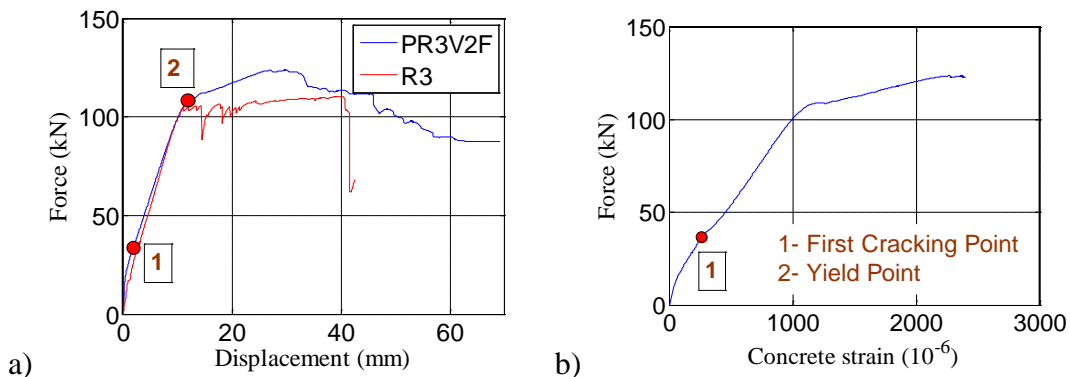
Figure 60: Test results for specimen P-R3-V2-F a) load vs displacement and b) load vs concrete strain
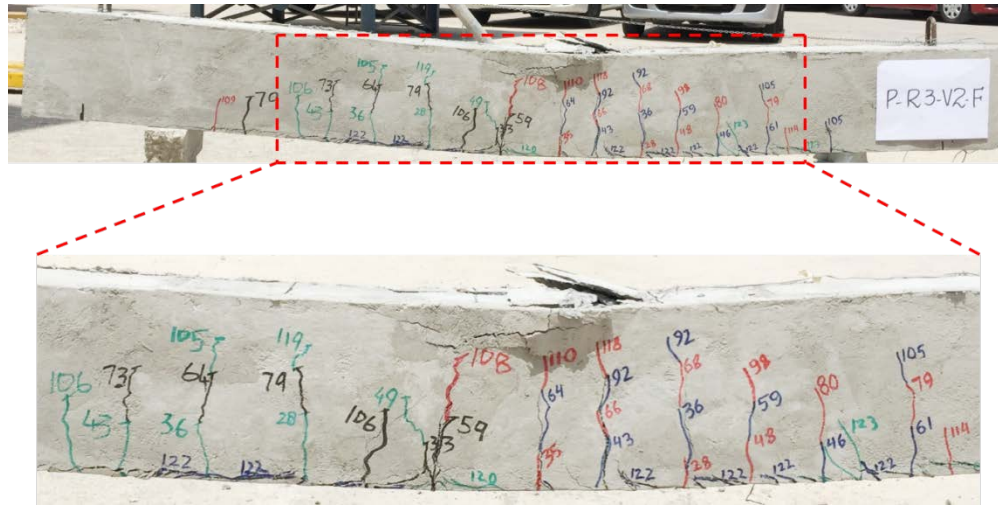
Figure 61: Mode of failure and crack patterns for test beam P-R3-V2-F

4.17 Discussion of test results

The following discussions are made on the observed ultimate load carrying capacities and the deformational characteristics in terms of the deflection at mid span, ductility index and energy absorption in both the TRM systems.

4.17.1 Load deflection and load carrying capacities:

Columns 3 and 4 in Table 11 list the ultimate load carrying capacity P_u for each specimen and gain in P_u (in terms of strengthened beams), respectively. Figure 62 (a and b) depicts the load versus mid-span deflection for strengthened beams having D10 as main longitudinal reinforcement. Figure 62a is for carbon and Figure 62b is for PBO strengthened specimens. From these figures, it is observed that for carbon TRM system, the increments/gains in P_u were: C-R1-V1-F with single textile layer - 38%, C-R1-V2-F with double textile layer - 35%, and C-R1-V3-F with three textile layers - 68%. For PBO TRM system, these gains were: P-R1-V1-F with single textile

layer - 25%, and P-R1-V2-F with two textile layers - 66%. Both the TRM systems showed considerable enhancement in ultimate load compared to the control specimen R1.
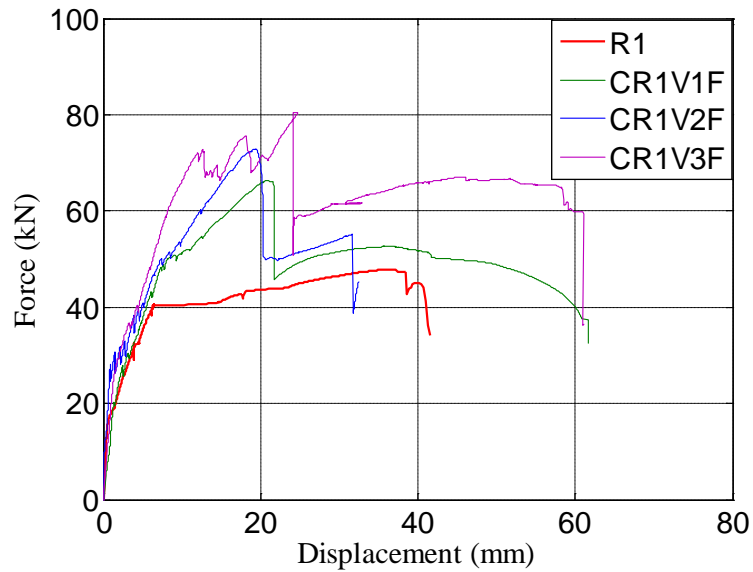
.

a)   Specimens strengthened with carbon TRM system
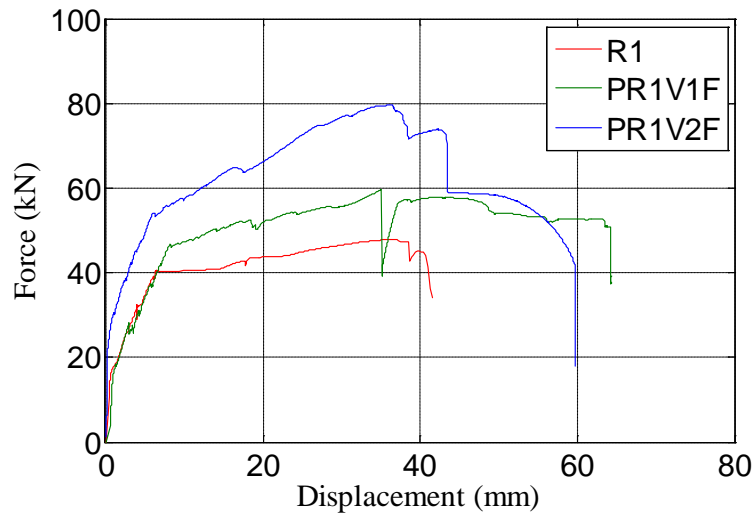
b)   Specimens strengthened with PBO TRM system

Figure 62: Comparison on load versus mid span deflection for specimens having D10 reinforcement.

Figure 63 (a and b) shows the load versus mid-span deflection for strengthened beams having D12 as main longitudinal reinforcement. It is observed that for carbon TRM system, the increments/gains in P_u were: C-R2-V1-F with single textile layer – 23.13%, C-R2-V2-F with double textile layer – 26.11%, and C-R2-V3-F with three textile layers – 77.51%. For PBO TRM system, these gains were: P-R2-V1-F with single textile layer – 22.47%, and P-R2-V2-F with two textile layers – 27.51%. Both the TRM systems showed considerable increment in ultimate load compared to the control specimen R2.
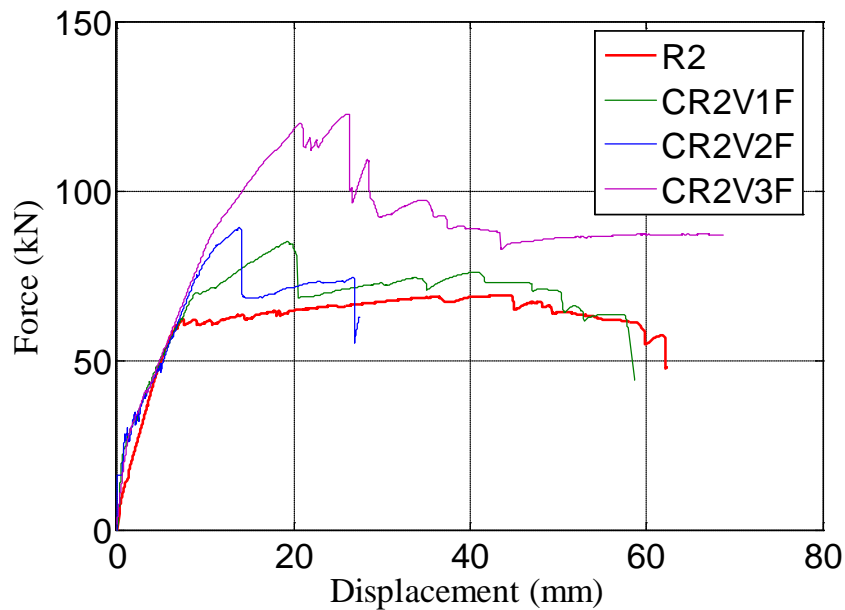
a) Specimens strengthened with carbon TRM system
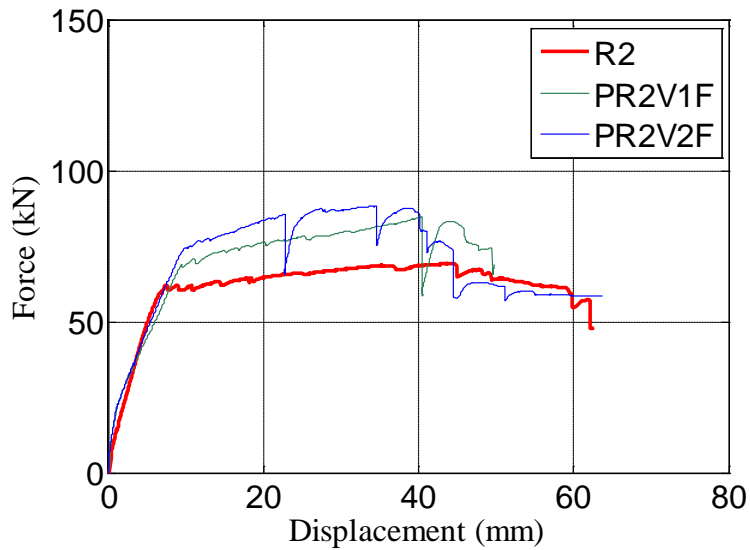
b) Specimens strengthened with PBO TRM system

Figure 63: Comparison on load versus mid span deflection for specimens having D12 reinforcement

Figure 64 (a and b) shows the load versus mid-span deflection for strengthened beams having D16 as main longitudinal reinforcement. Figure 64a is for carbon and Figure 64b is for the PBO strengthened specimens. It is observed that for carbon TRM system, the increments/gains in P_u were: C-R3-V1-F with single textile layer – 14.40%, C-R3-V2-F with double textile layer – 13.54%, and C-R3-V3-F with three textile layers – 45.41%. For PBO TRM system, these gains were: P-R3-V1-F with single textile layer – 6.60%, and P-R3-V2-F with two textile layers – 12.31%. Both the TRM systems showed considerable increment in ultimate load compared to the control specimen R3.
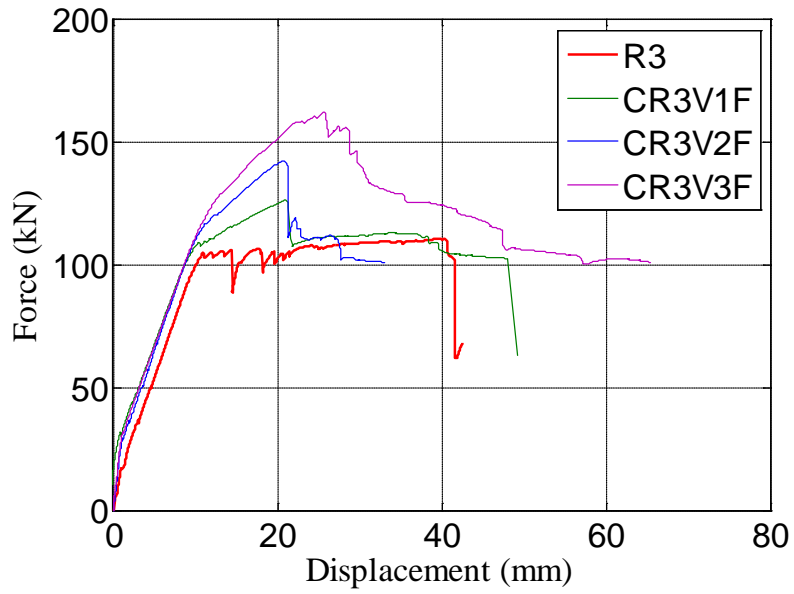
a) Specimens strengthened with carbon TRM system
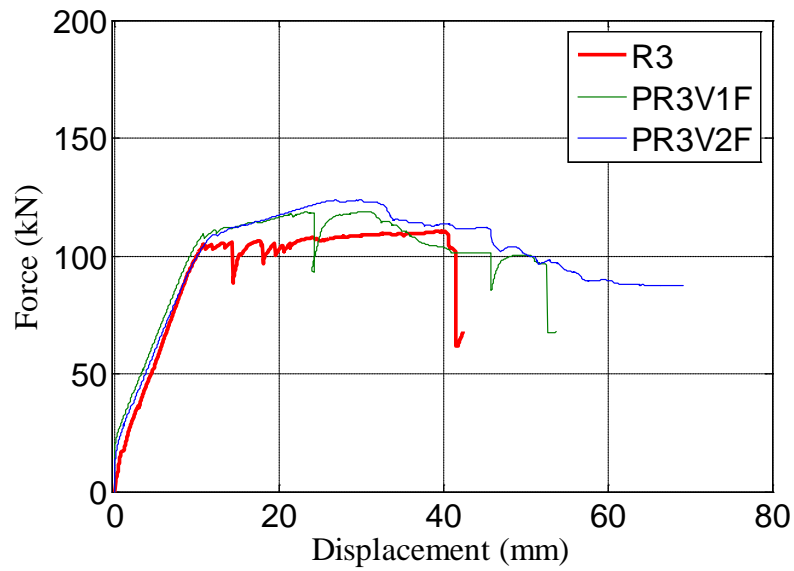
a) Specimens strengthened with PBO TRM system

Figure 64: Comparison on load versus mid span deflection for specimens having D16 reinforcement.

The bar chart in Figure 65 (a-c) depicts the ultimate and yield loads (P_u and P_y, respectively) for corresponding specimens. The yield load value is the load at which the steel rebar started to yield. The load value corresponding to the strain value of rebar (0.26% strain) where it started to yield was taken as the yield load. Figure 65 shows that the strengthening technique contributed to increase in both the yield and ultimate load carrying capacities of strengthened specimens as compared to control specimens. The increase in the ultimate capacity was also strongly affected by the number of layers of textiles.
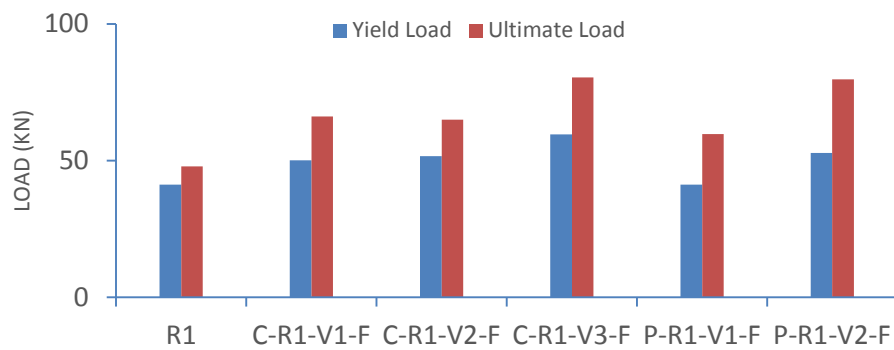
a) Specimens with D10 reinforcement
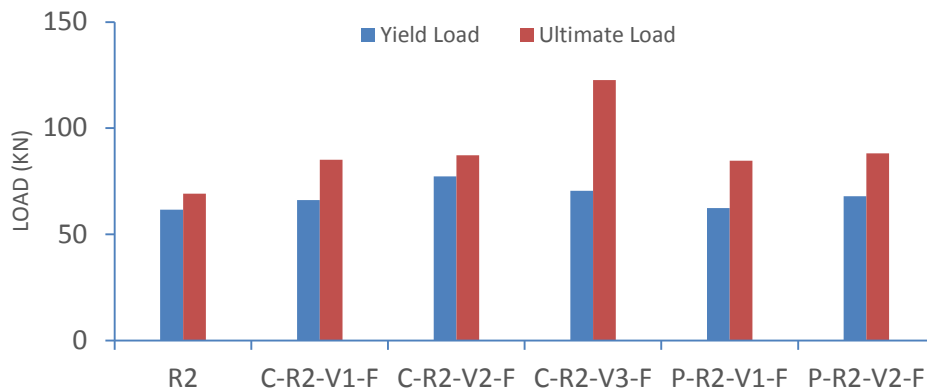
b) Specimens with D12 reinforcement
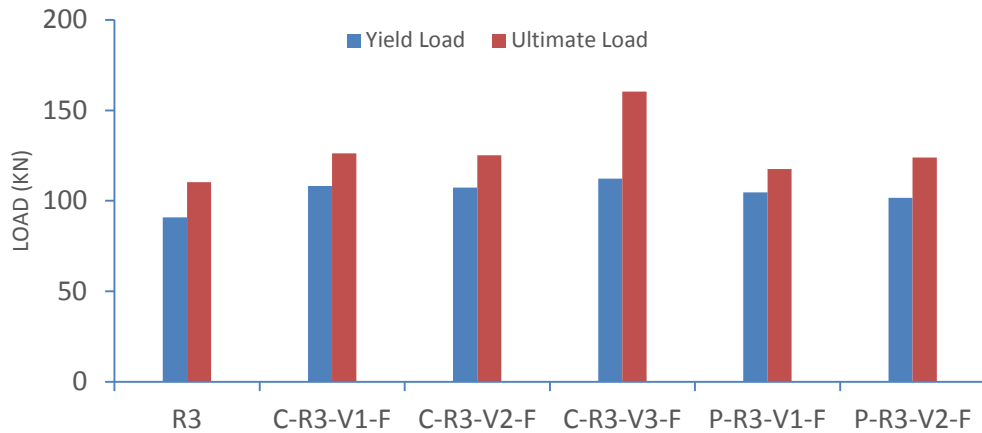
c) Specimens with D16 reinforcement

Figure 65: Ultimate and yield loads for all the tested specimens

4.17.2 Ductility characteristics

The ductility index (ΔI) is defined as the ratio between the deflection at the ultimate load and that at yield load [5]. The bar charts in Figure 66 (a-c) and column 8 in Table 12 summarize the values of ductility index (ΔI) for specimens having a different reinforcement ratio. For the D10 reinforcement ($\rho_s = 0.50\%$) beam specimens, the ductility index increased with the increase in the number of textile layers. PBO strengthened specimens were more ductile than that of specimens strengthened with the carbon textiles. However, beam specimens with the reinforcement D12($\rho_s = 0.72\%$), and D16($\rho_s = 1.27\%$), the ductility index values decreased with the higher number of textile layers. Nevertheless the beam specimens strengthened with PBO textiles were more ductile as compared to carbon textile.

The average values of ductility indices of using carbon as strengthening material were 1.1×, 1.2× and 0.5× for D10, D12 and D16 beam specimens respectively to that of the control specimen. Similarly the average values of ductility indices of using PBO as strengthening material were 2.42×, 0.75× and 0.56× for D10, D12 and D16 specimens respectively to that of the control specimen.

4.17.3 Energy absorption characteristics

The energy absorption (Ψ) is the area under the load deflection curve up to the ultimate load [5]. The bar charts in Figure 66 (a-c) and column 9 in Table 12 summarize the values of the energy absorption (Ψ) for specimens having a different reinforcement ratio. As shown in column 9 of Table 12, the increase in number of textile layers increases the energy absorption of all the strengthened specimens to that of the control specimens. A noticeable increase in the energy absorption was observed when using the carbon TRM system as compared to that when using PBO as shown in Figure 66.

The average values of energy absorption for using carbon as strengthening material were 1.8×, 1.2× and 1.6× for D10, D12 and D16 beam specimens respectively to that of the control specimen. Similarly the average values of energy absorption for using PBO as strengthening material were 2.0×, 1.0× and 1.5× for D10, D12 and D16 specimens respectively to that of the control specimen.
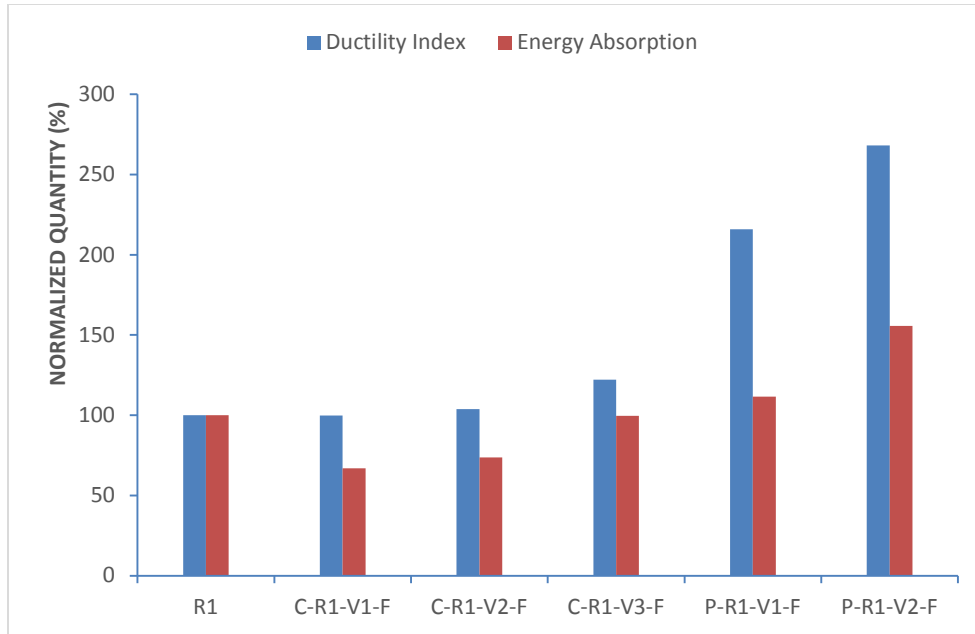
a)   Specimens with D10 reinforcement
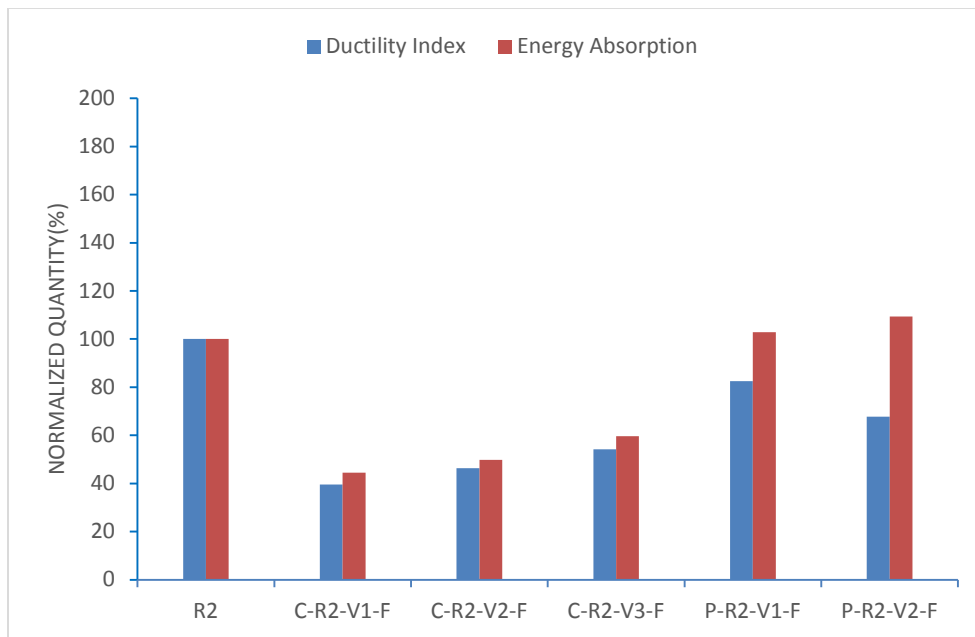
b)   Specimens with D12 reinforcement
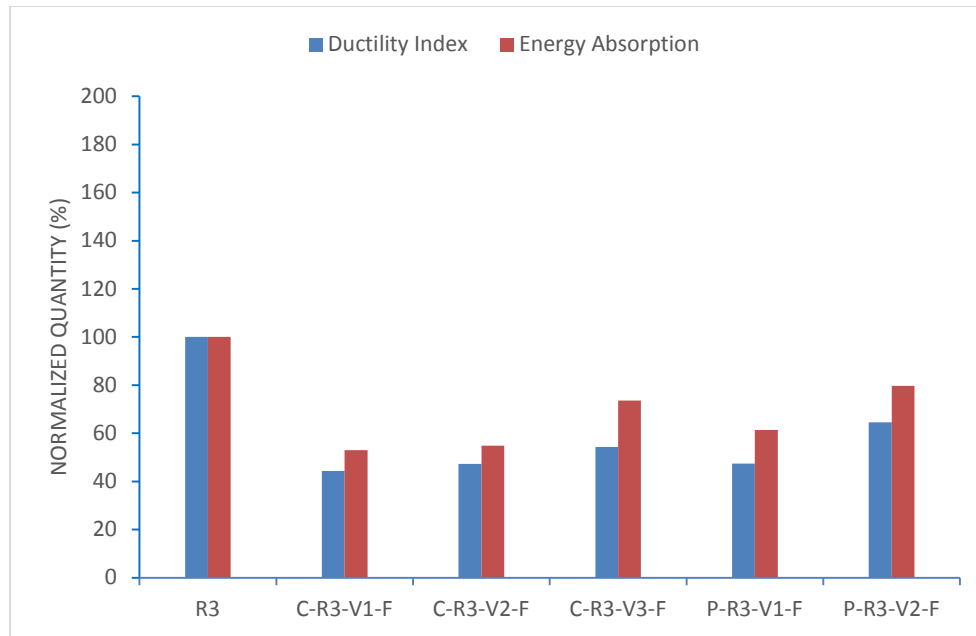
c) Specimens with D16 reinforcement

Figure 66: Ductility index and energy absorption values for all the specimens normalized to those of control specimens

4.18 Effect of investigated parameters

The three different parameters which were to be investigated in this research are steel reinforcement ratio, TRM systems and volume fraction. The detailed discussion of the effect of these parameters on the strengthened specimens using carbon and the PBO TRM system is highlighted below.

4.18.1 Effect of main steel reinforcement ratio

Specimens having different steel reinforcement ratios while having the same TRM reinforcement ratio are discussed in this section. Their behavior regarding the

increase in the ultimate strength and their mode of failure is highlighted for both the carbon and PBO TRM systems

4.18.1.1 Carbon TRM system

For the specimens (C-R1-V1-F, C-R2-V1-F and C-R3-V1-F) having different steel reinforcement ratio, but with textile of same $(EA)_C^1 = 12.56\ kN/mm$, a decrease in the gain in ultimate load value was observed from 37.97 % to 14.40 % respectively over their control specimens. Moreover the mode of failure, which was the rupture of textile at the mid-span (F+T+C), was similar for all of them.

Similarly, the specimens (C-R1-V2-F, C-R2-V2-F and C-R3-V2-F) with same textile $(EA)_C^2 = 25.12\ kN/mm$, had a decrease in the gain in P_u from 35.52 % to 13.54 % respectively over their control specimens. Moreover the mode of failure as mentioned above (F+T+C) was similar for all of them.

A similar trend was observed in specimens (C-R1-V3-F, C-R2-V3-F and C-R3-V3-F) having the same $(EA)_C^3 = 37.68\ kN/mm$ in which the gain in the ultimate load value was decreased from 67.85 % to 45.41%. All of these specimens had the similar mode of failure in which the TRM layer separated from concrete substrate (F+S+C).

4.18.1.2 PBO TRM system

For specimens (P-R1-V1-F, P-R2-V1-F and P-R3-V1-F) having the different steel reinforcement ratios, but with textile of same $(EA)_{PBO}^1 = 6.4\ kN/mm$, a decrease in the gain in ultimate load value was observed from 24.69 % to 6.60 % respectively

over their control specimens. The mode of failure which was cracking within the mortar layer (F+L+C) was similar for all of them.

Similarly for specimens (P-R1-V2-F, P-R2-V2-F and P-R3-V2-F) having the constant EA value $((EA)_{PBO}^2 = 12.8 \, kN/mm)$ while the ρ_s value changed from 0.57% to 1.27%, the gain in the ultimate load decreased from 66.49% to 12.31% though having the similar mode of failure as mentioned above (F+L+C).

It can be concluded that for the specimens strengthened either with carbon TRM system or PBO TRM system, as the steel reinforcement ratio was increased by keeping the TRM volumetric fraction constant, there was decrease in gain in the ultimate load value. The mode of failure was however similar for all the beams.

4.18.2 Effect of TRM system

Here discussion on two different TRM systems for strengthening the beam specimens is done comparing the efficiency of each system in enhancing the ductility and capacity of the strengthened beams.

4.18.2.1 Specimens with D10 reinforcement ($\rho_s = 0.50\%$)

For the specimens with ($\rho_s = 0.50\%$) strengthened with carbon and the PBO TRM system, the average increase in the load capacity of the strengthened beams were 47.11% and 45.59 % respectively over the control specimen R1. Moreover the average values of ductility index were $1.1 \times$ and $2.42 \times$ to that of the control specimens for carbon and PBO TRM system respectively. Also the energy absorption

increased from 998.7 kN-m to 1,485 kN-m for carbon TRM system and from 1,665.1 kN-m to 2,323.2 kN-m for the PBO TRM system.

4.18.2.2 Specimens with D12 reinforcement ($\rho_s = 0.72\%$)

For the specimens having $\rho_s = 0.72\%$ and strengthened with carbon and the PBO TRM system, the average increase in the capacity of the strengthened beams were 42.25% and 25% respectively over the control specimen R2. Moreover the average values of ductility index was $0.40\times$ and $0.75\times$ to that of the control specimen for carbon and PBO TRM system respectively. For carbon TRM system the energy absorption value increased from 1,210.7 kN-m to 1,623.8 kN-m and for PBO TRM system, the energy absorption value increased from 2,804.2 kN to 2,980.1 kN-m as the volume fraction increased.

4.18.2.3 Specimens with D16 reinforcement ($\rho_s = 1.27\%$)

Similar patterns of specimens having the $\rho_s = 0.72\%$ had been observed for specimens having $\rho_s = 1.27\%$ PBO strengthened specimens were more ductile and were having more average ductility index value of $0.56\times$ to that of the control specimen compared to specimens that were strengthened with carbon TRM system which had the average ductility index value of $0.47\times$ to that of control specimen. This decrease in ductility for strengthened beams with higher percentage of steel reinforcement $\rho_s = 1.27\%$ is understandable. Nevertheless, there was a gain in the energy absorption value for both strengthened beams, from 1,959.3 kN-m to 2,719.5 kN-m for carbon TRM system and from 2,266.5 kN-m to 2,943.2 kN-m for PBO

TRM systems respectively. Moreover the average increase in the ultimate capacity of strengthened specimens for carbon and the PBO TRM system were 24.5 % and 9.5 % respectively over the control specimen R3.

It can be concluded that for specimens of all three different reinforcement ratios, the ones strengthened with the PBO TRM system were more efficient in terms of ductility but less effective in enhancing the capacity of strengthened beams compared to the carbon TRM system. This was reflected in terms of the mode of failure (F+S+C) which showed the separation of TRM layer from concrete substrate for beam strengthened with carbon TRM system. But, in PBO TRM systems, there were cracks within the mortar layer (F+L+C) which showed the strong bond between TRM layer and concrete substrate and were hence more ductile. The higher value of ultimate load carrying capacity for the carbon TRM system corresponds to higher energy absorption value for beams strengthened with carbon TRM system as compared to the ones with PBO TRM.

4.18.3 Effect of volume fraction of textile

By keeping the steel reinforcement ratio (ρ_s) value constant, different volume fractions of textile were achieved by altering the number of layers of textiles that were embedded in the mortar. The behavior in terms of the increase in the load carrying capacity of strengthened beams, failure patterns observed, ductility and energy absorption among the two different TRM systems with different number of layers of textiles are discussed in this section.

4.18.3.1 Specimens with D10 reinforcement ($\rho_s = 0.50\%$)

As the number of layers of textiles increased from 1 to 3 in the carbon TRM system (EA values changes from 12.56 kN/mm to 37.68 kNmm), the gain in the ultimate load carrying capacity increased from 37.97 % to 67.85 % respectively to that of the control specimen R1. Also, there was an increase in the ductility index and energy absorption by increasing the volume fraction.

In PBO TRM system, as the number of layer of textiles increased from 1 to 2, (EA value increases from 6.4 kN/mm to 12.8 kN/mm) the ultimate load carrying capacity increased from 24.69 % to 66.49 %. Moreover, the ductility index and energy absorption values increased as well and are comparatively higher than the carbon TRM system. It can also be seen that specimens strengthened with two layers of PBO TRM system ($(EA)_{PBO}^2 = 12.8 \, kN/mm$) gave approximately the same increase in the ultimate load carrying capacity of 66.49 % compared with three layers of carbon ($(EA)_C^3 = 37.68 \, kN/mm$) TRM system of 67.85 %.

4.18.3.2 Specimens with D12 reinforcement ($\rho_s = 0.72\%$)

Here for the carbon TRM system, as the EA value for textile increased from $(EA)_C^1 = 12.56 \, kN/mm$ to $(EA)_C^3 = 37.68 \, kN/mm$, the ultimate load carrying capacity was increased from 23.13% to 77.51% to that of the control specimen R2. Energy absorption value also increases by increasing the number of layers of textile, however there was subsequent decrease in the ductility index.

For the PBO TRM system, as the EA value increased from from $(EA)_{PBO}^1 = 6.4\ kN/mm$ to $(EA)_{PBO}^2 = 12.8\ kN/mm$, the increase in the ultimate load carrying capacity was 22.47 % and 27.51 % respectively. The energy absorption value increased but relatively lowers than that of the carbon TRM system. The ductility index value decreased with the increase in textile volumetric fraction, however the energy absorption value increased, but relatively lower than that of the carbon TRM system.

4.18.3.3 Specimens with D16 reinforcement ($\rho_s = 1.27\%$)

A similar trend to specimens ($\rho_s = 0.72\%$) was observed for specimens having ($\rho_s = 1.27\%$) in which as the number of layers of textiles in the carbon TRM system increased from 1 to 3 layers, the ultimate load carrying capacity also increased from 14.40% to 45.41% to that of the control specimen R3. But for the PBO TRM system as the number of layers of textile increased from 1 to 2 there was no any remarkable increase in the ultimate load carrying capacity (gain in *Pu* was from 6.60% to 12.31% only). Moreover, similar trend of ductility index (reduction) and energy absorption (gain) were observed.

From the above observations, for lower reinforcement ratio ($\rho_s = 0.50\%$), as the textile volumetric fraction increased, the specimens strengthened with PBO TRM system were more efficient in terms of ductility as well as in increasing the ultimate load carrying capacity than that of carbon TRM system. For larger reinforcement ratios ($\rho_s = 0.72\%\ and\ \rho_s = 1.27\%$), the carbon TRM system was more efficient in

98

the ultimate load carrying capacity than that of PBO TRM system which was also the indication of higher energy absorption values in specimens strengthened with carbon TRM system. Moreover as the textile volumetric fraction increased with the increase in the reinforcement ratio, there was not any change in the failure pattern of specimens strengthened with PBO TRM system. On the other hand for all the reinforcement ratios of specimens strengthened by carbon TRM system, the increase in volume fraction tends to change the failure pattern. For lower volume fraction ($\rho_f = 0.014\%$ and 0.028%), the failure pattern was (F+T+C) in which the textile at the mid span ruptured from the mortar layers and for higher volume fraction ($\rho_f = 0.041\%$) it changed to (F+S+C) which means the separation of whole TRM layer with concrete substrate.

CHAPTER 5
THEORETICAL LOAD CALCULATIONS

5.1 Theoretical loads

The theoretical values of the load have been calculated in order to verify the experimentally observed flexural load value. Theoretical formulations for the analytical predictions of the flexural strength of the tested beams were done based on ACI 549.4R-13 [10]. Analogies will be made to state the applicability of the ACI formulations for predicting behavior of TRM system.

For theoretical computations, several assumptions were made to calculate the flexural resistanceof RC beam sections reinforced with TRM layer. These assumptions are:

1. Plane cross section remains plane before and after loading.

2. Whitney stress block is used to calculate compressive stress in concrete.

3. The maximum compressive strain in concrete is assumed to be 0.003. Tensile strength of concrete is neglected.

4. Steel is assumed to be elastic before yielding, and it maintains constant yielding stress (550 MPa) post yielding.

5. TRM / FRCM has a bilinear-elastic behavior up to failure. However, the contribution of TRM before cracking is neglected [33].

6. The interface between the reinforcing mortar and the textile is considered stronger than the concrete substrate and TRM interface.

7. The perfect bond between TRM layer and concrete substrate as well as the good bond between fabric and the matrix.

Of all the assumptions, the one with the perfect bond seems to be more arguable. However as the TRM tensile properties are characterized in ACI 549, the fabric slip within the matrix is built in the constitutive law of material [10]. Similarly, at failure the TRM separation / debonding from the concrete substrate occurs without affecting the flexural performance of the member.

The following sections present step-by-step formulations adopted for calculating the flexural resistance of typical doubly-reinforced concrete beam with TRM strengthening. Sample calculations for two of the beams have been done accordingly and are given in Appendix A. The typical bending moment and shear force diagram for the tested beam is shown in Figure 67 for reference.

The theoretical computations and experimentally observed values are compared in Table13.
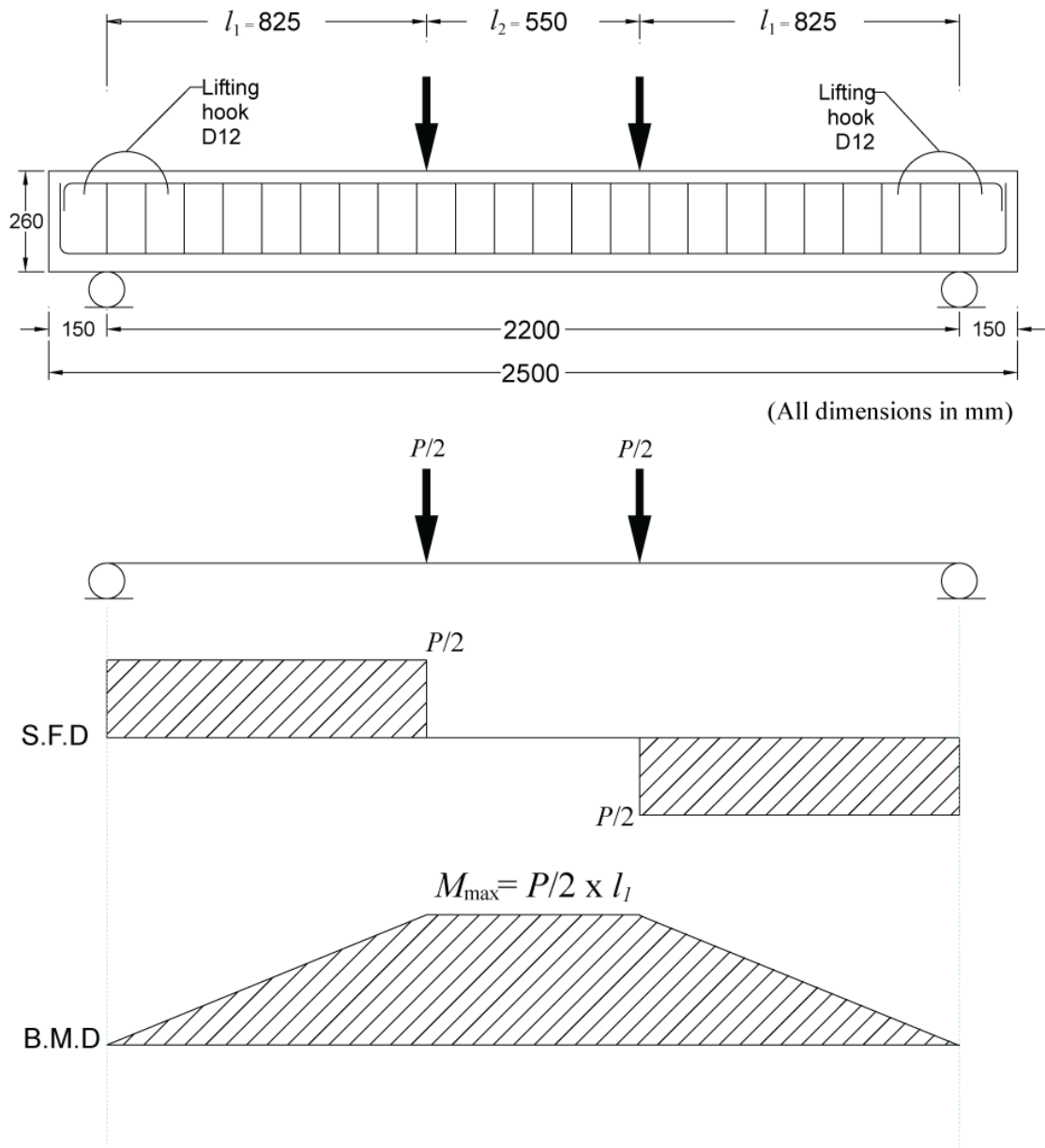
Figure 67: Bending moment and shear force diagram for the tested beam

Table 13: Theoretical load computation results for all tested beams.

No.	Beam	"c" mm	Nominal Moment (Mn) kN-m	Theoretical Ultimate Load (P_T) kN	Test Ultimate Load (P_U) kN	$\dfrac{P_U}{P_T}$
1	R1	30.16	17.305	46.87	47.90	1.02
2	R2	37.5	24.094	58.41	69.14	1.18
3	R3	60.6	40.434	98.02	110.32	1.12
4	C-R1-V1-F	16.96	26.10	63.28	66.084	1.04
5	C-R1-V2-F	19.72	31.34	74.99	72.94	0.99
6	C-R1-V3-F	22.47	36.10	87.52	80.40	0.92
7	C-R2-V1-F	21.35	32.28	78.26	85.15	1.09
8	C-R2-V2-F	24.10	37.21	90.27	89.12	0.99
9	C-R2-V3-F	26.84	42.10	102.06	122.71	1.20
10	C-R3-V1-F	32.34	47.22	114.48	126.17	1.10
11	C-R3-V2-F	35.19	52.10	126.29	142.29	1.12
12	C-R3-V3-F	37.89	57.15	138.44	160.36	1.15
13	P-R1-V1-F	15.60	23.62	57.25	59.72	1.04
14	P-R1-V2-F	17.01	26.21	63.51	79.74	1.25
15	P-R2-V1-F	20	29.84	72.34	84.68	1.17
16	P-R2-V2-F	21.40	32.37	78.50	88.15	1.13
17	P-R3-V1-F	31.14	45.05	109.24	117.6	1.07
18	P-R3-V2-F	32.52	47.47	115.10	123.86	1.08

5.1.2 Moment capacity of beam specimens with TRM layers

Following ACI 549 (Reference), TRM ultimate tensile strain ε_{fu}, is the average minus one standard deviation derived from the tensile test conducted according to AC434. So, based on this the effective tensile strain level in TRM at failure, ε_{fe}, is limited to the ultimate tensile strain, ε_{fu}, defined in Eq. (1). The internal stress and strain distribution of doubly reinforced concrete beam with the TRM strengthening is shown in Figure 68.
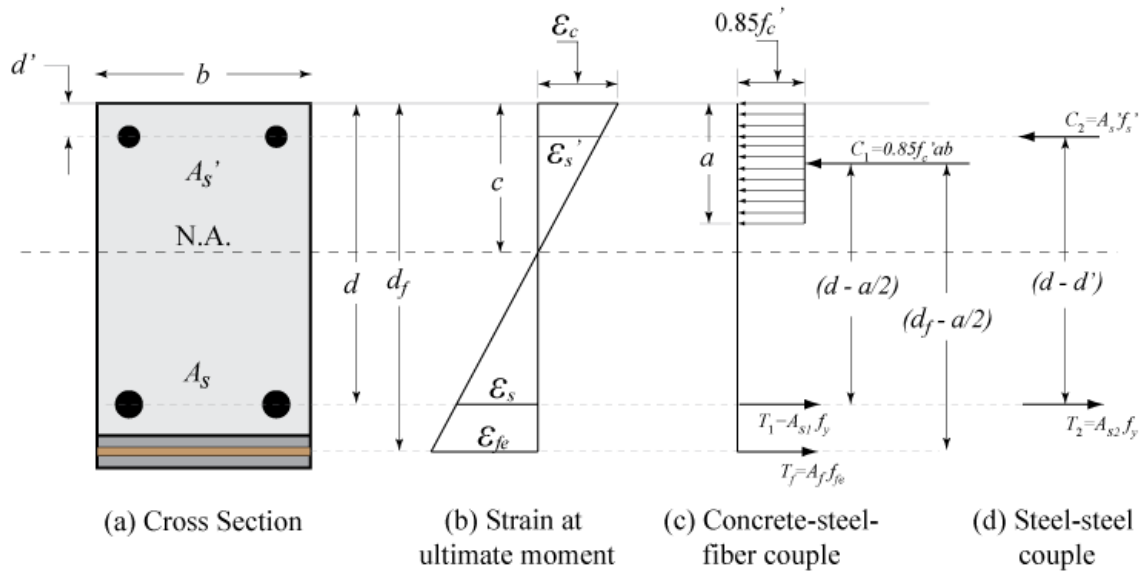
Figure 68: Internal stress and strain distribution for a doubly-reinforced rectangular beam section strengthened with TRM under flexure at ultimate limit state

$$\varepsilon_{fe} = \varepsilon_{fu} \leq 0.012 \tag{1}$$

The effective tensile stress level in the TRM reinforcement achieved at failure, f_{fe}, can be computed from Eq. (2)

$$f_{fe} = E_f \times \varepsilon_{fe} \tag{2}$$

The flexural strength is calculated in accordance with Eq. (3)

$$M_n = M_{ns1} + M_{ns2} + M_f \tag{3}$$

Where M_n = nominal flexural strength; and M_{ns1}, M_{ns2} and M_f is equal to the contribution of tension steel reinforcement, compression steel reinforcement and TRM respectively. They are expressed according to Eq. (4), (5) and (6) respectively

$$M_{ns1} = A_s f_y \left(d - \frac{\beta c}{2} \right) \tag{4}$$

$$M_{ns2} = A_s' f_s'(d - d') \tag{5}$$

$$M_f = A_f b f_{fe} \left(h - \frac{\beta c}{2} \right) \tag{6}$$

With assumed neutral axis depth, the strain and stress level in the TRM layer and steel reinforcement can be calculated with the hit and trial method using the internal force equilibrium Eq. (9)

Referring to Figure 68

$$T_1 + T_f = C_1 + C_2 \tag{7}$$

$$As\, fy + A_f b f_{fe} = (0.85 \times fc')\beta cb + fs'A_s' \tag{8}$$

Where $a = \beta c$ and $\beta = 0.85$

$$c = \frac{A_s f_y + A_f b f_{fe} - A_s' f_s'}{0.85\, f_c'\, \beta b} \tag{9}$$

The effective stresses on compression and tension steel rebars can be computed as

$$f_s = E_s \times \varepsilon_{sy} \text{ and } f_s' = E_s \times \varepsilon_{sy}' \tag{10}$$

Using the strain compatibility, the effective tensile strain level in TRM (ε_{fe}), tension steel yield strain (ε_{sy}), compression steel yield strain (ε_{sy}') and the compressive strain in the concrete (ε_c), are related in accordance with Eq. (11).

$$\frac{\varepsilon_{fe}}{h-c} = \frac{\varepsilon_{sy}}{d-c} = \frac{\varepsilon_{sy}'}{c-d'} = \frac{\varepsilon_c}{c} \tag{11}$$

As the maximum value of moment is know from Figure 67,

$$M_{max} = \frac{P}{2} \times l_1 \tag{12}$$

The value of P can be obtained by the following relation

$$P = \frac{M_n \times 2}{l_1} \tag{13}$$

Based on the theoretical load calculations as described above, computational results comparable to the experimental values were achieved. Average variation of theoretically computed load to the experimentally observed values was 3% which shows relatively satisfactory computational results. It should be noted that the scope of theoretical computation adopted in this work is relatively simple and is based on formulations based on ACI 549 [10]. Future work will be concentrated on more detailed finite element.

CHAPTER 6
CONCLUSION AND RECOMMENDATIONS

The experimental as well as analytical work for using textile reinforced mortar to increase the flexural capacity of reinforced concrete beams was performed in this study. Two different types of TRM systems, namely carbon TRM system and PBO TRM system were used as a strengthening material. The effect of three different parameters; steel reinforcement ratio, different TRM systems and volume fraction (EA) of textiles have been studied in order to know the behavior of each TRM system and to make comparisons between the two systems. Eighteen (18) beam specimens were tested under four point bending until failure. After successful completion of experimental work, an increase in the capacity of all tested strengthened specimens was achieved. The major conclusion derived from this research is discussed for each parameter respectively.

6.1 Effect of reinforcement ratio

For the specimens strengthened either with the carbon TRM system or by a PBO TRM system, it was observed that as the steel reinforcement ratio increased by keeping the (EA) value of TRM constant, the gain in the ultimate load value decreased. Also the change in the reinforcement ratio did not affect the mode of failure. Higher the reinforcement ratio, while having the same (EA) value gave the same mode of failure. Similarly for lower reinforcement ratio specimens having same textile (EA) also gave the same mode of failure.

.For both types of TRM systems, increased in reinforcement ratio resulted in a reduced ductility index, which is commonly observed for RC beams with higher reinforcement content. However, energy absorption increased for all the specimens with subsequent increase in reinforcement ratio.

6.2 Effect of TRM system

Specimens for all three different reinforcement ratios, the ones strengthened with the PBO TRM system was more efficient in terms of ductility but less effective in enhancing the capacity of strengthened beams as compared to the carbon TRM system. This also had been reflected in terms of the mode of failure (F+S+C) for carbon TRM system which showed the separation of TRM layer from concrete substrate but in PBO TRM systems, there were cracks within the mortar layer (F+L+C) which shows the strong bond between TRM layer and concrete substrate and were hence more ductile. However, due to the higher ultimate load carrying capacity of carbon TRM system, the energy absorption value was also relatively higher as compared to the PBO TRM system.

6.3 Effect of volume fraction of textile

For lower reinforcement ratio ($\rho_s = 0.50\%$), as the (EA) value increased, the specimens strengthened with the PBO TRM system was more effective in terms of ductility as well as enhancing the ultimate load carrying capacity than that of the carbon TRM system. For larger reinforcement ratios ($\rho_s = 0.72\%$ and $\rho_s = 1.27\%$), the carbon TRM system was more effective in the ultimate load carrying capacity

than that of a PBO TRM system which was also the indication of higher energy absorption values in specimens strengthened with carbon TRM system.

However, as the (EA) value of TRM increased with the increase in the reinforcement ratio, there was no change in the failure pattern of specimens strengthened with the PBO TRM system. On the other hand, for all the reinforcement ratios of specimens strengthened by a carbon TRM system, the increased in (EA) also resulted in change in the failure pattern. For lower EA values of TRM; $(EA)_C^1 = 12.56 \, kN/mm$ and $(EA)_C^2 = 25.12 \, kN/mm$, the failure pattern was (F+T+C) in which the textile at the mid span was close to rupture (close to the tensile strength) and for a higher values $(EA)_C^3 = 37.68 \, kN/mm$, it changed to (F+S+C), the separation of whole TRM layer with concrete substrate, with relatively low stressed textiles.

6.4 Final conclusion and future work

It can be concluded that a reasonable gain in the flexural strength was achieved for both the TRM systems, with an average increase of 38% for the carbon TRM system and an average of 26.7% for the PBO TRM system compared to that of their respective control specimen. So, both the systems performed considerably well and objective of gaining in an increase in flexural strength (by using different volume fractions and different steel reinforcement ratio) with TRM has been achieved successfully with this work.

Further, PBO system showed comparatively stronger interfacial bond behavior within the TRM system as well as between the TRM layer and concrete substrate, which

resulted in higher ductility index and high energy absorption. It should be noted that for lightly reinforced beam specimen (R1 types), PBO TRM reinforced specimens performed well both in strength gain as well as in ductility index. For higher reinforcement ratios (R2 and R3 types), carbon TRM system was better in enhancing the flexural capacity, but during experimentation, as the load increased, there were cracks along the TRM surface and ultimately resulted in the separation from the concrete substrate which was the final mode of failure. This showed that the carbon TRM system had a weaker bond among the TRM systems and was less ductile. Therefore, both the adopted TRM systems performed exceptionally well within the scope of the work, with carbon TRM system showing a relatively higher increase in the capacity of strengthened specimens and PBO TRM systems exhibiting relatively more ductile failure with higher bond strength between the TRM surface and concrete substrate.

Moreover, during the experimentation, it was seen that the technique of applying the TRM system also considers the contractor's ease where the construction workers (although not very skilled) can easily adopt the technique after being given simple demonstrations.

The reported work is limited to apply the TRM strengthening technique on newly constructed beams. The potential future work will concentrate on the study of TRM effectiveness for the corrosion damaged specimens which will highlight the behavior of TRM-strengthened structures with a focus on the corrosion aspect and its effect on

the structure's performance. Further, more detailed finite element modeling of TRM

strengthened beams will be performed in near future.

REFERENCES

[1]   Shalaby, H.M., and Daoud, O.K., "Case studies of deterioration of coastal concrete," vol. 20, no. c, pp. 975–985, 1990.

[2]   M. Khanzadeh Moradllo, M. Shekarchi, and M. Hoseini, "Time-dependent performance of concrete surface coatings in tidal zone of marine environment," *Constr. Build. Mater.*, vol. 30, pp. 198–205, 2012.

[3]   Tann, D.B., and Delpark. R, "Eperimental investigation of concrete bems reinforced with narrow carbon strips," in *Intl. Conf. Structural Faults & Repair*, 1999.

[4]   L. L.C., Hollaway, and M. B., *Strengthening of reinforced concrete structures: Using externally-bonded FRP composites in structural and civil engineering*. Elsevier Ltd, 1999, p. 325.

[5]   U. Ebead, "Inexpensive strengthening technique for partially loaded reinforced concrete beams : Experimental study," pp. 1–11, 2013.

[6]   M. Badawi and K. Soudki, "Control of corrosion-induced damage in reinforced concrete beams using carbon fiber-reinforced polymer laminates," *J. Compos. Constr.*, vol. 9, no. 2, pp. 195–201, 2005.

[7]   R. Al-Hammoud, K. Soudki, and T. H. Topper, "Fatigue flexural behavior of corroded reinforced concrete beams repaired with CFRP sheets," *J. Compos. Constr.*, vol. 15, no. February, pp. 42–51, 2011.

[8]   J. C. P. H. Gamage, R. Al-Mahaidi, and M. B. Wong, "Bond characteristics of CFRP plated concrete members under elevated temperatures," *Compos. Struct.*, vol. 75, pp. 199–205, 2006.

[9]   M. Leone, S. Matthys, and M. A. Aiello, "Effect of elevated service temperature on bond between FRP EBR systems and concrete," *Compos. Part B Eng.*, vol. 40, no. 1, pp. 85–93, 2009.

[10]   American Concrete Instutute (ACI)., "Design and construction of externally bonded Fabric-Reinforced Cementitious Matrix (FRCM) systems for repair and strengthening concrete and masonry Structures," *ACI 549, Farmingt. Hills, MI.*, 2013.

[11]   U. Ebead, "Hybrid externally bonded / mechanically fastened fiber- reinforced polymer for RC beam strengthening," no. 108, pp. 1–10, 2012.

[12]   U. Ebead and H. Marzouk, "Fiber-reinforced polymer strengthening of two-way slabs," *ACI Struct. J.*, vol. 101, no. 101, pp. 650–659, 2004.

[13] T. Triantafillou, "A new generation of composite materials as alternative to fibre-reinforced ploymers (FRP) for strengthening and seismic retrofitting of structures," pp. 113–127, 2011.

[14] Y. Al-Salloum, "Experimental and numerical study for the shear strengthening of reinforced concrete beams using textile-reinforced mortar," *J. Compos. Constr.*, no. February, pp. 74–90, 2012.

[15] Brameshuber W., "State-of-the-art report of RILEM technical committee TC 201-TRC: Textile reinforced concrete," *RILEM Publ.*

[16] "Project succeeds in processing carbon fibre heavy tows," *[online] 2015, www.knittingindustry.com/project-succeeds-in-processing-carbon-fibre-heavy-tows/ (Accessed: 2 July, 2015). .*

[17] "Photo Gallery | Structures Laboratory - University of Patras," *[online] 2015, www.strulab.civil.upatras.gr/resources/photo-gallery (Accessed: 2 July, 2015). .*

[18] T. C. Bournas, D. A., Lontou, P., Papanicolaou, C. G., and Triantafillou, "Textile-reinforced mortar (TRM) versus FRP confinement in reinforced concrete columns," *ACI Struct. J.*, vol. 104, no. 6, pp. 740–748, 2007.

[19] M. Jesse, F., Weiland, S., and Curbach, "Flexural strengthening of RC structures with textile-reinforced concrete," *Text. Concr. (ACI-SP250), Dubey, A. Ed. Am. Concr. Institute, Farmingt. Hill, MI, USA*, pp. 41–50, 2007.

[20] T. Taljsten, B. and Blanksvard, "Mineral-based bonding of carbon FRP to strengthen concrete structures," *ASCE J. Compos. Constr.*, vol. 11, no. 2, pp. 120–128, 2007.

[21] A. Blanksvard, T., Taljsten, B., and Carolin, "Shear strengthening of concrete structures with the use of mineral-based composites," *ASCE J. Compos. Constr.*, vol. 13, no. 1, pp. 25–34, 2009.

[22] T. C. Triantafillou, "Textile-reinforced mortars (TRM) versus fiber-reinforced polymers (FRP) as strengthening and seismic retrofitting materials for reinforced concrete and masonry structures.," *Int. Conf. Adv. Compos. Constr. (ACIC07), April 2-4, Univ. Bath.*

[23] H. M. Elsanadedy, T. H. Almusallam, S. H. Alsayed, and Y. a. Al-Salloum, "Flexural strengthening of RC beams using textile reinforced mortar - Experimental and numerical study," *Compos. Struct.*, vol. 97, pp. 40–55, 2013.

[24] D'Ambrisi A. D. and Focacci F., "Flexural strengthening of RC beams with cement based composites.," *ASCE J. Compos. Constr.*, vol. 15, no. 5, pp. 707–720, 2011.

[25] R. Kotynia, H. Abdel Baky, K. W. Neale, and U. Ebead, "Flexural strengthening of RC beams with externally bonded CFRP Systems: Test results and 3D nonlinear FE analysis," *J. Compos. Constr.*, vol. 12, no. 2, pp. 190–201, 2008.

[26] C. Papanicolaou, C. G., Triantafillou, T. C., Papantoniou, I., and Balioukos, "Strengthening of two-way slabs with textile-reinforced mortars (TRM)," *11th Int. fib Symp. London, UK*, 2009.

[27] A. Si Larbi, A. Agbossou, and P. Hamelin, "Experimental and numerical investigations about textile-reinforced concrete and hybrid solutions for repairing and/or strengthening reinforced concrete beams," *Compos. Struct.*, vol. 99, pp. 152–162, 2013.

[28] B. Gencoglu, M. and Mobasher, "Monotonic and cyclic flexural behavior of plain concrete beams strengthened by fabric-cement based composites," *3rd Int. Conf. Struct. Eng. Mech. Comput. (SEMC 2007),Zingoni, A. Ed. Africa, Sept. 10-12*, pp. 1961–1966.

[29] B. Gencoglu, M. and Mobasher, "Static and impact behavior of fabric reinforced cement composites in flexure.," *High Perform. Fiber Reinf. Cem. Compos. - HPFRCC 5, Reinhardt, H.W. Naaman, A. E. Ed. RILEM Proceeding 53, S.A.R.L., Cachan, Fr.*, pp. 463–470, 2007.

[30] B. Mobasher, "Mechanics of fiber and textile reinforced cement composites," *Compos. Struct.*, vol. 107, pp. 711–725, 2014.

[31] B. Soranakom, C. and Mobasher, "Modeling of tension stiffening in reinforced cement.," *Mater. Struct.*, vol. 43, pp. 1231–1243, 2010.

[32] S. Verbruggen, T. Tysmans, and J. Wastiels, "TRC or CFRP strengthening for reinforced concrete beams: An experimental study of the cracking behaviour," *Eng. Struct.*, vol. 77, pp. 49–56, 2014.

[33] S. Babaeidarabad, G. Loreto, and A. Nanni, "Flexural strengthening of RC beams with an externally bonded fabric-reinforced cementitious matrix," *J. Compos. Constr.*, vol. 18, no. 5, pp. 1–12, 2014.

[34] D. Arboleda, F. G. Carozzi, A. Nanni, and C. Poggi, "Testing procedures for the uniaxial tensile characterization of fabric-reinforced cementitious matrix composites," *J. Compos. Constr.*, no. 10.1061(ASCE)CC.1943–5614.0000626, pp. 1–11, 2015.

[35] B. Supernant And W. Malisch, "Equipment for cleaning or preparing concrete surfaces for repair," *C860927*, 1986.

[36] "Types Of sandblasting equipment and machines," *[online] 2015, www.knowsandblasting.com/types-sandblasting-equipment (Accessed: 2 July, 2015). .*

[37] "Captive shot blasting, blast technology LTD," *[online] 2015, www.gritblasters.co.uk/captive_shot_blasting.php (Accessed: 2 July, 2015). .*

[38] "Benefits of high pressure water jetting," *[online] 2015, www.leobest.com/benefits-high-pressure-water-jetting Accessed: 2 July, 2015). .*

[39] T. Sen and H. N. Jagannatha Reddy, "Strengthening of RC beams in flexure using natural jute fibre textile reinforced composite system and its comparative study with CFRP and GFRP strengthening systems," *Int. J. Sustain. Built Environ.*, vol. 2, no. 1, pp. 41–55, 2013.

[40] "Qatar Steel," *[online] 2015, http://www.qatarsteel.com.qa/Products/Specification/SitePages/bars.aspx (Accessed: 2 August, 2015). .*

[41] "S&P ARMO-mesh," *[online] 2015, http://www.sp-reinforcement.com.br/pdf/armomesh_sep.pdf (Accessed: 20 July, 2015). .*

[42] "Ruredil X Mesh Gold," *[online] 2015, http://www.bob-fr.com/DOCPDF/ruredilmeshgold_datasheet_0114en.pdf (Accessed: 20 July, 2015). .*

[43] ASTM C109/C109M (2013), "Standard test method for compressive strength of hydraulic cement mortars," *ASTM International, West Conshohocken, PA, USA*.

APPENDIX A

Detailed theoretical calculations for two of the beam specimen based on Chapter 5 are given in this section. The sample calculations are presented for two characteristic beam specimens: i) the strengthened specimen with three layers of carbon textile (C-R2-V3-F), and ii) the strengthened specimen with two layers of PBO textile (P-R2-V2-F). Also, the sample calculation for specimen showing the shear capacity of strengthened specimen is not exceeding the flexural one are also presented.

A.1 Sample calculation for R2 with three layers of carbon textile (C-R2-V3- F)

Beam Properties

Clear Length of beam	$L_b = = 2200$ mm
Width of beam	$W_b = 150$ mm
Effective depth of steel reinforcement	$d = 210$ mm
Thickness of the beam	$h = 260$ mm
Effective depth of compression steel	$d' = 36$ mm
Nominal compressive strength	$f_c' = 67$ MPa
Area of steel bar	$A_s = 226.2$ mm^2
Area of compression steel bar	$A_s' = 100.53$ mm^2
Yield Strength	$f_y = 550$ MPa

| Steel Modulus of elasticity | $E_s = 200$ GPa |
| Concrete Modulus of Elasticity | $E_c = 38.47$ GPa |

TRM Properties

Area of fabric per unit width	$A_f = 0.157$ mm^2 / mm
Ultimate tensile strain	$\varepsilon_{fu} = 0.012$
Tensile Modulus of elasticity	$E_f = 80$ GPa
Ultimate tensile strength	$f_{fu} = 1031$ MPa
Number of layers of fabric	$N = 3$
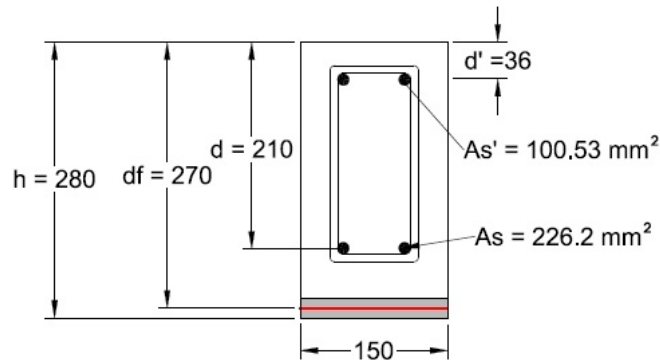
Calculation

Referring to section 5.1.2, the TRM delamination is assumed as the final mode of failure at the maximum strain of TRM while the compressive strain in the concrete does not exceed ε_c'.

After hit and trial method, internal force equilibrium should be satisfied according to Eq. (7) by taking $c = 27.67$ mm from equation (9)

$$c = \frac{A_s f_y + A_f b\, f_{fe} - A_{s'} f_{s'}}{0.85\, f_c'\, \beta b} = 27.67 \text{ mm}$$

The strain levels in concrete, tension steel and compression steel are computed as

$$\varepsilon_c = \frac{c}{h-c}\varepsilon_{fe} = 0.0014 \text{ mm / mm}$$

$$\varepsilon_s = \frac{d-c}{h-c}\varepsilon_{fe} = 0.0094 \text{ mm / mm}$$

$$\varepsilon_s' = \frac{c-d'}{c}\varepsilon_c = \text{-0.00043} \cong 0 \text{ mm / mm}$$

$$\varepsilon_c = \frac{1.7\, f_{c'}}{Ec} = 0.00296 \text{ mm / mm}$$

Internal force equilibrium equation

$$T_1 + T_f = C_1 + C_2$$

$$T_1 = A_s f_y = 124.41 \text{ kN}$$

$$T_f = N A_f b E_f \varepsilon_f = 67.82 \text{ kN}$$

$$C_1 = 0.85 f_c' \beta c b = 200.91 \text{kN}$$

$$C_2 = A_s' \varepsilon_s' E_s = 0 \text{ kN}$$

The flexural strength is calculated in accordance with Eq. (3)

$$M_n = M_{ns1} + M_{ns2} + M_f$$

$$M_{ns1} = A_s f_y \left(d - \frac{\beta c}{2} \right) = 26.37 \text{ kN-m}$$

$$M_{ns2} = A_s'f_s'(d - d') = 0 \text{ kN-m}$$

$$M_f = A_f bf_{fe}\left(h - \frac{\beta c}{2}\right) = 16.83 \text{ kN-m}$$

So, the total Nominal moment is equal to

$$M_n = 43.24 \text{ kN-m}$$

As the maximum moment is

$$Mmax = \frac{P}{2} \times 0.825$$

$$43.24 = \frac{P}{2} \times 0.825$$

$$\boldsymbol{Pmax = 104.76\ kN}$$

A.2 Sample calculation for R2 with two layers of PBO textile (P-R2-V2- F)

Beam Properties

Clear Length of beam	$L_b = = 2200$ mm
Width of beam	$W_b = 150$ mm
Effective depth of steel reinforcement	$d = 210$ mm
Thickness of the beam	$h = 260$ mm
Effective depth of compression steel	$d' = 36$ m
Nominal compressive strength	$f_c' = 67$ MPa
Area of steel bar	$A_s = 226.2$ mm^2
Area of compression steel bar	$A_s' = 100.53$ mm^2
Yield Strength	$f_y = 550$ MPa
Steel Modulus of elasticity	$E_s = 200$ GPa
Concrete Modulus of Elasticity	$E_c = 38.47$ GPa

TRM Properties

Area of fabric per unit width	$A_f = 0.05$ mm^2 / mm
Ultimate tensile strain	$\varepsilon_{fu} = 0.016$
Tensile Modulus of elasticity	$E_f = 128$ GPa
Ultimate tensile strength	$f_{fu} = 1664$ MPa
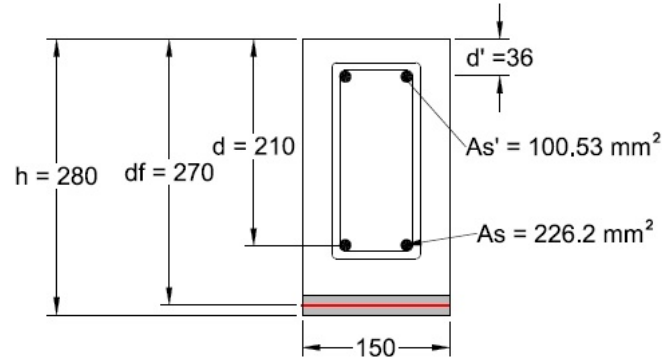
Number of layers of fabric $\qquad$ N = 2

Calculation

Referring to section 5.1.2, the TRM delamination is assumed as the final mode of failure at the maximum strain of TRM while the compressive strain in the concrete does not exceed ε_c'.

After hit and trial method, internal force equilibrium should be satisfied according to Eq. (7) by taking c = 22.23 mm from equation (9)

$$c = \frac{A_s f_y + A_f b\, f_{fe} - A_s' f_s'}{0.85\, f_c'\, \beta b} = 22.23 \text{ mm}$$

The strain levels in concrete, tension steel and compression steel are computed as

$$\varepsilon_c = \frac{c}{h-c} \varepsilon_{fe} = 0.0011 \text{ mm / mm}$$

$$\varepsilon_s = \frac{d-c}{h-c} \varepsilon_{fe} = 0.0095 \text{ mm / mm}$$

$$\varepsilon_s' = \frac{c-d'}{c} \varepsilon_c = \text{-0.0069} \cong 0 \text{ mm / mm}$$

$$\varepsilon_c = \frac{1.7\,f_{c'}}{Ec} = 0.00296 \text{ mm / mm}$$

Internal force equilibrium equation

$$T_1 + T_f = C_1 + C_2$$

$$T_1 = A_s f_y = 138.3 \text{ kN}$$

$$T_f = NA_f bE_f \varepsilon_f = 23.04 \text{ kN}$$

$$C_1 = 0.85 f_c' \beta cb = 161.41 \text{ kN}$$

$$C_2 = A_s' \varepsilon_s' E_s = 0 \text{ kN}$$

The flexural strength is calculated in accordance with Eq. (3)

$$M_n = M_{ns1} + M_{ns2} + M_f$$

$$M_{ns1} = A_s f_y \left(d - \frac{\beta c}{2}\right) = 27.75 \text{ kN-m}$$

$$M_{ns2} = A_s' f_s'(d - d') = 0 \text{ kN-m}$$

$$M_f = A_f bf_{fe} \left(h - \frac{\beta c}{2}\right) = 57.72 \text{ kN-m}$$

So, the total Nominal moment is equal to

$$M_n = 33.52 \text{ kN-m}$$

As the maximum moment is

$$M_{max} = \frac{P}{2} \times 0.825$$

$$33.52 = \frac{P}{2} \times 0.825$$

$$\boldsymbol{Pmax = 81.27\ kN}$$

APPENDIX B

B.1 Check for the shear capacity not exceeding the flexural strength [10]

The TRM composite material bonded to the surfaces of an RC member can be used to enhance the design shear strength by acting as external shear reinforcement. The sample calculation for two of the specimens C-R3-V2-F and C-R3-V3-F were done here to show that the shear capacity exceeds the flexural capacity.

The design tensile strain in TRM shear reinforcement, ε_{fv}, is calculated by Eq. (B.1a) [10].

$$\varepsilon_{fv} = \varepsilon_{fu} \leq 0.004 \qquad \text{(B.1a)}$$

So, the design tensile strength of the TRM shear reinforcement is calculated based on the Eq. (B.1b)

$$f_{fv} = E_f \varepsilon_{fv} \qquad \text{(B.1b)}$$

Where E_f is the tensile modulus of elasticity of the cracked TRM composite material

The shear strength can be computed by using Eq. (B.1c)

$$V_n = V_c + V_s + V_f \qquad \text{(B.1c)}$$

Where V_n is the nominal shear strength and V_c, V_s and V_f are the contribution of steel reinforcement , concrete and TRM composite material to the nominal shear strength

respectively and their corresponding relations are computed in Eq. (B.1d), (B.1e) and

(B.1f) respectively

$$V_s = \frac{A_v f_y d}{s} \tag{B.1d}$$

$$V_c = \frac{1}{6}\sqrt{f_c'}(b_w d) \tag{B.1e}$$

$$V_f = nA_f f_{fv} d_f \tag{B.1f}$$

B.2 Sample calculation of computing shear strength for C-R3-V2-F

Beam Properties

Clear Length of beam	$L_b = {} = 2200$ mm
Width of beam	$W_b = 150$ mm
Effective depth of steel reinforcement	$d = 210$ mm
Nominal compressive strength	$f_c' = 67$ MPa
Area of steel bar (stirrups)	$A_v = 100.4$ mm^2
Yield Strength	$f_y = 550$ MPa
Spacing of stirrups	$s = 100$ mm
Steel Modulus of elasticity	$E_s = 200$ GPa
Concrete Modulus of Elasticity	$E_c = 38.47$ GPa

TRM Properties

Area of fabric per unit width	$A_f = 0.157 \text{ mm}^2 / \text{mm}$
Ultimate tensile strain	$\varepsilon_{fu} = 0.016$
Design Tensile strain	$\varepsilon_{fv} = 0.0004$
Tensile Modulus of elasticity	$E_f = 80 \text{ GPa}$
Ultimate tensile strength	$f_{fu} = 1664 \text{ MPa}$
Number of layers of fabric	$N = 2$

Calculation:

According to the Eq. (B.1c)

$$V_n = V_c + V_s + V_f$$

$$V_s = \frac{A_v f_y d}{s} \qquad = \qquad 115.9 \text{ kN}$$

$$V_c = \frac{1}{6} \sqrt{f_c'} (b_w d) \quad = \qquad 42.97 \text{ kN}$$

$$V_f = n A_f f_{fv} d_f \qquad = \qquad 2.67 \text{ kN}$$

So, by summing all three of them

$$V_n = 161.54 \text{ kN} \geq 142.25 \text{ kN} \textit{ (Flexural Failure occurs)}$$

B.3 Sample calculation of computing shear strength for C-R3-V3-F

Beam Properties

Clear Length of beam	$L_b = = 2200$ mm
Width of beam	$W_b = 150$ mm
Effective depth of steel reinforcement	$d = 210$ mm
Nominal compressive strength	$f_c' = 67$ MPa
Area of steel bar (stirrups)	$A_v = 100.4$ mm^2
Yield Strength	$f_y = 550$ MPa
Spacing of stirrups	$s = 100$ mm
Steel Modulus of elasticity	$E_s = 200$ GPa
Concrete Modulus of Elasticity	$E_c = 38.47$ GPa

TRM Properties

Area of fabric per unit width	$A_f = 0.157$ mm^2 / mm
Ultimate tensile strain	$\varepsilon_{fu} = 0.016$
Design Tensile strain	$\varepsilon_{fv} = 0.0004$
Tensile Modulus of elasticity	$E_f = 80$ GPa
Ultimate tensile strength	$f_{fu} = 1664$ MPa
Number of layers of fabric	$N = 3$

Calculation:

According to the Eq. (B.1c)

$$V_n = V_c + V_s + V_f$$

$$V_s = \frac{A_v f_y d}{s} \qquad = \qquad 115.9 \text{ kN}$$

$$V_c = \frac{1}{6}\sqrt{f_c'}(b_w d) \quad = \qquad 42.97 \text{ kN}$$

$$V_f = nA_f f_{fv} d_f \qquad = \qquad 3.99 \text{ kN}$$

So, by summing all three of them

$$V_n = 162.86 \text{ kN} \geq 160.36 \text{ kN } \textbf{\textit{(Flexural Failure occurs)}}$$

APPENDIX C

C.1 Sample Calculation to find the Ductility Index (ΔI) and Energy Absorption (Ψ)

This section will briefly show the sample calculation to find the Ductility Index as well as Energy Absorption values. Appendix C (Table 14) shows the ductility index and energy absorption values for all of the beam specimens used in the experimentation.

C.2 Ductility Index (ΔI) value for C-R2-V1-F and P-R2-V1-F

The ductility Index **(ΔI)** is defined as the ratio between the deflection at the ultimate load($\boldsymbol{\delta_u}$) and that at the yield load($\boldsymbol{\delta_y}$).

While doing the experimentation, the data was measured using the data acquisition system which have been discussed in section 3.7 as well. Two strain gauges were installed on the steel rebar in order to measure the average strain values in the steel rebar. Also, the displacement measurements at the mid span of the specimens were measured using the displacement transducers. The ultimate load value of each specimen was computed directly from the load vs displacement relationship and the displacement corresponding to the ultimate load value was taken as the ultimate load displacement($\boldsymbol{\delta_u}$).

The yield load value is the load at which the steel rebar started to yield. As strain values in the rebar had been recorded by the data acquisition system, the load value corresponding to the strain value of rebar (0.26% strain) where it started to yield (as

illustrated in Table 6) was taken as the yield load and the corresponding displacement measured from displacement transducer was taken as the displacement at yield load(δ_y).

C.2.1 Sample calculation for specimen C-R2-V1-F

Ultimate load value recorded Pu = 85.15 kN

Displacement at the ultimate load value (δ_u) = 19.33 mm

Load value corresponding to 2600μ strain in rebar Py = 66.18 kN *(Yield Load)*

Displacement at the yield load value (δ_y) = 8.02 mm

$$\text{Ductility Index } (\Delta I) = \frac{(\delta_u)}{(\delta_y)} = \frac{19.33}{8.02} = \mathbf{2.41}$$

C.2.2 Sample calculation for specimen P-R2-V1-F

Ultimate load value recorded Pu = 84.68 kN

Displacement at the ultimate load value (δ_u) = 40.45 mm

Load value corresponding to 2600μ strain in rebar Py = 62.36 kN *(Yield Load)*

Displacement at the yield load value (δ_y) = 8.05 mm

$$\text{Ductility Index } (\Delta I) = \frac{(\delta_u)}{(\delta_y)} = \frac{40.45}{8.05} = \mathbf{5.02}$$

C.3 Energy Absorption (Ψ) value for C-R3-V1-F

The energy absorption **(Ψ)** is defined as the area under the load deflection curve up to the ultimate load value. The area under the curve can be computed easily using the Excel Software or any other related software. As, in this research project Mat-Lab software had been used to plot all the relationships (graphs). Therefore the energy absorption value had also been calculated using the Mat-Lab software.

The required code in Mat-Lab software to get the energy absorption of any beam specimen:

Energy_absorption = trapz (displacement_mid(1:the ultimate load value number)**,**

force(1:ultimate load value number)**)**

The Appendix C (Figure 69) shows the Mat- Lab code for calculating the Energy Absorption for C-R3-V1-F beam specimen.
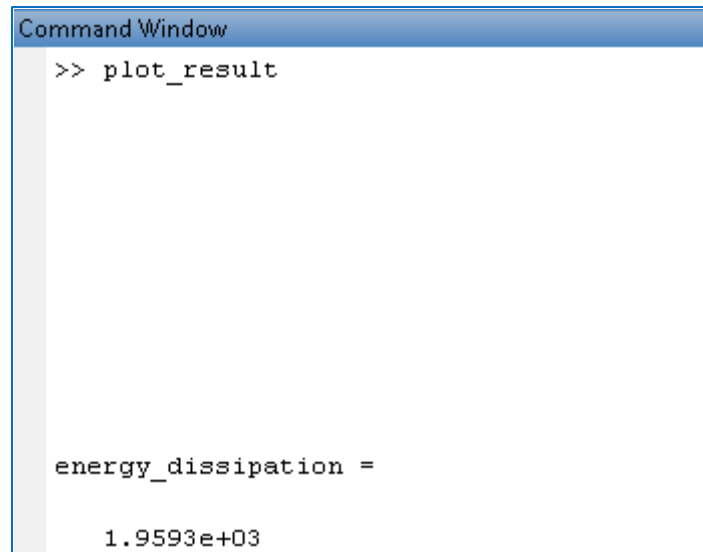
Energy_absorption = trapz (displacement_mid(1:1309)**, force**(1:1309)**)**

```
xlabel('Concrete strain (10^-^6)','FontSize',20,'FontName','Times New Roman')
ylabel('Force (kN)','FontSize',20,'FontName','Times New Roman')
legend('CR3V1F','FontSize',20,'FontName','Times New Roman')

energy_absortion = trapz(-displacement_mid(1:1309),force(1:1309))
```

Appendix C Figure 69: Mat-Lab code for C-R3-V1-F to calculate Energy Absorption

The calculated value of Energy Absorption had been displayed in the command window of Mat-Lab as shown in Appendix C (Figure 70). The Energy Absorption value came out to be 1959.3 kN-mm. On similar pattern, the energy absorption of all the beam specimens had been calculated. The values are shown in column 5 of Appendix C (Table 14).

Appendix C Figure 70: Print screen of Command window of Mat-Lab software

Appendix C Table 14: Ductility Index and Energy Absorption values

1	2	3	4	5
Specimen	δ_Y (mm)	δ_u (mm)	Ductility Index (ΔI)	Energy Absorption Ψ (kN-mm)
R1	15.03	36.49	2.43	1491.7
R2	7.14	43.46	6.09	2724.9
R3	8.8	39.51	4.49	3692.1
C-R1-V1-F	8.38	20.33	2.43	998.7
C-R1-V2-F	7.74	17.29	2.23	1132
C-R1-V3-F	8.15	24.17	2.97	1485
C-R2-V1-F	8.02	19.33	2.41	1210.7
C-R2-V2-F	11.91	17.97	1.51	1358.8
C-R2-V3-F	7.99	26.33	3.30	1623.8
C-R3-V1-F	10.50	20.93	1.99	1959.3
C-R3-V2-F	10.29	18.81	1.83	2025.4
C-R3-V3-F	10.06	24.53	2.44	2719.5
P-R1-V1-F	6.7	35.14	5.24	1665.1
P-R1-V2-F	5.61	36.52	6.51	2323.2
P-R2-V1-F	8.05	40.45	5.02	2804.2
P-R2-V2-F	8.38	34.56	4.12	2980.1
P-R3-V1-F	10.13	21.54	2.13	2266.5
P-R3-V2-F	10.39	30.15	2.90	2943.2

APPENDIX D

Cost Efficiency of TRM system compared to FRPs

This section will give a brief overview of the cost for a beam that is being strengthened using TRM strengthening system (Flat – Type) of one layer; having dimensions of (150 x 260 x 2500) mm and then comparison has been made along with the FRP materials (Appendix D Figure 71).

D.1 Cost details of the Carbon TRM system used in this research project

Appendix D Tables (15) and (16) depicts the cost required to prepare one beam specimen strengthen with one layer of carbon TRM system.

Appendix D Table 15: Cost details of the product

Sr. No	Product Name	Unit	Price per unit (QAR)
1	Full roll of ARMO-mesh L600 Fabric	per m^2	60 QAR / m^2
2	Mortar Armo-crete (1bag = 25 kg)	kg	107 QAR / bag

Appendix D Table 16: Cost used to prepare 1 beam specimen using one layer of TRM system.

Sr. No	Product Name	Layers	Quantity used	Cost (QAR)
1	Carbon Fabric	1	0.315 m^2	19/-
2	Mortar used	1	8.33 kg	36/-
	Total cost of material to prepare beam specimen strengthened with one layer of carbon textile			**55/-**

D.2 Cost details of the PBO TRM system used in this research project

Appendix D Tables (17) and (18) shows the cost required to prepare one beam specimen strengthen with one layer of PBO TRM system.

Appendix D Table 17: Cost details of the product

Sr. No	Product Name	Unit	Price per unit (QAR)
1	Ruridel X Mesh Gold Fabric	per meter	275 QAR / m
2	Rureidel X Mortar -750 (1bag = 25 kg)	kg	145 QAR / bag

Appendix D Table 18: Cost used to prepare 1 beam specimen using one layer of TRM system.

Sr. No	Product Name	Layers	Quantity used	Cost (QAR)
1	Ruridel X Mesh Gold Fabric	1	0.315 m^2	42/-
2	Rureidel X Mortar -750	1	8.33 kg	49/-
	Total cost of material to prepare beam specimen strengthened with one layer of PBO textile			**91/-**

D.3 Cost details of the FRP system available in the market

Appendix D Tables (19) and (20) shows the cost required to prepare one beam specimen strengthen with Carbon Fiber Sheet using Sikadur Epoxy- 30 PL.

Appendix D Table 19: Cost details of the product

Sr. No	Product Name	Unit	Price per unit (QAR)
1	Carbon Fiber Sheet	per meter	540 QAR / m
2	Sikadur Epoxy- 30 PL (6 kg)	6 kg	300 QAR

Appendix D Table 20: Cost used to prepare 1 beam specimen using one layer of TRM system.

Sr. No	Product Name	Layers	Quantity used	Cost (QAR)
1	Carbon Fiber Sheet	1	0.315 m^2	81/-
2	Sikadur Epoxy- 30 PL (6 kg)	1	2 kg	100/-
	Total cost of material to prepare beam specimen strengthen by Carbon fiber sheet with Sikadur Epoxy			**181/-**

(The cost used here is changed to QAR based on the currency exchange rate available on date **2/1/2016**).
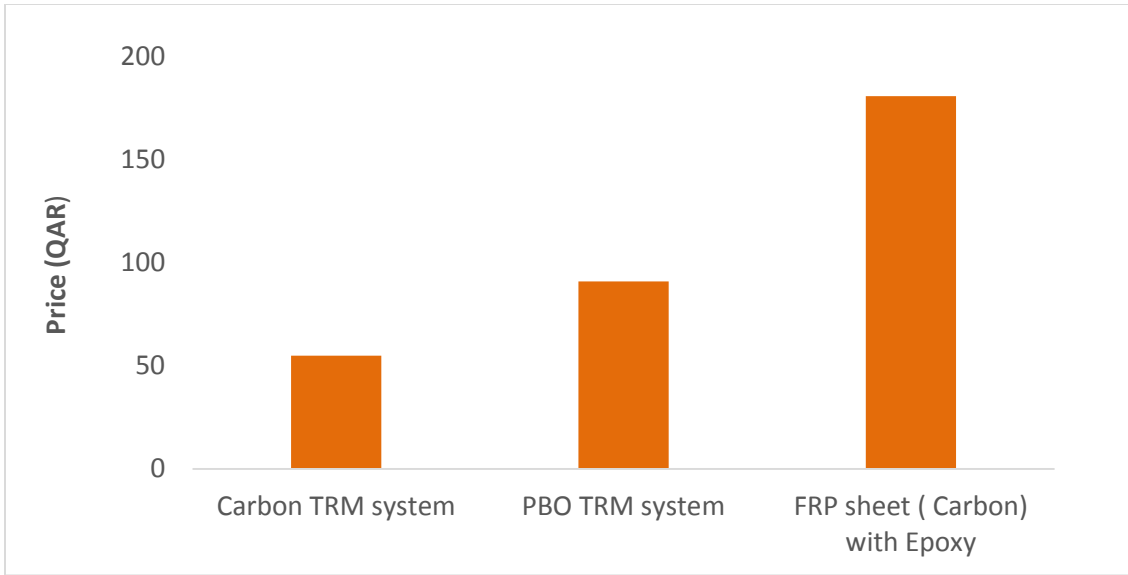
Appendix D Figure 71: Cost comparison between the (Carbon and PBO) TRM systems and FRP